



Michigan Technological University
Create the Future Digital Commons @ Michigan Tech

Dissertations, Master's Theses and Master's
Reports - Open

Dissertations, Master's Theses and Master's
Reports

2011

Structural capacity of steel tubular cast-in-place piling

Kevin A. Mears

Michigan Technological University

Follow this and additional works at: <https://digitalcommons.mtu.edu/etds>



Part of the [Civil and Environmental Engineering Commons](#)

Copyright 2011 Kevin A. Mears

Recommended Citation

Mears, Kevin A., "Structural capacity of steel tubular cast-in-place piling ", Master's Thesis, Michigan Technological University, 2011.

<https://doi.org/10.37099/mtu.dc.etds/258>

Follow this and additional works at: <https://digitalcommons.mtu.edu/etds>



Part of the [Civil and Environmental Engineering Commons](#)

STRUCTURAL CAPACITY OF STEEL TUBULAR CAST-IN-PLACE PILING

By

Kevin A. Mears

A THESIS

Submitted in partial fulfillment of the requirements for the degree of

MASTER OF SCIENCE

Civil Engineering

MICHIGAN TECHNOLOGICAL UNIVERSITY

2011

This thesis, "Structural Capacity of Steel Tubular cast-in-place piling," is hereby approved in partial fulfillment of the requirements for the Degree of MASTER OF SCIENCE IN CIVIL ENGINEERING.

Department of Civil and Environmental Engineering

Signatures:

Thesis Advisor

Devin Harris

Department Chair

William M. Bulleit

Date

Table of Contents

LIST OF FIGURES.....	VI
LIST OF TABLES	X
ACKNOWLEDGEMENTS	XI
ABSTRACT.....	XII
1 INTRODUCTION.....	1
2 LITERATURE REVIEW.....	4
2.1 FOUNDATIONS	4
2.1.1 <i>Shallow Foundations</i>	4
2.1.2 <i>Deep Foundations</i>	5
2.1.2.1 Pile Foundations.....	6
2.1.2.2 Drilled Shafts	7
2.1.2.3 Caissons.....	8
2.1.3 <i>Foundation Summary</i>	8
2.2 FOUNDATION DESIGN	8
2.2.1 <i>Resistance Based Design</i>	8
2.2.2 <i>Structural Capacity</i>	10
2.2.2.1 AASHTO LRFD.....	10
2.2.2.2 State Specific Design Codes.....	12
2.2.2.3 Other Design Methods	13
2.3 PREVIOUS RESEARCH	16
2.3.1 <i>CFT Experimental Studies</i>	16
2.4 SUMMARY OF LITERATURE REVIEW	19

3	PROCEDURES	21
3.1	DRIVING THE PILES	21
3.2	CASTING THE PILES.....	24
3.3	CURING THE PILES	25
3.4	CUTTING THE PILES.....	27
3.5	TESTING THE PILES	31
3.5.1	<i>Testing Machines.....</i>	<i>31</i>
3.5.2	<i>Data Acquisition and Instrumentation.....</i>	<i>32</i>
3.5.3	<i>Axial Compression Testing</i>	<i>33</i>
3.5.3.1	Full Section Compression Tests	33
3.5.3.2	Section Core Compression Tests	34
3.5.3.3	Cored Sample Tests	36
3.5.3.4	Push-through Tests	37
3.6	FINITE ELEMENT MODEL.....	38
4	ANALYSIS	44
4.1	CONCRETE CORE SAMPLES.....	44
4.2	FULL CROSS SECTION LOADING.....	46
4.2.1	<i>10 ¾" specimens (0.375" wall)</i>	<i>47</i>
4.2.2	<i>10 ¾" specimens (0.5" wall)</i>	<i>51</i>
4.2.3	<i>12 ¾" specimen (0.375" wall)</i>	<i>55</i>
4.2.4	<i>Summary of Full Cross Section Loading</i>	<i>58</i>
4.3	SECTION CORE ONLY LOADING.....	60
4.3.1	<i>10 ¾" specimen (0.375" wall)</i>	<i>61</i>
4.3.2	<i>10 ¾" specimen (0.5" wall)</i>	<i>64</i>
4.3.3	<i>12 ¾" specimen (0.375" wall)</i>	<i>68</i>

4.3.4	<i>Summary of Section Core Only Loading</i>	71
4.4	PUSH-THROUGH TESTING.....	73
4.5	SUMMARY OF ANALYSIS	76
5	CONCLUSION AND RECOMMENDATIONS	77
5.1	FINDINGS, OBSERVATIONS, AND CONCLUSIONS	77
5.1.1	<i>Findings</i>	77
5.1.2	<i>Observations</i>	78
5.1.3	<i>Conclusions</i>	78
5.2	RECOMMENDATIONS	80
	BIBLIOGRAPHY	82
	APPENDIX A – CORE SAMPLE TEST DATA	84
	APPENDIX B – ADDITIONAL COMPRESSION DATA	88
	APPENDIX C – CALCULATIONS	94
C.1	TRANSFORMED SECTION CALCULATIONS	94
C.2	TRANSFORMED SECTION EXAMPLE	95
C.3	10- ³ / ₄ " (0.375" WALL) MEMBER CAPACITIES.....	96
C.4	10- ³ / ₄ " (0.5" WALL) MEMBER CAPACITIES.....	99
C.5	12- ³ / ₄ " (0.375" WALL) MEMBER CAPACITIES.....	102

List of Figures

FIGURE 3.1: THE FOUR PILES AND THE CAISSONS	22
FIGURE 3.2: PILE DRIVE HEAD	22
FIGURE 3.3: PILE DRIVER.....	23
FIGURE 3.4: UNFILLED PILES WITH THE CAISSON PLACED AROUND THEM.....	24
FIGURE 3.5: CONCRETE POUR INTO PILES.....	25
FIGURE 3.6: CAISSONS BEING FILLED WITH SOIL	26
FIGURE 3.7: PILES AFTER BEING PULLED	26
FIGURE 3.8: PILE SUPPORTS FOR CUTTING	28
FIGURE 3.9: DIAMOND WIRE SAW.	28
FIGURE 3.10: DIAMOND WIRE SAW CUTTING.....	29
FIGURE 3.11: PILE CUT SECTION USE DIAGRAM	30
FIGURE 3.12: MTS 315.03 LOAD FRAME	31
FIGURE 3.13: BALDWIN CYLINDER TEST MACHINE.....	32
FIGURE 3.14: FULL SECTION LOADS	34
FIGURE 3.15: FULL SECTION LOADING SETUP	34
FIGURE 3.16: SECTION CORE LOADS	35
FIGURE 3.17: SECTION CORE LOADING SETUP.....	35
FIGURE 3.18: DRILL PRESS SETUP.....	36
FIGURE 3.19: PUSH-THROUGH LOADS	37
FIGURE 3.20: PUSH-THROUGH RINGS	38
FIGURE 3.21: PUSH-THROUGH SETUP.....	38
FIGURE 3.22: CONCRETE MODEL VERIFICATION	41
FIGURE 3.23: STEEL MODEL VERIFICATION.....	41
FIGURE 3.24: 12- $\frac{3}{4}$ " (0.375" WALL) MODEL STRAINS	42

FIGURE 3.25: 10- $\frac{3}{4}$ " (0.375" WALL) MODEL STRAINS	43
FIGURE 3.26: 10- $\frac{3}{4}$ " (0.5" WALL) MODEL STRAINS	43
FIGURE 4.1: AVERAGE CORE SAMPLE COMPRESSION STRENGTHS THROUGH THE DEPTH	45
FIGURE 4.2: FULL CROSS SECTION LOADING – AXIAL LOAD VS. LONGITUDINAL STRAINS, 10- $\frac{3}{4}$ " (0.375" WALL)	48
FIGURE 4.3: FULL CROSS SECTION LOADING – AXIAL LOAD VS. TANGENTIAL STRAINS, 10- $\frac{3}{4}$ " (0.375" WALL)	48
FIGURE 4.4: FULL CROSS SECTION LOADING – LONGITUDINAL STRESS VS. LONGITUDINAL STRAINS, 10- $\frac{3}{4}$ " (0.375" WALL)	49
FIGURE 4.5: FULL CROSS SECTION LOADING – LONGITUDINAL STRESS VS. TANGENTIAL STRAINS, 10- $\frac{3}{4}$ " (0.375" WALL)	49
FIGURE 4.6: FULL CROSS SECTION LOADING – AXIAL LOAD VS. LONGITUDINAL STRAINS, 10- $\frac{3}{4}$ " (0.5" WALL)	52
FIGURE 4.7: FULL CROSS SECTION LOADING – AXIAL LOAD VS. TANGENTIAL STRAINS, 10- $\frac{3}{4}$ " (0.5" WALL)	52
FIGURE 4.8: FULL CROSS SECTION LOADING – LONGITUDINAL STRESS VS. LONGITUDINAL STRAINS, 10- $\frac{3}{4}$ " (0.5" WALL)	53
FIGURE 4.9: FULL CROSS SECTION LOADING – LONGITUDINAL STRESS VS. TANGENTIAL STRAINS, 10- $\frac{3}{4}$ " (0.5" WALL)	53
FIGURE 4.10: FULL CROSS SECTION LOADING – AXIAL LOAD VS. LONGITUDINAL STRAINS, 12- $\frac{3}{4}$ " (0.375" WALL)	56
FIGURE 4.11: FULL CROSS SECTION LOADING – AXIAL LOAD VS. TANGENTIAL STRAINS, 12- $\frac{3}{4}$ " (0.375" WALL)	56
FIGURE 4.12: FULL CROSS SECTION LOADING – LONGITUDINAL STRESS VS. LONGITUDINAL STRAINS, 12- $\frac{3}{4}$ " (0.375" WALL)	57

FIGURE 4.13: FULL CROSS SECTION LOADING – LONGITUDINAL STRESS VS. TANGENTIAL STRAINS, 12- $\frac{3}{4}$ " (0.375" WALL)	57
FIGURE 4.14: SECTION CORE ONLY LOADING – AXIAL LOAD VS. LONGITUDINAL STRAINS, 10- $\frac{3}{4}$ " (0.375" WALL)	61
FIGURE 4.15: SECTION CORE ONLY LOADING – AXIAL LOAD VS. TANGENTIAL STRAINS, 10- $\frac{3}{4}$ " (0.375" WALL)	62
FIGURE 4.16: SECTION CORE ONLY LOADING – LONGITUDINAL STRESS VS. LONGITUDINAL STRAINS, 10- $\frac{3}{4}$ " (0.375" WALL)	62
FIGURE 4.17: SECTION CORE ONLY LOADING – LONGITUDINAL STRESS VS. TANGENTIAL STRAINS, 10- $\frac{3}{4}$ " (0.375" WALL)	63
FIGURE 4.18: SECTION CORE ONLY LOADING – AXIAL LOAD VS. LONGITUDINAL STRAINS, 10- $\frac{3}{4}$ " (0.5" WALL)	65
FIGURE 4.19: SECTION CORE ONLY LOADING – AXIAL LOAD VS. TANGENTIAL STRAINS, 10- $\frac{3}{4}$ " (0.5" WALL)	66
FIGURE 4.20: SECTION CORE ONLY LOADING – LONGITUDINAL STRESS VS. LONGITUDINAL STRAINS, 10- $\frac{3}{4}$ " (0.5" WALL)	66
FIGURE 4.21: SECTION CORE ONLY LOADING – LONGITUDINAL STRESS VS. TANGENTIAL STRAINS, 10- $\frac{3}{4}$ " (0.5" WALL)	67
FIGURE 4.22: SECTION CORE ONLY LOADING – AXIAL LOAD VS. LONGITUDINAL STRAINS, 12- $\frac{3}{4}$ " (0.375" WALL)	69
FIGURE 4.23: SECTION CORE ONLY LOADING – AXIAL LOAD VS. TANGENTIAL STRAINS, 12- $\frac{3}{4}$ " (0.375" WALL)	69
FIGURE 4.24: SECTION CORE ONLY LOADING – LONGITUDINAL STRESS VS. LONGITUDINAL STRAINS, 12- $\frac{3}{4}$ " (0.375" WALL)	70

FIGURE 4.25: SECTION CORE ONLY LOADING – LONGITUDINAL STRESS VS. TANGENTIAL STRAINS, 12- $\frac{3}{4}$ " (0.375" WALL)	70
FIGURE 4.26: BOND STRENGTH – 10- $\frac{3}{4}$ " (0.375" WALL)	74
FIGURE 4.27: BOND STRENGTH – 10- $\frac{3}{4}$ " (0.5" WALL)	74
FIGURE 4.28: BOND STRENGTH – 12- $\frac{3}{4}$ " (0.375" WALL)	75
FIGURE B.1: FULL CROSS SECTION LOADING – AXIAL LOAD VS. DISPLACEMENT, 10- $\frac{3}{4}$ " (0.375" WALL)	88
FIGURE B.2: FULL CROSS SECTION LOADING - DISPLACEMENTS, 10- $\frac{3}{4}$ " (0.375" WALL)	88
FIGURE B.3: FULL CROSS SECTION LOADING – AXIAL LOAD VS. DISPLACEMENT, 10- $\frac{3}{4}$ " (0.5" WALL)	89
FIGURE B.4: FULL CROSS SECTION LOADING – DISPLACEMENTS, 10- $\frac{3}{4}$ " (0.5" WALL)	89
FIGURE B.5: FULL CROSS SECTION LOADING – AXIAL LOAD VS. DISPLACEMENT, 12- $\frac{3}{4}$ " (0.375" WALL)	90
FIGURE B.6: FULL CROSS SECTION LOADING – DISPLACEMENTS, 12- $\frac{3}{4}$ " (0.375" WALL)	90
FIGURE B.7: SECTION CORE ONLY LOADING – AXIAL LOAD VS. DISPLACEMENT, 10- $\frac{3}{4}$ " (0.375" WALL)	91
FIGURE B.8: SECTION CORE ONLY LOADING – DISPLACEMENTS, 10- $\frac{3}{4}$ " (0.375" WALL)	91
FIGURE B.9: SECTION CORE ONLY LOADING – AXIAL LOAD VS. DISPLACEMENT, 10- $\frac{3}{4}$ " (0.5" WALL)	92
FIGURE B.10: SECTION CORE ONLY LOADING – DISPLACEMENTS, 10- $\frac{3}{4}$ " (0.5" WALL)	92
FIGURE B.11: SECTION CORE ONLY LOADING – AXIAL LOAD VS. DISPLACEMENT, 12- $\frac{3}{4}$ " (0.375" WALL)	93
FIGURE B.12: SECTION CORE ONLY LOADING – DISPLACEMENTS, 12- $\frac{3}{4}$ " (0.375" WALL)	93

List of Tables

TABLE 2.1: COMPOSITE SECTION CONSTANTS	12
TABLE 2.2: AVAILABLE STATE/DISTRICT TRANSPORTATION AGENCY METHODOLOGIES	13
TABLE 4.1: AVERAGE CORE SAMPLE COMPRESSIVE STRENGTHS	45
TABLE 4.2: 10 $\frac{3}{4}$ " (0.375" WALL) NOMINAL CAPACITY	47
TABLE 4.3: 10- $\frac{3}{4}$ " (0.5" WALL) NOMINAL CAPACITY	51
TABLE 4.4: 12- $\frac{3}{4}$ " (0.375" WALL) NOMINAL CAPACITY	55
TABLE 4.5: CONCRETE-STEEL BOND STRENGTH	75
TABLE A.1: CORE SAMPLE TEST DATA	84

Acknowledgements

First, I would like to thank my advisor, Dr. Devin Harris, for the guidance and help along the way throughout this project and with my graduate studies. I would also like to thank Kiko, Mike Yokie, Adam Holcomb and the rest of the Benedict staff for all the help along the process of this project, along with Cutting Edge services for the assistance with the cutting of the sections and donation of materials and time. I would also like to thank Pheifer Bros. Construction for their assistance with the driving and casting of the piles used for this project. WisDOT was the funding agency for this project, to which I am extremely grateful for the opportunity to do this work. I would also like to thank Dr. Barbara Dai and Dr. Brett Hamlin for serving on my committee and helping guide me through the final stages of this project. Finally, I would like to thank all my friends, family, and colleagues for all the help and inspiration throughout the years.

Abstract

Steel tubular cast-in-place pilings are used throughout the country for many different project types. These piles are a closed-end pipe with varying wall thicknesses and outer diameters, that are driven to depth and then the core is filled with concrete. These piles are typically used for smaller bridges, or secondary structures. Mostly the piling is designed based on a resistance based method which is a function of the soil properties of which the pile is driven through, however there is a structural capacity of these members that is considered to be the upper bound on the loading of the member. This structural capacity is given by the AASHTO LRFD (2010), with two methods. These two methods are based on a composite or non-composite section. Many state agencies and corporations use the non-composite equation because it requires much less computation and is known to be conservative. However with the trends of the time, more and more structural elements are being investigated to determine ways to better understand the mechanics of the members, which could lead to more efficient and safer designs.

In this project, a set of these piling are investigated. The way the cross section reacts to several different loading conditions, along with a more detailed observation of the material properties is considered as part of this research. The evaluation consisted of testing stub sections of pile with varying sizes ($10\frac{3}{4}$ ", $12\frac{3}{4}$ "), wall thicknesses (0.375", 0.5"), and testing methods (whole compression, composite compression, push through, core sampling). These stub sections were chosen as they would represent a similar bracing length to many different soils. In addition, a finite element model was developed using ANSYS to predict the strains from the testing of the pile cross sections. This model was able to simulate the strains from most of the loading conditions and

sizes that were tested. The bond between the steel shell and the concrete core, along with the concrete strength through the depth of the cross section were some of the material properties of these sections that were investigated.

1 Introduction

Concrete-filled steel tubular members, when designed correctly, can take advantage of both components strengths and behave as a single unit. The shell is typically the steel element, which is then infilled with concrete. The steel shell works as formwork for the concrete and because of the location of the steel, typically there is no need for longitudinal reinforcement. Locating steel at the farthest point from the centroid, such as in the shell, maximizes the moment of inertia in the cross section, which then increases the flexural capacity. To achieve the same moment of inertia from a column with longitudinal reinforcing bars would require a larger pile because of the required cover over the steel bars. Also, the steel shell provides a confining pressure to the concrete, which can increase the compressive strength of the concrete to a much higher level (Baig et al. 2006). Lastly the presence of the concrete core fills the space in the steel tube which would normally be an air void, enhancing the buckling capacity of the steel shell.

Concrete-filled steel tubular sections are used for many different construction elements, ranging from foundation elements to columns. This research highlights how a certain type of concrete-filled steel tubular member is used as a foundation element and examines their structural capacity. The piles investigated are closed ended on the drive side and are backfilled with concrete after they are fully driven. The main focus of the project was to quantify the true axial capacity of the pile sections and determine whether composite action can be considered in design. Currently, some state codes, like Wisconsin, assume that the steel shell is not present due to the possibility of corrosion over time and damage from driving. The goal of this research was to determine if there is a better way to use the full material properties and design the piles for a larger load.

Piles were tested in multiple configurations to determine how they behave under different boundary and loading scenarios. The major considerations in this project were the structural capacity of the pile under axial loading, and whether the piles act as a composite member, or whether there is slip between the materials in the pile, making each material act independently.

There are several main goals and possible advantages that can be accomplished from this research. The first major goal is to accurately determine the true capacity of the piles section. At this point the design capacity of the pile is based on the percentage of steel in the cross section. If there is enough steel, it is assumed the member acts as a composite member. If there is not enough steel, it is assumed that the steel only acts as formwork and the capacity is solely based on the concrete core and any reinforcing steel inside the concrete. Some possible advantages include a better understanding of the actual full capacity of the pile sections, which will allow for better designs on future projects, along with the need for extra piles that can be eliminated because the increased capacity of these piles, which in turn could also reduce project costs by eliminating the installation, concrete material, and work costs associated with each additional pile, in addition to the pile cost itself. Another primary goal is to determine the strength of the bond between materials and to determine if the pile sections act as a composite section, or as two independent elements. To use the composite action in design there has to be significant composite behavior. Determining the amount of composite action present is another major goal of this research project. After all the testing was completed, the results were compared with a finite element model that was created as part of this research project. This model is an analytical tool based on the theoretical properties of the cross sections, but provides a mechanism to evaluate how

the system behaves. This model was also modified with different concrete properties, to determine how the concrete strength affects the overall member.

This thesis covers an experimental investigation of steel tubular cast in place piling loaded axially and is divided into the following sections: 1) Chapter 2: Literature Review, 2) Chapter 3: Procedure, 3) Chapter 4: Analysis, and 4) Chapter 5: Conclusion.

2 Literature Review

Included in this section is a summary of literature pertinent to the performance of cast-in-place steel tubular piles. A general summary on their application is presented followed by typical design methods and a synopsis of previous research related to piles.

2.1 Foundations

The foundation is one of the most important elements of a structure because it serves as the component that anchors the structure to the earth. A failure in the foundation could lead to a catastrophic failure of the entire structure. This is one reason most substructure elements are over-designed and have a high factor of safety (Coduto 2001). However, with the advancement of construction technology creating larger buildings and bridges, structures require larger foundation elements and there is a need to better understand the behavior of these elements. With an increased understanding, better designs which optimize material usage and geometry can be implemented. In general, there are two main categories of foundations, shallow and deep foundations.

2.1.1 Shallow Foundations

Shallow foundations are typical for structures with smaller loads and when the soil beneath the structure can easily support the weight of the structure, such as a house with a block wall foundation. The main two types of shallow foundations are spread footing foundations and mat foundations (Coduto 2001). A spread footing transfers the loads from a single column, group of columns, or wall down to an enlarged bottom, which distributes the load over a much larger bearing area. These are by far the most common type of foundation due to their low price and ease of construction. Spread

footings can be built in many different shapes, with the most common shapes being square, rectangular, circular, continuous, combined, and ring.

The mat foundation is actually very similar to the spread footing, but instead of supporting only one column or wall, the entire structure has a single “mat” beneath the entire footprint of the building. Typically, mat foundations are used when loads are large or the soil is so poor as to make the spread footings cover about 50 percent or more of the building footprint area. They are also used when there is high potential for differential settlement due to soil conditions, erratic loading, and non-uniformly distributed lateral loads. Mat foundations are also practical when the uplift loads are larger than what a spread foundation can support, and when the foundation is below the groundwater table, so waterproofing is a large concern (Coduto 2001).

2.1.2 Deep Foundations

Deep foundations are used when standard shallow foundations are not capable of supporting the structure. Deep foundations transfer the loads of the structure down to soil layers below the main structure that are capable of supporting the loads of the building (Coduto 2001). As with shallow foundations, there are several types of deep foundations including: piles, drilled shafts, and caissons. Other types of deep foundations include mandrel-driven thin shells filled with concrete, auger-cast piles, pressure injected footings, and anchors. Pile foundations are typically prefabricated members that are driven or forced into the ground. Drilled shafts are made by drilling a cylindrical hole in the ground, adding reinforcing steel and filling the hole with concrete. Caissons are prefabricated like piles, however, they are much larger. Generally caissons are boxes or cylinders that are sunk into the ground to the desired depth by digging around them, and then filled with either concrete or soil (Coduto 2001).

2.1.2.1 Pile Foundations

In pile foundations there are many different types of piles used, and many different ways of driving the piles (Coduto 2001). The oldest type of piles are timber piles. These have been around for thousands of years, and still continue to be a good choice for many applications. They are driven so that the largest cross section of the timber is at the top. These piles are suggested for use in loose sands or soft to medium clay, and should not be used in dense or hard soils or as end bearing piles.

Another type of pile is a steel pile. One of the most common types of steel piles is the rolled H-pile. These sections resemble the wide-flange shapes of steel members used in the construction of buildings, but H-piles have the same thickness on the flanges and web, whereas the wide flange beams have a thinner web than flange. The steel piles have an advantage over timber in that another section of pile may be simply spliced on if the pile needs to be driven further than a single length of piling. Also they can be easily cut to the height above ground if driven into rock at a higher depth than was expected.

Another type of steel pile is a pipe pile, which is constructed using both concrete and steel. The pile is a steel cylinder with either a closed or open bottom end that is driven into the ground to a specified depth. Once it is driven, the core of the steel cylinder is filled with concrete to add both weight and strength to the pile. With the steel being located along the perimeter, pipe piles have a larger moment of inertia when compared to the H-piles, and are often a better choice for scenarios with large lateral loads.

Piles are also made from concrete, which are typically pre-cast and pre-stressed with a number of steel prestressing strands running along their length. These pre-stressed concrete piles have almost completely replaced conventionally reinforced

concrete piles, and have strengths similar to steel piles, but at a lower cost. However, they are the most costly to cut, and as such, are not recommended when refusal is possible. Concrete piles are also more susceptible to damage during installation and transportation. Nevertheless, they are very popular because they are cheaper than full steel piles, and have a large load capacity (Coduto 2001).

2.1.2.2 Drilled Shafts

Drilled shafts are another type of deep foundation that is used frequently. The major difference between drilled shafts and piles is that drilled shafts are drilled and cast in place, whereas the piles are prefabricated and driven into the ground.

The most used construction procedure for drilled shafts is the dry method. This construction starts with drilling a cylindrical hole to the required depth, followed by filling the lower portion of the shaft with concrete. After this lower portion is filled with concrete a prefabricated steel reinforcing cage is lowered into the shaft and, the rest of the shaft is filled with concrete. There is a portion of the steel cage that remains above ground as a tie in point between the shaft and the rest of the substructure. Drilled shafts are used instead of piles due to a lower mobilization cost for the drilling rigs, less vibration and noise, the ability to verify and evaluate soil layers as they are removed, the ease of changing the required length based on observed soil conditions, and the potential to penetrate layers of large rock. Conversely, drilled shafts are not used in favor of piles because the construction of drilled shafts is very dependent on the contractor's skill, driving piles actually increases the lateral stress in the soil by displacing the soil which increases the side friction capacity, and the added benefit of soil densification beneath the tip that occurs with pile driving (Coduto 2001).

2.1.2.3 Caissons

A caisson is another common type of deep foundation, primarily used for bridge piers. They are usually in the shape of a box or cylinder and are hollow inside. The caisson is sunk into the ground and then filled with concrete to create the foundation. The most common method used to sink a caisson is through excavation of the soil on the inside and near the edges of the member. Often water must be pumped out prior to this excavation (Coduto 2001).

2.1.3 Foundation Summary

In this study only pipe piles filled with concrete were investigated. The following sections describe how pipe piles are designed, their structural capacity, and research in the area of concrete filled steel members subjected to axial loading.

2.2 Foundation Design

In the design of pile foundations, the two main design components considered are the resistance from friction provided by the pile and the supporting soil, and the structural capacity of the pile. The latter serves as the upper bound on the load that can be safely applied if the pile was driven to refusal in a solid bed with a capacity greater than that of the pile.

2.2.1 Resistance Based Design

The total capacity of the pile in a resistance-based design is the summation of the side friction strength (P_s) and the end bearing strength (P_t). Both of these strengths are based on the characteristics of the soil into which the pile is driven. The side friction

is also variable, based on every different layer of soil the pile passes through. The side friction strength value is then determined by;

$$P_s = \sum f_s A_s \quad 2-1$$

where:

f_s = unit side friction resistance of each soil layer
 A_s = side friction contact area

The unit side friction resistance is highly variable and often determined using a sliding-friction model, which considers factors such as the material in contact with the soil, the smoothness of surface, the driving techniques, the soil type, the friction angle of the soil, the horizontal effective stress of the soil, and how consistent the soil is.

The end bearing capacity is determined in a similar manner, and is a function of the contact area at the base of the pile and the bearing resistance of the soil. The end bearing strength can be found using the following equation:

$$P_t = q'_t A_t \quad 2-2$$

where:

q'_t = unit toe – bearing resistance
 A_t = toe bearing contact area

The unit toe-bearing resistance is a function of the soil type (sand, clay, rock, etc.) and includes consideration of factors such as soil weight, shear stress, and vertical effective stress.

The total allowable load for an individual pile can be determined by considering the self-weight of the pile and an appropriate factor of safety using equation 2-3.

$$P_a = \frac{P_t + P_s - W_f}{F} \quad 2-3$$

where:

P_t = end bearing strength
 P_s = side bearing strength
 W_f = weight of pile
 F = factor of safety

This is the typical method for determining the pile capacity, as generally the soil is the controlling factor in design (Coduto 2001).

2.2.2 Structural Capacity

2.2.2.1 AASHTO LRFD

In addition to the bearing resistance, the pile itself has a structural capacity based on its constituent materials and geometry. A structural failure of the pile is typically uncommon due to the fact that most materials used for piling have a greater capacity than the supporting soil. Piles are frequently used in bridges, where design is governed by the AASHTO LRFD Bridge Design Manual (2010). AASHTO LRFD provides two alternatives to determine the capacity of a steel tubular pipe pile. The first approach is a simplification that considers the concrete core, while the second approach considers composite action between the steel and concrete, and evaluates the member as a fully bonded system.

The AASHTO LRFD sets out the two methods quite explicitly and specifies when each can be used. For composite action to be considered, the area of steel of the shell must be greater than or equal to four percent of the entire cross-section. The case of non-composite action considers the partial contribution of the concrete core and any steel (rebar, prestressing) inside this concrete in determining nominal capacity, P_n . For a spiral reinforced non-composite pile, the nominal capacity (P_n) would be calculated using equation 2-4:

$$P_n = .85[.85f'_c(A_g - A_{st} - A_{ps}) + f_y A_{st} - A_{ps}(f_{pe} - E_p \epsilon_{cu})] \quad 2-4$$

For a non-composite pile with standard tie reinforcement, the nominal capacity would be calculated using equation 2-5:

$$P_n = .80[.85f'_c(A_g - A_{st} - A_{ps}) + f_y A_{st} - A_{ps}(f_{pe} - E_p \epsilon_{cu})] \quad 2-5$$

where:

P_n = nominal axial resistance
 f_c = concrete compressive strength
 A_g = gross area
 A_{st} = area of longitudinal reinforcement
 f_y = yield strength of steel
 A_{ps} = area of prestressing steel
 E_p = elastic modulus of prestressing tendons
 f_{ps} = effective stress in prestressing tendons after losses
 ϵ_{cu} = failure strain of concrete in compression

When composite action can be considered, the nominal capacity (P_n) is based on elastic and inelastic compression member behavior. The nominal capacity of the composite section is determined using an effective section of steel and concrete. This method is similar to the composite section behavior within the AISC Steel Construction Manual (2005). The composite section capacity would be calculated by the following set of equations.

$$P_n = \begin{cases} 0.66^\lambda F_e A_s & \text{if } \lambda \leq 2.25 \\ \frac{0.88 F_e A_s}{\lambda} & \text{if } \lambda > 2.25 \end{cases} \quad 2-6$$

where:

$$\lambda = \left(\frac{Kl}{r_s \pi} \right)^2 \frac{F_e}{E_e}$$

$$F_e = F_y + C_1 F_{yr} \frac{A_r}{A_s} + C_2 f'_c \frac{A_c}{A_s}$$

$$E_e = E \left[1 + \frac{C_3 A_c}{n A_s} \right]$$

and where:

K = effective length factor
 l = unbraced length
 r_s = radius of gyration of the steel section
 A_s = cross sectional area of steel
 A_c = cross sectional area of concrete
 A_r = cross sectional area of longitudinal reinforcement

F_y = yeild strength of steel

F_{yr} = yield strength of longitudinal reinforcement

f_c = concrete compressive strength

E = modulus of elasticity of steel shell

C_1, C_2, C_3 = coefficients seen in Table 2.1

Table 2.1:
Composite Section Constants

	Filled Tubes	Encased Tubes
C_1	1.00	0.70
C_2	0.85	0.60
C_3	0.40	0.20

Once the nominal capacity is determined, whether by non-composite or composite means, the member strength (ϕP_n) is determined by applying the appropriate strength reduction factor, ϕ . For axial compression members ϕ equals 0.75.

2.2.2.2 State Specific Design Codes

While new bridge designs use the AASHTO LRFD, states also maintain their own design codes, many of which are based on current and historical AASHTO design standards. A survey and summary of available design approaches is presented in this section.

The designs approaches adopted by most states can be categorized as composite, non-composite, state-specific or no explicit information. The composite design approaches used are similar to that of the AASHTO LFRD and are used by Indiana, Maine, Massachusetts, Nebraska, Nevada, and South Carolina. The non-composite design approach considers only the concrete or reinforced concrete core and is used by Florida, Idaho, Missouri, Montana, New Jersey, Pennsylvania and Wisconsin. However, Idaho and Montana are based on a non-composite section with only the steel

contributing to the capacity, while Missouri allows the steel shell to count as reinforcement in the section and New Jersey refers to a previous version of the AASHTO, which also uses a non-composite section.

Some states have their own methodology as to how to design or use piles. Some of these include tabulated capacities of specified pile sizes and types, allowable stresses or even prohibit the use of pipe piles. Alabama, Connecticut, Delaware, Minnesota, North Carolina, Texas, Virginia all use tables to give the engineers the values for the capacity of their standard size piles, while Michigan, Ohio, Oregon, Rhode Island, Washington D.C. only design piles by the resistance based method. California requires allowable stress design and Iowa does not allow for the use of pipe piles at all. A summary of the available state methodologies is presented in Table 2.2

**Table 2.2:
Available State/District Transportation Agency Methodologies**

Design Method	States
Composite	Indiana, Maine, Massachusetts, Nebraska, Nevada, and South Carolina
Non-Composite	Florida, Idaho, Missouri, Montana, New Jersey, Pennsylvania and Wisconsin
Tables	Alabama, Connecticut, Delaware, Minnesota, North Carolina, Texas, Virginia
Resistance Based	Michigan, Ohio, Oregon, Rhode Island, Washington D.C.
Other	California (allowable stress), Iowa (pipe piles not allowed)
Not Specified or Available	Alaska, Arizona, Arkansas, Colorado, Georgia, Hawaii, Illinois, Kansas, Kentucky, Louisiana, Maryland, Mississippi, New Hampshire, New Mexico, New York, North Dakota, Oklahoma, South Dakota, Tennessee, Utah, Vermont, Washington, West Virginia, Wyoming

2.2.2.3 Other Design Methods

Members similar to steel pipe piles, mainly concrete-filled tubular (CFT), are used in other infrastructure, such as columns in building systems. The following sections discuss other design methods pertinent to these members including the AISC method

which is relevant to structural steel building frame systems and the ACI 318-08 which is applicable to reinforced concrete design. While these are not cast-in-place steel pipe piles, their general configuration is the same and hence is expected to demonstrate similar structural behavior.

2.2.2.3.1 AISC LRFD

The method presented in the AISC Steel Construction Manual (2005) is fairly similar to the composite section method of the AASHTO LRFD (2010). The composite section analysis considers both the steel and concrete properties, and is based on principles of elastic and inelastic buckling. The nominal capacity (P_n) is determined by equations 2-7:

$$P_n = \begin{cases} \left(0.658^{\frac{P_o}{P_e}}\right) P_o & \text{for } P_e \geq 0.44P_o \\ 0.877P_e & \text{for } P_e < 0.44P_o \end{cases} \quad 2-7$$

where:

$$P_o = A_s F_y + A_{sr} F_{yr} + 0.85 A_c f_c'$$

$$P_e = \pi^2 \frac{EI_{eff}}{(KL)^2}$$

and where:

P_o = nominal axial compressive strength without consideration of length

P_e = Euler buckling load

K = effective length factor

L = unbraced length

A_s = cross sectional area of steel

A_c = cross sectional area of concrete

A_{sr} = cross sectional area of longitudinal reinforcement

F_y = yield strength of steel

F_{yr} = yield strength of longitudinal reinforcement

f_c' = concrete compressive strength

E_s = modulus of elasticity of steel

E_c = modulus of elasticity of concrete

I_c = moment of inertia of the concrete

I_s = moment of inertia of the steel

I_{sr} = moment of inertia of the reinforcement

w_c = unit weight of concrete

Several research studies have compared the experimental results to the capacity predicted by this approach and found this method to be conservative. Schneider (1998) tested several concrete filled tubular members to capacity, and found that the capacity of the sections are around 1.32 times greater than the AISC method predicted. Similarly, Baig et al. (2006) tested a series of circular concrete-filled tubular sections, and found around a 1.3 times greater capacity than the AISC method predicted.

2.2.2.3.2 ACI Code

The ACI 318 Code (2008) uses a fairly simple equation (2-8) and methodology for the nominal structural capacity of steel encased concrete composite sections. The equations are for the axial capacity, or “squash load” of the cross section:

$$N_u = 0.85A_c f'_c + A_a f_y \quad 2-8$$

where:

A_c = area of concrete
 f'_c = concrete compressive strength
 A_a = area of steel
 f_y = steel strength

A study by Baig et al. (2006) demonstrated that this method is conservative because it does not account for the increased strength from the confining effects provided by the tubular shell. Their research suggested a modification of the ACI approach to that given in equation 2-9.

$$N_u = 1.3A_c f'_c + A_a f_y \quad 2-9$$

where:

A_c = area of concrete
 f'_c = concrete compressive strength
 A_a = area of steel
 f_y = steel strength

2.3 Previous Research

A literature survey on cast in place steel tubular piles yielded little results with the exception of resistance-based design capacity. All of this research on the resistance-based method was dealing with drivability and how different soil types reacted under different loads and applications, and as such this was deemed irrelevant for this research project. However, extensive studies have been performed on concrete-filled tubular members (CFT), which are more common in building infrastructure. CFTs are basically piles with longer unbraced lengths. The lateral restraint provided by the soil is such that the full length of the pile may be upwards of forty feet, but the unbraced length may be as little as a few feet or the pile may even be continuously braced, all based on the stiffness of the soil into which the pile is driven. CFTs, on the contrary, have unbraced lengths on the order of twelve to thirty feet, depending on story height of the building in which they are used.

2.3.1 CFT Experimental Studies

Most experimental studies on CFTs have been performed on stub sections due to testing challenges associated with full length sections. These shorter test sections would be expected to be more representative of in-service piles, where unbraced lengths are short due to the restraint provided by the surrounding soil. Much of the research evaluated the behavior of different shapes (circular and rectangular) and sizes (diameter and wall thickness) of the steel shells, along with variations in concrete core compressive strength.

Many of the different studies varied the cross section and material properties of the CFTs. In a study by Yamamoto (2000), CFTs with three different diameters (4", 8.5", 12.5"), three different rectangular side dimensions (3.9", 7.8", 11.8"), and four different

concrete strength (4, 5, 7, 10 ksi) were tested to failure. Three different loading conditions were used in the test. The sections were either loaded completely, only the concrete core was loaded, or only the hollow steel shell was loaded. From the strains obtained during testing, it was found that strains would increase until local buckling started, at this point, the strains would essentially plateau, neither rising nor falling with any increase in load while the steel shell was buckling. This study developed recommendations for a new design equation able to predict capacities with no more than ten percent error. In another study by O'Shea (2000), three different loading methods for CFTs were investigated. The sections were loaded the in same three methods as in the study by Yamamoto. From these different loading patterns, it was determined that, when only the steel shell is loaded, the core does not contribute to change the capacity. When loading only the core or the entire section, the core significantly adds to the capacity. Fujimoto (2004) studied how the ratio of the diameter to wall thickness or side length to wall thickness affected eccentrically loaded CFTs. The test sections had three steel strengths (29, 85, 110 ksi), three concrete strengths (3, 6, 12 ksi), and three ratios of size to thickness (50, 100, 150). A constant concentric load was applied followed by an increasing eccentric load; however the concentric load was decreased such that the total load remained constant. Fujimoto found that the CFTs exhibited a very stable moment-curvature relationship, but also warned that mixing high strength concrete with lower strength steel may yield lower overall strengths than using both high strength steel and high strength concrete. In another study by Gupta (2007), the effects of the chemical composition of concrete, and different additives and admixtures, on the strength of different sized CFTs, was examined. Differing amounts of flyash, two industrial additives, and steel tubes of three different sizes (2", 3", 4") were used. The capacities obtained from testing were greater than the original theoretical capacities, due

to the lack of considerations of the confinement effects. The capacities obtained from testing were also compared with the values obtained using equation 2-9, by Baig et al. (2006), and the capacities calculated from the equation were found to give the most accurate capacities. In a study by Lam (2005), CFTs with different grade steel shells were investigated. Lam examined how a rectangular stainless steel shell would affect the capacity. A total of three different concrete strengths (4, 9, 14 ksi), and varying wall thicknesses (0.1"-0.2") were tested. Their study determined that the stainless steel shells did not provide the same level of confinement as conventional steel shells.

Several of these studies also examined how the capacities predicted by the design methods compared with actual testing. Baig et al. (2006) studied the capacity of CFTs compared with the theoretical capacities from several different design methods. The size and wall thickness of the pipe sections varied greatly, with only the steel strength (36 ksi) and concrete strength (4ksi) remaining constant. The author compared the test results with the theoretical design methods of the Eurocode-4, ACI (American Concrete Institute), the Australian Standard Codes, AISC (American Institute of Steel Construction) LRFD (load and resistance factored design), and the Chinese Code. During this testing, it was noted that when localized and member buckling occurred, the concrete assumed the shape of any steel deformations. The capacity predicted by Eurocode-4 was found to underestimate the actual capacity by 14-21%, the ACI and Australian Codes also underestimate the capacity by 16-32%, the AISC LRFD underestimated the capacity by 10-40%, while the Chinese Code overestimated by 7-30%.

Some studies also looked at how to better model the behavior of CFT sections. Hu (2003) studied how to model confining pressure in ABAQUS using test data from previous research as a baseline. When creating the model, it was determined that both

a confining pressure and an increased concrete strength were needed. The confining pressure is due to the fact that the two materials have different poisson ratios, causing them to expand at different rates. The model also needed to take the confined concrete strength into consideration because the presence of confining pressure holds the concrete back from spalling. After these elements were included in the model it was found to have very good agreement with the test data.

Other research examined better potential design methods for CFTs. In a study by Xiao (2009), confined CFTs were examined. Confined CFTs are normal CFTs with additional transverse reinforcement at locations with local buckling potential. This additional reinforcement was thought to delay the local buckling observed in normal CFTs, and could be easily retrofitted onto existing columns. The confined CFTs exhibited improved capacity until rupture of the wrap. Even after rupture, the capacity of the wrapped CFT was higher than that of a normal CFT until high strain values were observed. Gilbert (2005) studied incorporating a lower bound into the capacity of the LRFD method. It was found that offshore applications were using a lower bound and had much lower failure rates. This was thought to be caused by a physical limit to the smallest load a pile can support, which is greater than zero. After some testing, the authors suggested a few methods to incorporate the lower bounds into future designs.

2.4 Summary of Literature Review

There are many different types of foundation element. In this research project one particular deep foundation type is investigated, steel tubular cast in place piling. These piles are a steel tubular shell that is closed-ended on the drive side and open-ended on the top side. This open end is where the concrete core is typically cast through. These piles are typically used for many different applications. There are also

many different methodologies for the design of both cast-in-place steel tubular piling and structural CFTs. The main design methods used to analyze the structural behavior of piles are introduced in the AASHTO LRFD Manual (2010), and the other method is the resistance based design, that is a function of the soil friction and end bearing resulting from the soil the pile is driven into. Many other methods exist for a structural CFTs capacity, with a few coming from ACI and AISC. While extensive research has been conducted on CFTs, there has been essentially no investigation in the structural capacity of cast-in-place steel tubular piling. It should be noted that a CFT and a cast-in-place steel tubular pile are the same element, but used for different purposes in a structure, which is why much of the research was conducted on the CFT elements.

3 Procedures

This study focuses on evaluating the structural capacity of 10- $\frac{3}{4}$ " and 12- $\frac{3}{4}$ " piles, which are typically used in moderately deep foundations in Wisconsin. The goal of the investigation was to determine the capacity of representative in service piles. In this project, several test piles were cast in conditions as similar as possible to in service conditions. These full length pile sections were later cut up into smaller sections for testing. The tests performed included, composite section loading, non-composite section loading, cored sample testing, and a test on the bond strength between the core and shell. Additionally a finite element model was created to simulate the behavior of the stub sections which were tested. This section highlights the details of pile fabrication, cutting, and test procedures used. Also included is the validation details of a finite element model used to simulate test specimen response.

3.1 Driving the Piles

The driving of the piles occurred in parallel with a new bridge construction near Waupaca, Wisconsin. This site was chosen for its location away from any major highway and the dates available for driving. The piles used for the project were circular closed end steel pipe piles, which were driven and filled simultaneously with the bridge piers for this new bridge. Four sample piles were installed in a row next to the bridge site. These piles were removed and used for this research project. Two of the piles were 10- $\frac{3}{4}$ " diameter piles, one with 0.375 in. wall (pile 1) and one with a 0.5 in. wall (pile 2). The other two piles were 12- $\frac{3}{4}$ " diameter piles (piles 3 and 4), both had a wall thickness of 0.375 in. All four of the piles were around forty feet long. The 12- $\frac{3}{4}$ "

diameter piles were spiral formed, whereas the 10- $\frac{3}{4}$ " diameter piles were cold rolled and seam welded. The piles before driving are shown in Figure 3.1.



Figure 3.1: The four piles and the caissons

The pile driver (Figure 3.3) used on this project was a single piston diesel hammer, it was chosen based on the sandy soil conditions of the site. The pile driver had a single head that could install many different sizes of circular piles (10- $\frac{3}{4}$ ", 12- $\frac{3}{4}$ ", and 14"), as shown in Figure 3.2. This head allowed the installation to go much smoother and faster when changing the size of circular piles on job sites and reduced the need for multiple drive heads when dealing with the steel tubular piles.



Figure 3.2: Pile drive head



Figure 3.3: Pile driver

The driving of the piles proceeded quickly, due to soil conditions in the area. The piles were only being partially driven (15ft), to allow for ease of installation and removal. If the piles were fully driven, much more work would be required to remove the piles because the piles get their strength from the frictional resistance between the side of the pile and the soil. Fifteen feet was chosen because the soil directly beneath the pile was capable of supporting the pile vertically and a filled caisson placed around the pile provided enough lateral support to counter any horizontal loads the pile would experience.

Because the piles were not driven to full depth, they were insulated to mimic in-situ condition to which typical piles are exposed. Several alternatives to insulate the portion of the pile above ground were investigated. One idea was to build a set of walls around the piles and backfill the voids between the piles and the wall with soil. This was found to be too costly, due to the required number of supports and bracing in the walls necessary to hold back the soil pressure. Another idea was to use a full size concrete caisson, typically used for bridge piers, to surround the piles and fill the caisson with soil. This is similar to the wall idea, but no longer required the construction of walls and

bracing. Finally, it was determined that the best solution was to use individual caissons that are a few inches larger than the piles and then fill the void between the pile and the caisson with soil. This would require much less time and cure as similar to the piles that were fully driven into soil while being more economical.

The selected caissons were a steel shell that was open on both ends and was several inches in diameter larger than the pile it was going to be placed around. The four caissons were lifted placed around each one of the piles. These caissons can be seen in Figure 3.4, which shows the caissons placed around the piles before they were filled with soil from the site, and before the piles were filled with concrete.

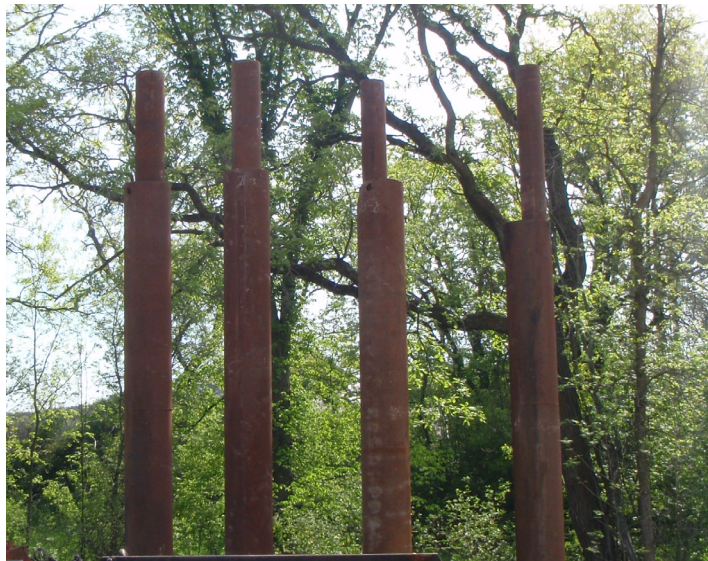


Figure 3.4: Unfilled piles with the caisson placed around them

3.2 Casting the Piles

The concrete for the piles was placed using a pump truck which takes the concrete from the concrete truck and pumps it through a hose. The hose was lowered slightly into the piles as can be seen in Figure 3.5 for the pour. The piles were filled by allowing the concrete to simply fall, which is standard practice for the contractor. To prevent a cavity from forming at the top of the section, the hose was slowly removed

while still pumping. Several standard on-site tests were performed on the wet concrete during casting to ensure it was within specifications. The slump of the mix was 2- $\frac{3}{4}$ in., and the entrained air content was 5%, both of these were within WisDOT specifications (2005). Along with these standard tests, a total of 20 four by eight inch cylinders were cast for testing later. Nine of these cylinders were transported back with the researchers after casting and the remaining eleven were left wrapped by soil from the site to cure in a similar manner to the piles. The nine that were transported back were used to run compression tests to verify that the concrete in the piles had sufficient capacity for extraction.



Figure 3.5: Concrete pour into piles

3.3 Curing the Piles

The area between the caissons and the piles was filled with soil from the area to help reasonably simulate underground temperature and moisture conditions. Since the

caissons are far too high to reach by hand, a concrete bucket was used to fill the void between the piles and the caissons (Figure 3.6).



Figure 3.6: Caissons being filled with soil

With soil filling the voids between the pile and the caisson, the piles were left to cure before removal. Cylinders were tested at five and seven days to ensure that the concrete strength was high enough for the piles to be safely removed and stored. The five day average strength was 3,915 psi, while the seven day average strength was 4,349 psi. This was determined to be sufficient strength, and the following day, the piles were extracted. After the piles were removed, they were set aside for pickup (Figure 3.7).



Figure 3.7: Piles after being pulled

3.4 Cutting the Piles

Different methods for cutting the full length piles down to testable section sizes were investigated. One method was a large hydraulic shear, as it would be quick and could be done on site. However the finished surface of the piles after cutting would be deformed and crushing of the concrete was expected. Another method was water jetting, with a computer-aided cutting machine, which leaves a very smooth and clean surface. However there were no local businesses capable of handling such large samples on their water jet. Alternatively, a company would have to use a mobile unit, which is not as easily controlled and cannot guarantee an even cut each time. Most of the mobile units are a backpack based system and are used for simple removal, not for perfectly straight cutting. The chosen method was a diamond wire saw. These saws are used to remove large sections of buildings, sever underwater pipelines, cut large bricks of rock in quarries, and many other heavy-duty tasks. This method was found to leave a flat, clean surface after cutting, very similar to that of ones cut by a stationary water jet. Another advantage to the wire saw over the water jet is the portability of the wire saw. These systems are made to be used on site and can be adapted for use in many different configurations. It was determined that a wire saw typically used to cut underwater pipe would be best suited for this situation.

To support the piles during the cutting, stands were needed. The support was constructed using 8x8 timbers, which were of minimal cost, and such a large timber would easily support the load. The original plan was to use four two-foot sections for each support, but during construction, this was modified to three two-foot sections for each support, allowing more supports to be built while still easily supporting the load, see Figure 3.8. To help hold the piles on the support and prevent them from sliding,

some 2x4s were cut at a forty-five degree angle and screwed down to the top of the timber, giving lateral support by acting as wedges.



Figure 3.8: Pile supports for cutting

The saw that was used to cut the piles can be seen in Figure 3.9 and Figure 3.10. Once the saw was clamped onto the section, it averaged about twenty minutes per cut. The diamond wire itself was cooled with water and the water was also used as a lubricant to help cut through the material and keep dust down. There were a total of eighty-two cuts for the four piles.



Figure 3.9: Diamond wire saw.



Figure 3.10: Diamond wire saw cutting

The piles were cut into 12", 18", and 11' sections, with the specimen size based on the intended testing plan. These tests include: full section compression, section core compression, cored samples, and push-through testing, and can be found in more detail in the next section. The sections were numbered according to which pile they were cut from, and then lettered in the order they were removed, with A being at the top and Z being at the bottom. The numbering nomenclature and intended test scheme for each pile is shown in Figure 3.11.

The test specimens selected for compression testing were 18" long, as this size fit into the test frame. The stub sections dimensions were selected to mimic the short unbraced length of the continuously supported piles in the ground. Specimen lengths of 18" and 12" were selected to extract core samples at various locations along the piles. These sizes were chosen as it would allow for 4 by 8 cylinders to be cored out, while fully using the most of each pile length. The eleven foot long sections were reserved for flexural testing which allowed for a ten foot clear span to be tested as part of a future project. Six inches on either side was determined to be adequate for the supports on the load frame at Michigan Tech. Out of each pile section, a total of one 11 ft. section, two 12 in. sections, and fifteen to eighteen 18 in. sections were cut.

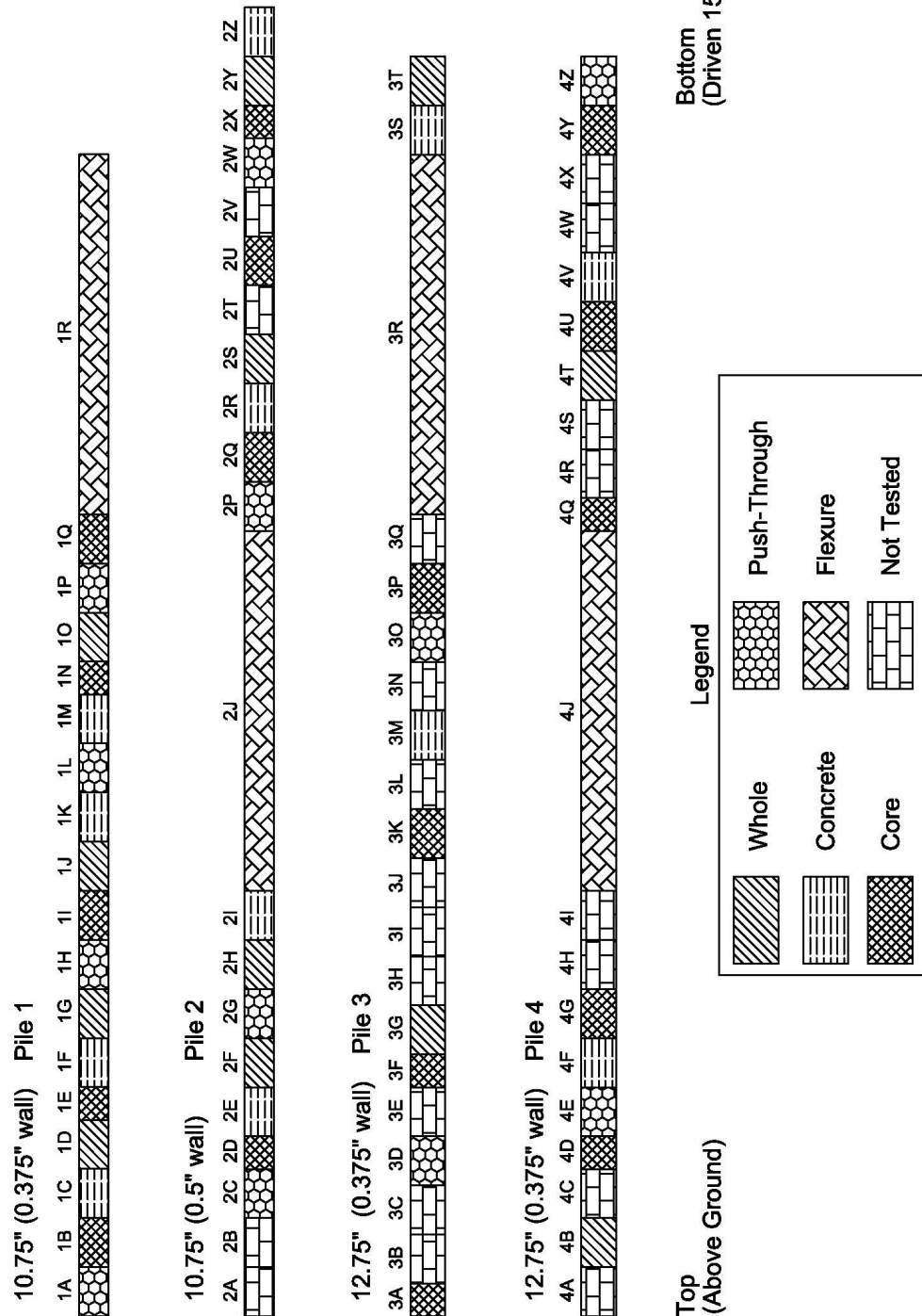


Figure 3.11: Pile cut section use diagram

3.5 Testing the Piles

This section describes the full section compression (composite loading), section core compression (non-composite loading), cored samples, and push-through (bond) testing performed on the stub sections of each pile, along with the machines and instrumentation used for the different testing.

3.5.1 Testing Machines

The load frame used for the compression testing was a MTS 315.03. This frame is capable of exerting a total load of 1 million pounds and has a total stroke of 4 in (Figure 3.12). The frame was calibrated by a MTS technician before the testing was started. The software that runs the frame was set up in displacement control, at a rate of 0.01 in. per minute. This load rate was calculated to give a test of a standard length and to provide a smooth data set.



Figure 3.12: MTS 315.03 Load Frame

The other testing machine, a Baldwin 300CT (Figure 3.13), was used for the testing of the core samples and cylinders and has a capacity of 300,000 pounds. The machine is set up to the ASTM Standard C31 for testing cylinders, which gives a loading rate of 35 psi per second.



Figure 3.13: Baldwin Cylinder Test Machine

3.5.2 Data Acquisition and Instrumentation

The axial compression testing used a Campbell Scientific CR9000X data acquisition system (DAQ), which is considered a modular measurement and control system. The DAQ has numerous input capabilities, but for this project only linear variable differential transformers (LVDT) and strain gauges.

The strain gauges were all from Vishay Micro-measurements. For the axial compression testing the strain gauges used were 1/8 in. long, 120 Ω series BT strain gauges (EA-06-125BT-120).

The other instrumentation used was a load cell and an LVDT. The LVDT measured total distance traveled by the loading head during testing, while the load cell measured the applied load. These measurements were used to find the stress in the samples and the amount of deflection the specimen experienced. The displacement from the LVDT was also used to verify that the frame was loading at the specified displacement control rate.

3.5.3 Axial Compression Testing

The first test conducted on the pile sections was the axial compression tests. The compression tests consisted of an axial compression of the entire cross section, a confined axial compression test on the concrete core, axial compression testing on each individual cored concrete core sample, and a push-through test, see Figure 3.11 for specimen details.

3.5.3.1 Full Section Compression Tests

The full section compression test was used to investigate the ultimate capacity of the pile stub sections (Figure 3.14). Four pile sections from each size configuration were tested. To obtain a better representative value of the true average capacity, 4 sections were taken from different areas of each pile. Each pile stub section had two strain gauges attached onto their surface. One strain gauge was placed to measure the longitudinal strain at the mid-height of the pile stub section and the other was placed to measure the tangential strain at the mid-height. The second strain gauge captured any outward deformation from Poisson's effects of the steel shell at the mid-height.

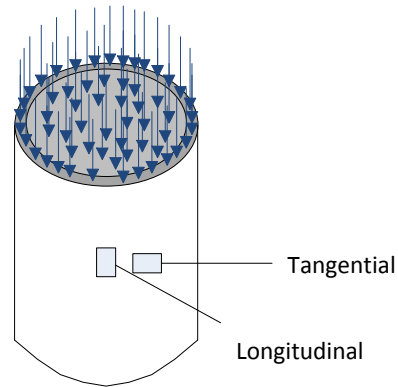


Figure 3.14: Full section Loads

The test specimens were placed into the load frame with a T-100 (100,000psi yield) plate steel cap at either end. This cap was used to protect the loading head of the test frame and to provide a flat surface for loading (Figure 3.15). All of the specimens were loaded in compression to evaluate the capacity of the section.



Figure 3.15: Full section loading setup

3.5.3.2 Section Core Compression Tests

The section core compression test was used to determine the capacity of the section if loaded only through the core section (Figure 3.16). The resultant capacity was expected to be some representation of the confined compressive strength of the concrete core.

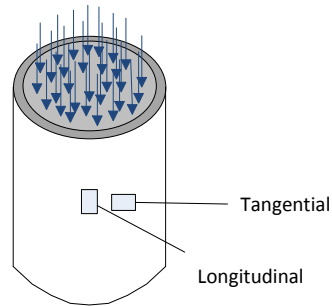


Figure 3.16: Section core loads

The setup for this test was very similar to the whole section compression test except the Grade 60 plates were used to load only the core section rather than the entire cross section. One inch thick plates were cut to fit just inside the pile's steel shell with enough clearance as to not contact the steel shell on both ends of the specimen (Figure 3.17). Each pile stub section had two strain gauges attached onto their surface. One strain gauge was placed to measure the longitudinal strain at the mid-height of the pile stub section and the other was placed to measure the tangential strain at the mid-height. The second strain gauge captured any outward deformation from Poisson's effects of the steel shell at the mid-height. These gauges were intended to observe the behavior of the steel shell when the concrete core was loaded. Ideally, this was expected to capture the failure of the concrete core, along with any expansion in the steel shell. All of the specimens were loaded in compression to evaluate the capacity of the section.

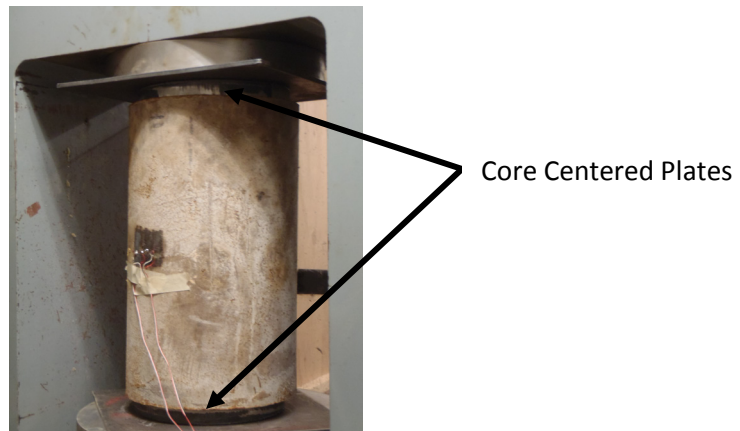


Figure 3.17: Section core loading setup

3.5.3.3 Cored Sample Tests

Core samples were taken from various locations in the pile sections, to determine the representative concrete strength throughout the pile; the sections used for this can be seen in Figure 3.11. From the sets of piles with the same outside diameter, at least one section was taken out of every five foot of length of the pile. Eight of these sections were 12 in. tall and ten sections were 18 in. tall specimens. A drill press with a four by thirteen inch core bit was used to core samples out of the pile sections (Figure 3.18).

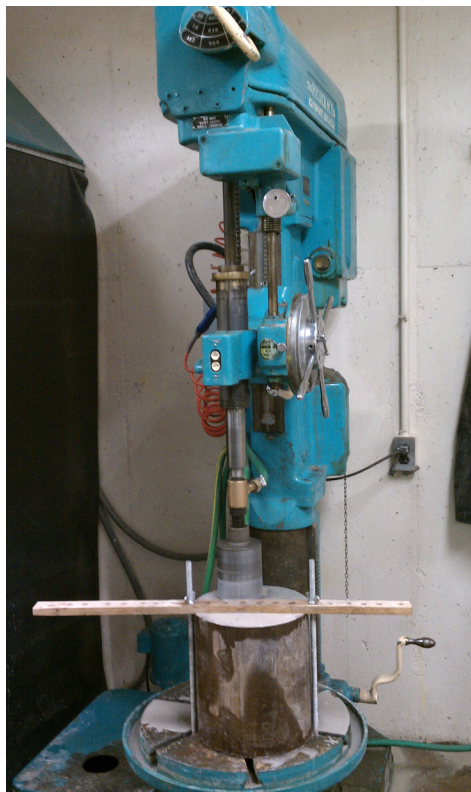


Figure 3.18: Drill press setup

The maximum numbers of cores were taken from each pile section. All cores were drilled out at the same rate and at a depth of ten inches, so that when the core was removed, it would still allow for enough material to be end ground to yield a 4 by 8 in. cylinder. These cylinders were then each individually tested in the Baldwin 300CT compression machine mentioned above following ASTM C-31 (2003).

3.5.3.4 Push-through Tests

The final compression testing conducted was a series of push-through tests. These tests were used to determine the bond strength between the concrete core and the outer steel shell. These tests were conducted using the MTS million pound test frame. Each test section had one strain gauge to record the vertical strain in the steel shell at the midpoint. This strain gauge and the displacements were used to capture the load under which the concrete core began to move in relation to the shell. At that point, the bond strength has been overcome and only friction is holding the sections together (Figure 3.19).

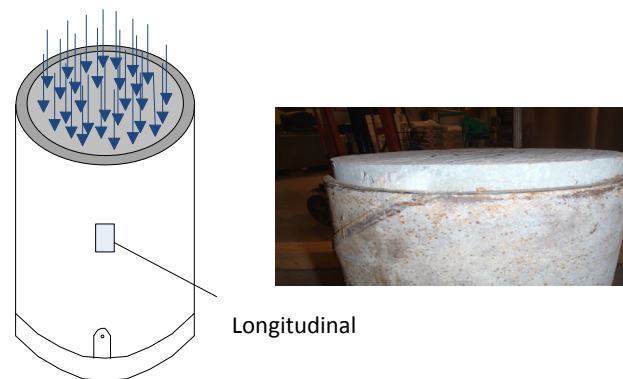


Figure 3.19: Push-through loads

For this setup, two rings were constructed using one inch thick grade 60 steel. These rings were cut so the outside had a diameter of fourteen inches to match the loading platens on the loading frame. The inside diameter was cut so there was enough clearance to allow the concrete core to be pushed through but also enough overlap over the steel to hold the shell back. Two rings had to be constructed to accommodate the diameters of test sections (Figure 3.20). The platens used for the confined concrete testing were also used in this test so that only the concrete would be loaded. This allowed for the core to be forced out of the shell, see Figure 3.21.



Figure 3.20: Push-through rings



Figure 3.21: Push-through setup

3.6 Finite Element Model

A finite element model, created in ANSYS (2009), was used to estimate the capacity of the sections before testing. A different model was required for each of the steel shell and concrete core configurations. A total of three models were created, one for each of the different sizes tested. To start with, only one model was created and then a syntax based code was generated and modified to model the other two configurations.

The first model developed was the 12- $\frac{3}{4}$ " model. This model was developed first because there were two piles in this size that were to be tested, while the other size

both only had one section. The model developed was a full model of the 18 in. stub section. It had two separate volumes to make up the cross section, to match the steel shell and concrete core. After the volumes were modeled, the material properties were added. Linear elastic material models were chosen for both the concrete and steel with the expectation that non-linearity and buckling could be added with consideration of the experimental results. These results could be used to validate the linear response and help in the extrapolation of the non-linear response. For the concrete core, an initial elastic modulus of 3.8 ksi was used with a Poisson's ratio of 0.15. This modulus was derived from a 4.5 ksi compressive strength concrete using the ACI Code (2008) relationships between compressive strength and elastic modulus, equation 3-1. The Poisson ratio selected was representative of a typical value for concrete (American Concrete Institute 2008). For the steel shell, the elastic modulus was the standard 29,000 ksi and the Poisson's ratio was 0.3 (American Institute of Steel Construction Inc. 2005).

$$E_c = 57,000\sqrt{f'_c} \quad 3-1$$

After the volumes were defined with their material properties, the model was meshed. SOLID92 elements were selected for the meshing of the materials. A SOLID92 element is a ten node tetrahedral element with three degrees of freedom at every node. Other element types and meshes were initially tested, including Solid 65 and Solid 45. The SOLID92 element was chosen as it had more nodes for refinement than the other solid elements. It also was a tetrahedral element which was needed for the meshing of the cylinder, rectangular meshing cannot easily implemented for circular cross sections, modeled in the Cartesian coordinates. To use a rectangular element the model would have needed to be in polar coordinates. The solid element was also

chosen over a shell element as shell elements are valid for thin elements not such large elements like the concrete core. For the meshing, separate meshes were initially created for the steel and concrete elements. However, this created a problem where the materials were able to move freely and through one another. By meshing both volumes with the same mesh, this problem was solved. A single mesh was chosen to account for the contact between the materials by not allowing one material to push through the other, and could be modified later if need be, with the addition of a contact element based on test data. In doing so, the mesh had to be refined, as some of the points contacted each other potentially creating problems or errors.

The end constraints were applied to the nodes instead of a surface or face, so that the nodes located on the top and bottom surfaces were fixed in the two directions where there was no load. At the centerline of the model, the nodes were fixed in the direction of loading to induce symmetric boundaries that were not restrained from movement.

The modeling approach was validated with a simple test case of a uniaxial load of a homogeneous section using Hooke's Law (Vable 2002), which can be seen below (Eqn. 3-2 - 3-4), on both a concrete (Figure 3.22) and steel only section (Figure 3.23).

$$\varepsilon_x = \frac{1}{E} [\sigma_x - v(\sigma_y + \sigma_z)] \quad 3-2$$

$$\varepsilon_y = \frac{1}{E} [\sigma_y - v(\sigma_x + \sigma_z)] \quad 3-3$$

$$\varepsilon_z = \frac{1}{E} [\sigma_z - v(\sigma_x + \sigma_y)] \quad 3-4$$

where:

E = Elastic Modulus

v = Poisson Ratio

σ_x = stress in the radial direction

σ_y = stress in the tangential direction

σ_z = stress in the longitudinal direction

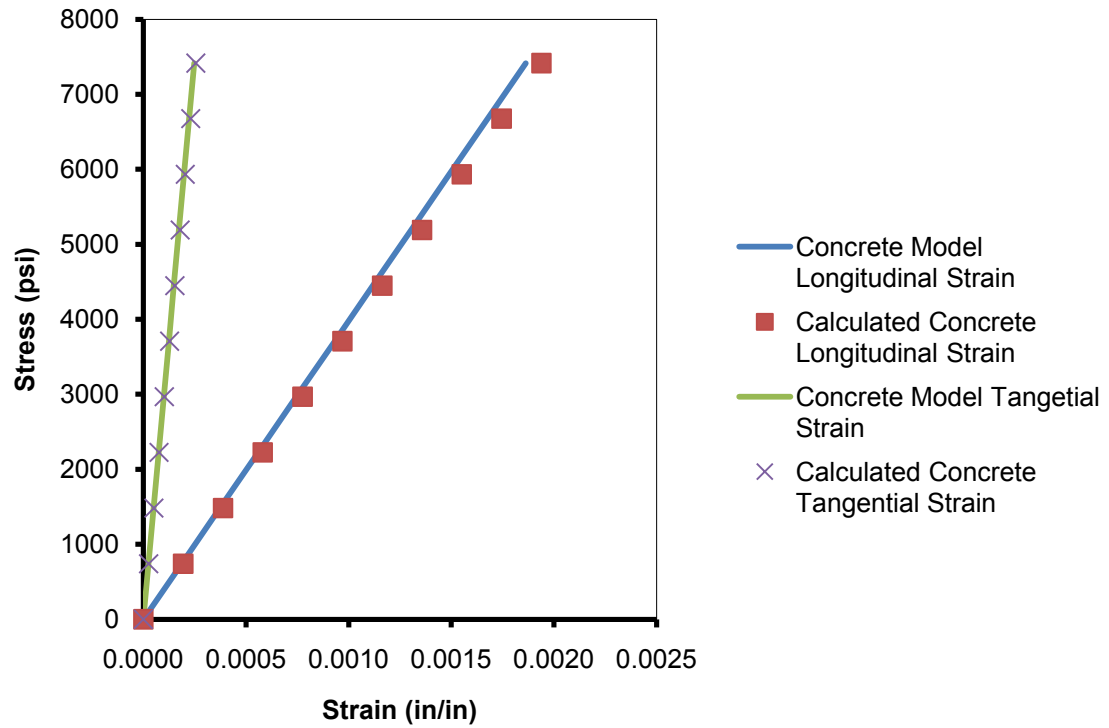


Figure 3.22: Concrete Model Verification

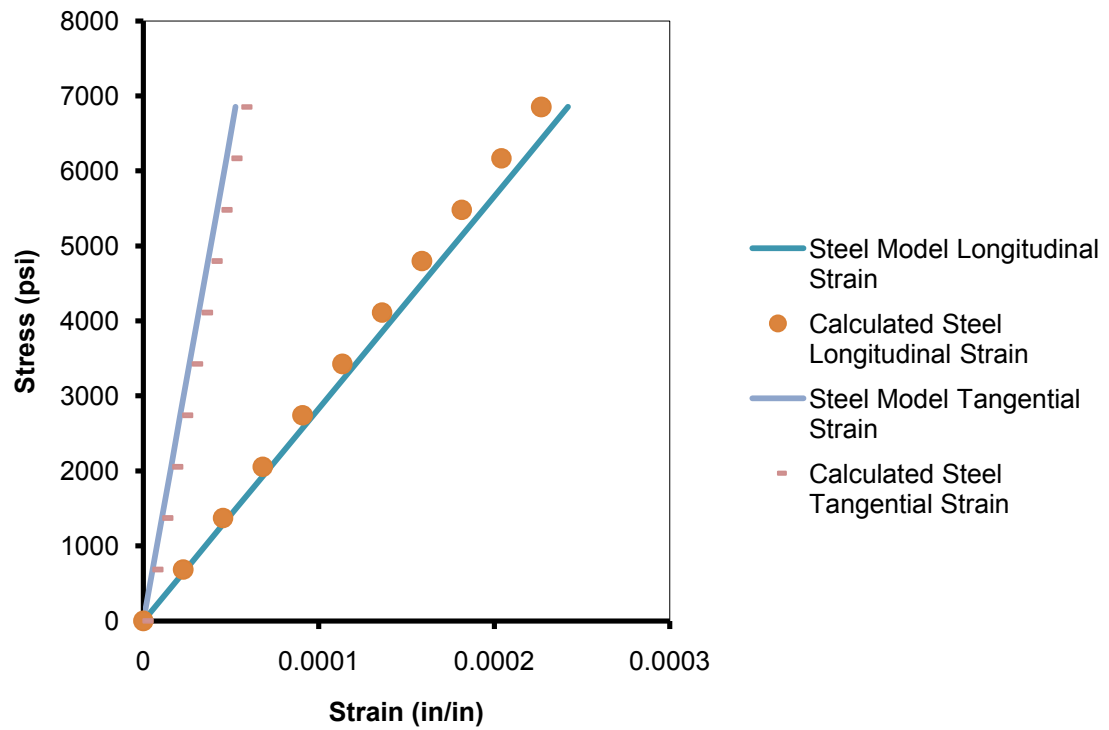


Figure 3.23: Steel Model Verification

Once the basic model was validated, the composite sections were analyzed under a concentric loading (full section and core only). For the loading of the entire cross section, a load was applied to the entire set of nodes on the top and bottom surfaces. Also, loading of the concrete core section was simulated. The core-only scenario was performed in a similar manner as loading the entire cross section, however the loading was applied only to the nodes completely inside the core. These loads were always set to match and varied incrementally from 100 kips to 1000 kip, which was the maximum load capability of the machine on which the testing was performed (Figure 3.24). From these different loading cases, the strains and stresses under the different loads in the different directions were used to predict the response from testing. Finally, the models were expanded to the other stub test sections of 10- $\frac{3}{4}$ " with 0.375" wall thickness (Figure 3.25), and 10- $\frac{3}{4}$ " with 0.5" wall thickness (Figure 3.26). From these models it was observed that only the 10- $\frac{3}{4}$ " (0.375" wall) specimens should yield under the applied load.

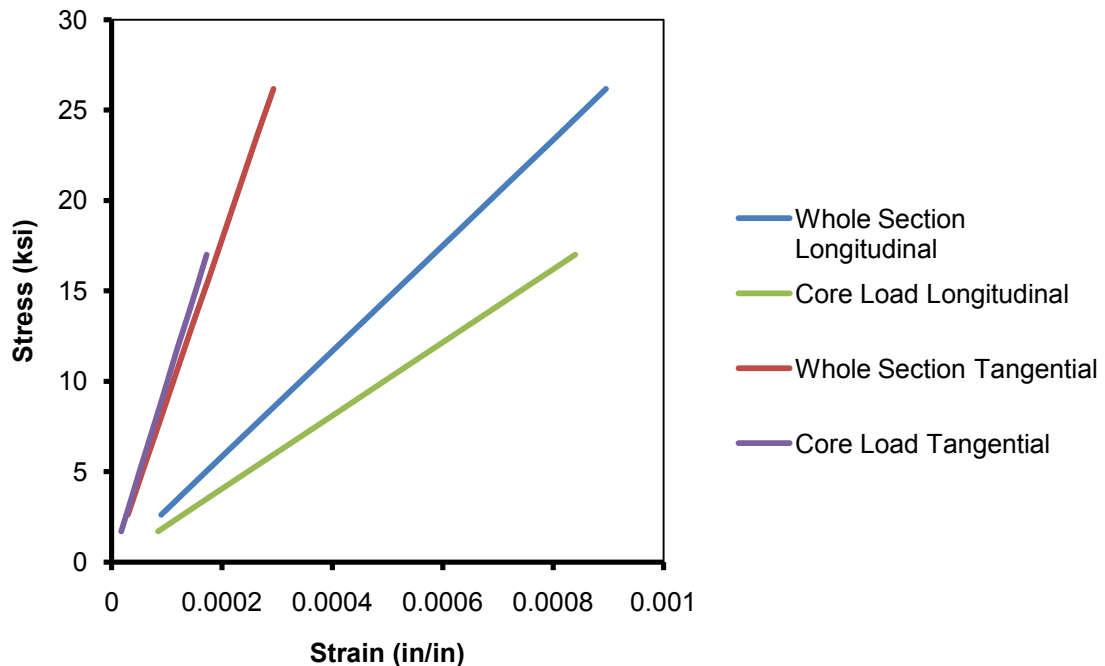


Figure 3.24: 12- $\frac{3}{4}$ " (0.375" wall) Model Strains

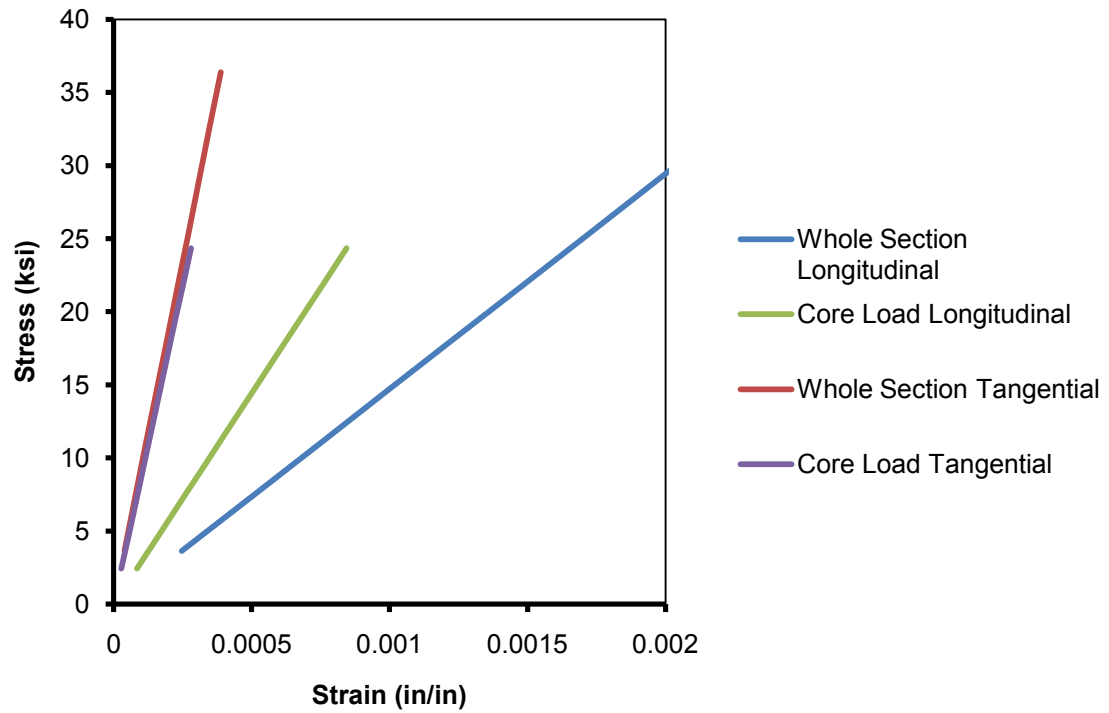


Figure 3.25: $10^{-3}/4''$ (0.375" wall) Model Strains

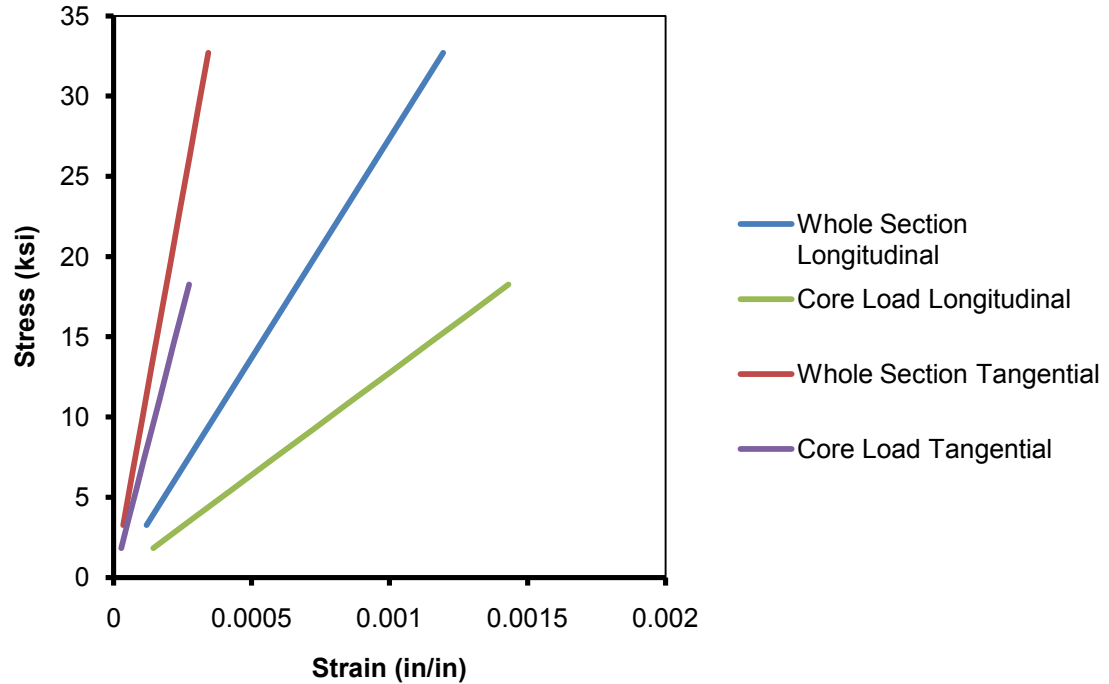


Figure 3.26: $10^{-3}/4''$ (0.5" wall) Model Strains

4 Analysis

In this section the tests, outlined earlier, are analyzed and several are compared to the finite element model solutions for the stub-sections. This finite element model comparison includes variations in the concrete strength obtained from core testing, along with revised concrete strengths that take into consideration confinement. The results in this section include the concrete core samples, loading of the whole section, loading of the core section only, and the push-through testing. It should be noted that none of the stub sections were tested to failure because the load frame was unable to provide sufficient load to induce failure.

4.1 Concrete Core Samples

The concrete core samples were taken from the different locations along the length of the pile (Figure 3.11) and were tested in compression on the Baldwin frame. The cores were tested following the procedures of ASTM C31 (2003), however some variations were required due to some of the cores breaking shorter than required. The full results from all of the tests are listed in Appendix A, and the average compressive strengths are presented in Table 4.1 and Figure 4.1. Some data points are missing because some of the cores broke, too short, during extraction and could not be tested as noted in Appendix A, also cores shorter than 7 inches were not used to calculate the averages. These average compressive strengths of the core samples are far greater than that of the test cylinders cast at the same time (7600 psi vs. 4700 psi).

**Table 4.1:
Average Core Sample Compressive Strengths**

	10-¾" Piles (Pile 1,2)		12-¾" Piles (Pile 3, 4)	
Depth	Compressive Strength (psi)	# of specimens	Compressive Strength (psi)	# of specimens
1-5 ft.	6008	3		
5-10 ft.	8218	4	7378	7
10-15 ft.			6509	4
15-20 ft.	9119	3		
20-25 ft.	7619	3		
25-30 ft.	7875	3	6545	1
30-35 ft.	7754	3	7073	4
35-40 ft.	9427	2	8195	3

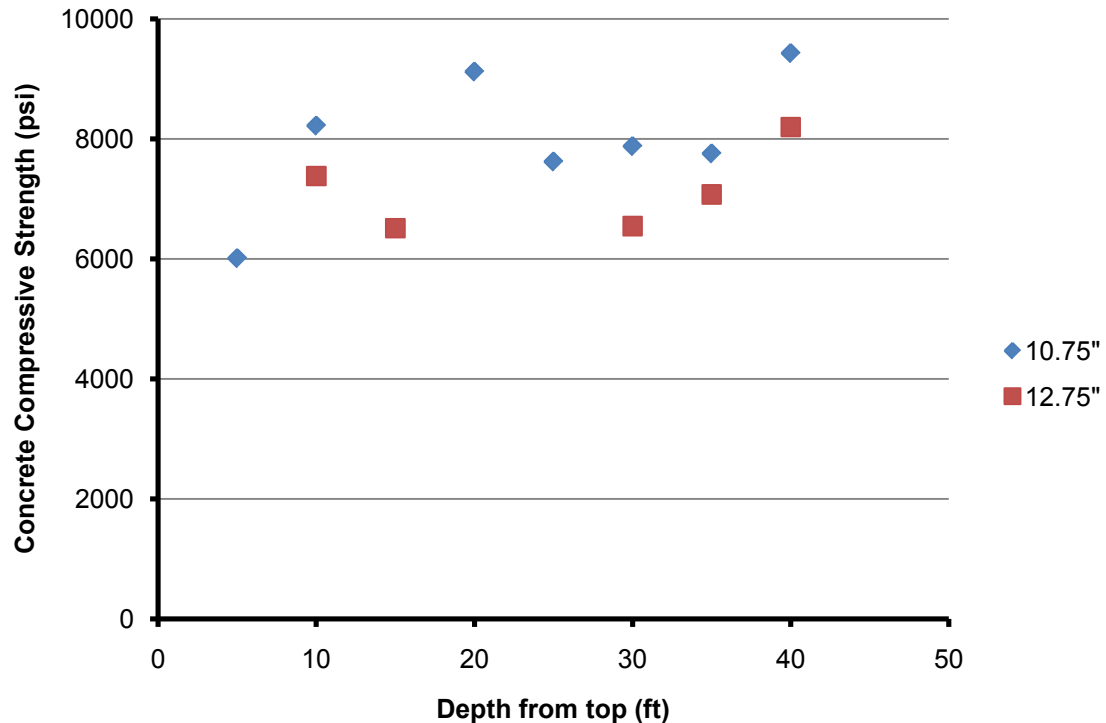


Figure 4.1: Average Core Sample Compression Strengths through the depth

This increase in strength could be attributed to many different things, the water in the concrete in the piles may not have been able to escape, so a larger portion of the cement was hydrated, or the weight of the concrete pushing down in conjunction with the confinement from the steel shell could have densified the concrete, or the coring process

may have relieved some stress from the sections and helped align the crystalline structure of the cement by re-hydrating more cement to make it stronger.

4.2 Full Cross Section Loading

Full cross-section load testing was performed on a total of twelve stub-sections, four of each cross section size. In this scenario the entire cross section was loaded using a steel plate between the loading head and the pile stub-sections. For all of the tests, load, longitudinal displacement, longitudinal strain at mid-height, and tangential (transverse) strain at mid-height were measured (Figure 3.14). To determine the stresses applied to these samples a transformed section analysis was performed, converting the concrete to an equivalent steel section (Eqn.4-1).

$$A_{eff} = A_s + \frac{A_c}{n} \quad 4-1$$

where:

A_{eff} = Effective area transformed to steel

A_s = Area of steel

A_c = Area of concrete

n = ratio of the modulus of elasticity of steel to the modulus of elasticity of concrete

For this analysis, the steel material properties assumed were an elastic modulus of 29,000 ksi and an overall yield strength of 57.5 ksi, which gives a yield strain of the steel at $2,000\mu\epsilon$. This yield strength was supplied by the contractors from the manufacturer for the steel shells used in this project. The concrete modulus was assumed as 3,800 ksi, based on compressive strength test results from the cylinders that were cast simultaneously with the piles. In some of the testing, the same pile sections were loaded several times to check that they had not yielded.

4.2.1 10 $\frac{3}{4}$ " specimens (0.375" wall)

This specimen size was the smallest cross section tested and, as such, experienced the most strains. This cross section also had the smallest theoretical design capacity as it had the smallest diameter and thinnest wall of the cross sections tested. The nominal capacities from the AASHTO LRFD (2010) composite (Eqn.2-5) and non-composite (Eqn. 2-6) design methods are presented in Table 4.2.

Table 4.2:
10 $\frac{3}{4}$ " (0.375" wall) Nominal Capacity

Design Method	Nominal Capacity
Composite	972 kips
Non-composite	240 kips

For all of the specimens, the load was applied concentrically to a maximum of 1,000 kips, the capacity of the testing frame. Figure 4.2 illustrates the load vs. longitudinal strains of all the 10 $\frac{3}{4}$ " (0.375" wall) specimens, while Figure 4.3 shows the load vs. tangential strains. In addition, the applied loads were converted into longitudinal stresses, by transforming the concrete to an equivalent steel area (Appendix C) for a comparison of stress-strain response (Figure 4.4 and Figure 4.5) for both the corresponding longitudinal and tangential strains. All of these figures also illustrate the simulated response from the finite element models.

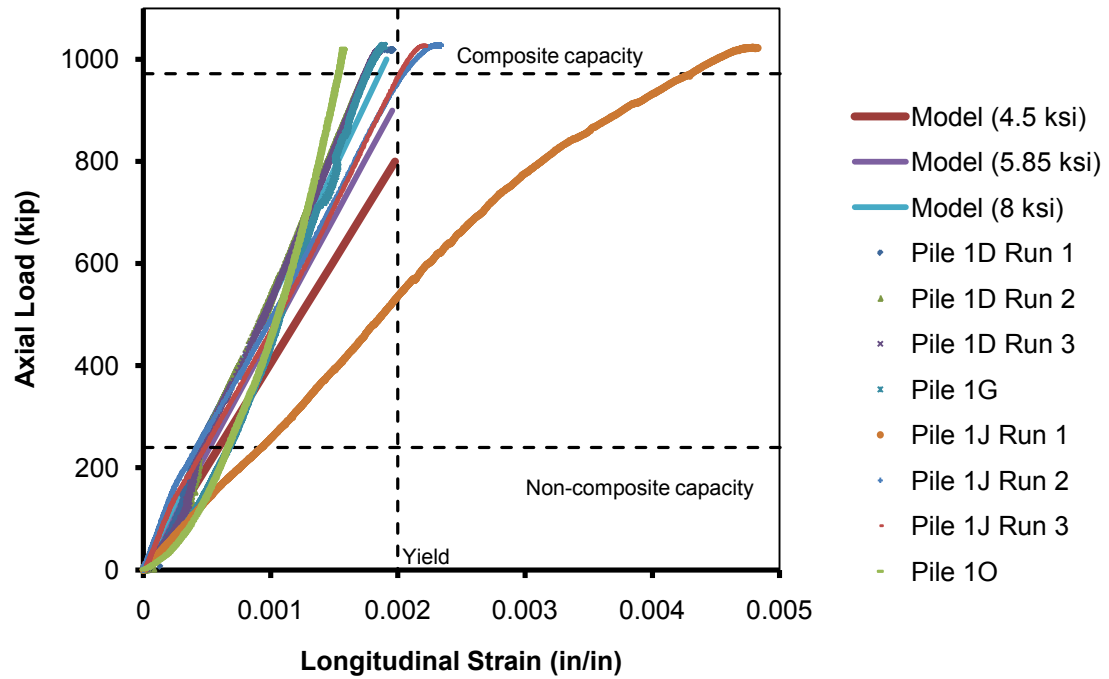


Figure 4.2: Full Cross Section Loading – Axial Load vs. Longitudinal Strains, 10- $\frac{3}{4}$ " (0.375" wall)

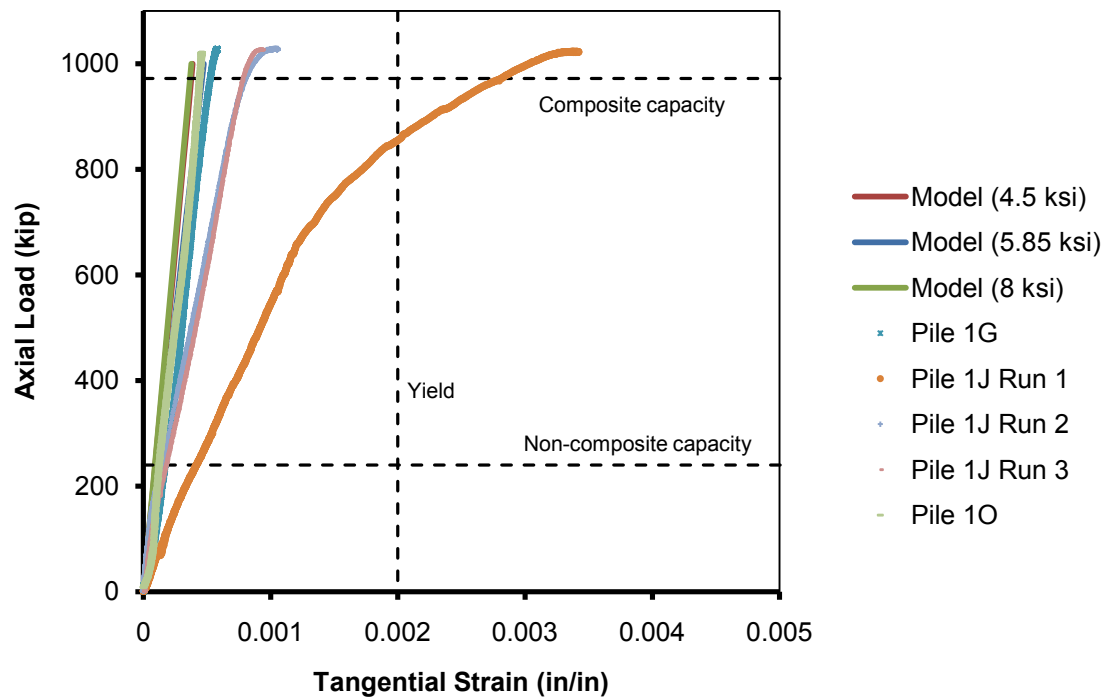


Figure 4.3: Full Cross Section Loading – Axial Load vs. Tangential Strains, 10- $\frac{3}{4}$ " (0.375" wall)

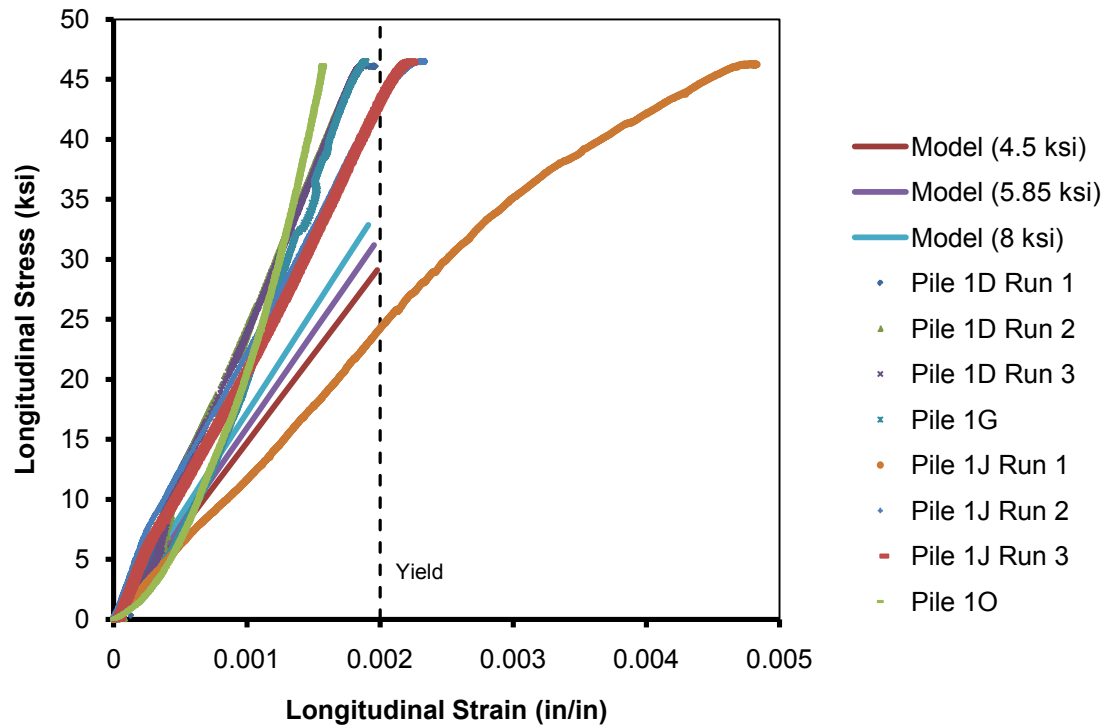


Figure 4.4: Full Cross Section Loading – Longitudinal Stress vs. Longitudinal Strains, 10-³/₄" (0.375" wall)

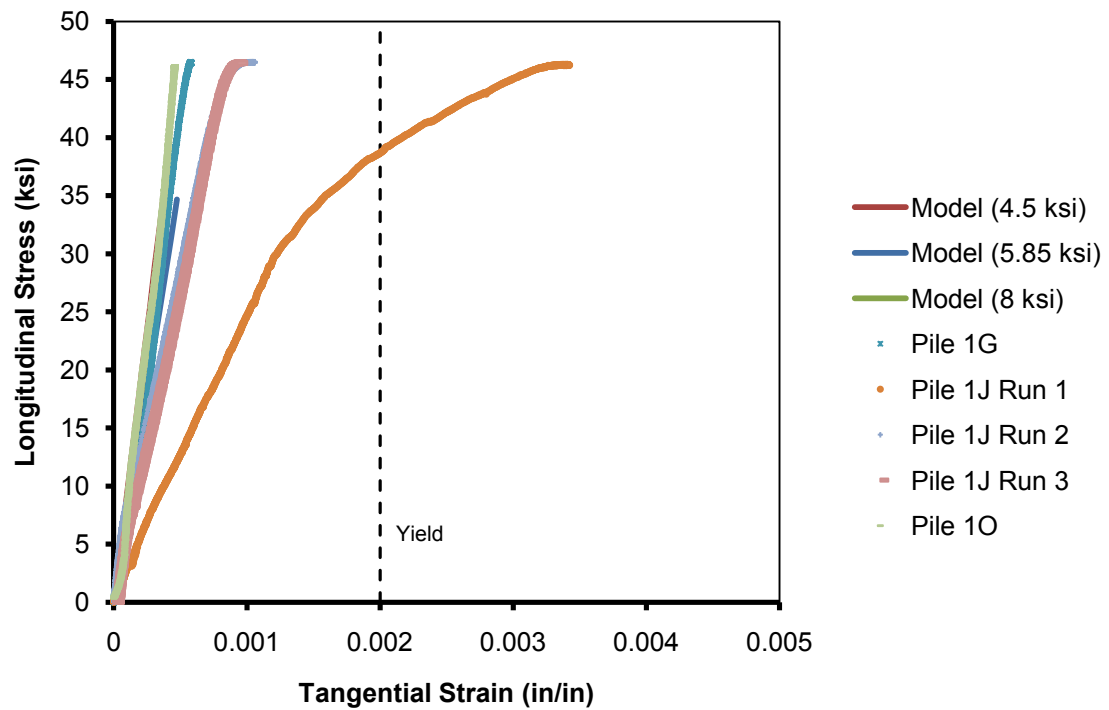


Figure 4.5: Full Cross Section Loading – Longitudinal Stress vs. Tangential Strains, 10-³/₄" (0.375" wall)

From Figure 4.4, it can be observed that most of the pile tests exhibited similar behavior, with only pile section 1J (Run 1), exhibiting more strains than the rest of the piles. This section was tested again (Pile 1J Run 2 and Run 3), and these other runs exhibited similar responses to the other cross-sections of the same size. Upon inspection of the specimen, it was found to have some irregularities on the top and bottom surfaces. This section had a small section of the steel shell and concrete core that was slightly elevated over the rest of the cross section, coincidentally directly above where the strain gauge was located. This caused the strain gauge to be located on the face with greatest pressure during the initial test. After the first test, the surfaces were flattened out to where the cross section was uniformly loaded. This was found to be a reoccurring problem for several test sections. There were two samples (Pile 1D all runs and Pile 1J Runs 2 and 3) that approached yielding; however the frame was at its capacity and more load could not be applied to cause yielding. Runs 2 and 3 for Pile 1J appear to have reached the yielding, but this cannot be verified as this was so close to the maximum load from the load frame that a change in slope cannot be seen. Neglecting Run 1 for specimen 1J, the finite element model provided a good representation of the member response, during testing, however it was found to be conservative, predicting strains greater than those actually recorded during loading.

Figure 4.5, shows corresponding longitudinal stress vs. tangential strain. These tangential strains are much lower than the longitudinal strains because the load was applied along the longitudinal axis, and the resulting strains are due to the radial expansion of the concrete and steel due to Poisson's effects. The finite element models were able to better represent the actual strains in the radial direction than the longitudinal strains under this same loading. When comparing the effect of concrete compressive strength on transverse system behavior (e.g. Model 1 vs. Model 2), the

impact is minimal. This is mostly attributed to the steel section being much stiffer (i.e. lower degree of radial expansion) than the concrete core.

4.2.2 10 ¾" specimens (0.5" wall)

This specimen size had the same outer diameter as the smallest cross section, but had a thicker steel wall. Due to the thicker shell, it was expected to have similar strengths to that of the 12-¾ in. specimen. The nominal capacities from the AASHTO LRFD (2010) composite (Eqn. 2-5) and non-composite (Eqn. 2-6) design methods are presented in Table 4.3.

Table 4.3:
10-¾" (0.5" wall) Nominal Capacity

Design Method	Nominal Capacity
Composite	1170 kips
Non-composite	228 kips

For all of the specimens, the load again was applied concentrically to a maximum of 1,000 kip. Figure 4.6 and Figure 4.7 illustrates the load vs. longitudinal strains and tangential strains, respectively, of all the 10 ¾" (0.5" wall) specimens. These applied loads were converted into longitudinal stresses, by transforming the concrete to an equivalent steel area (Appendix C) for a comparison of stress-strain response (Figure 4.8 and Figure 4.9) for both the corresponding longitudinal and tangential strains respectively. All of these figures also illustrate the simulated response from the finite element models.

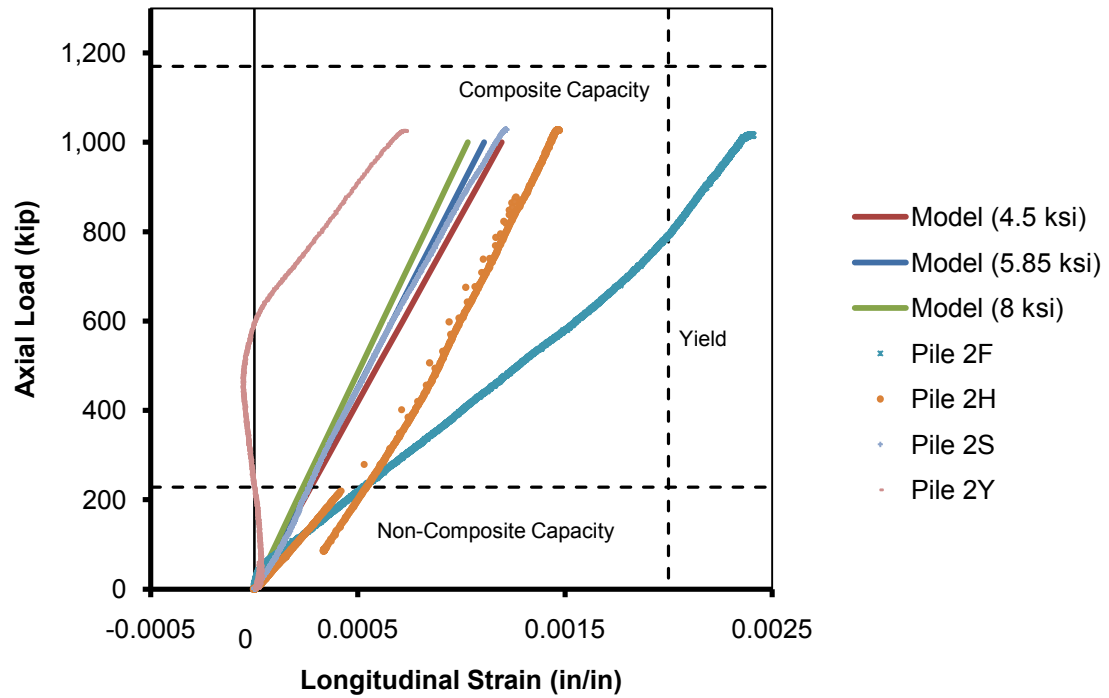


Figure 4.6: Full Cross Section Loading – Axial Load vs. Longitudinal Strains, 10-³/₄" (0.5" wall)

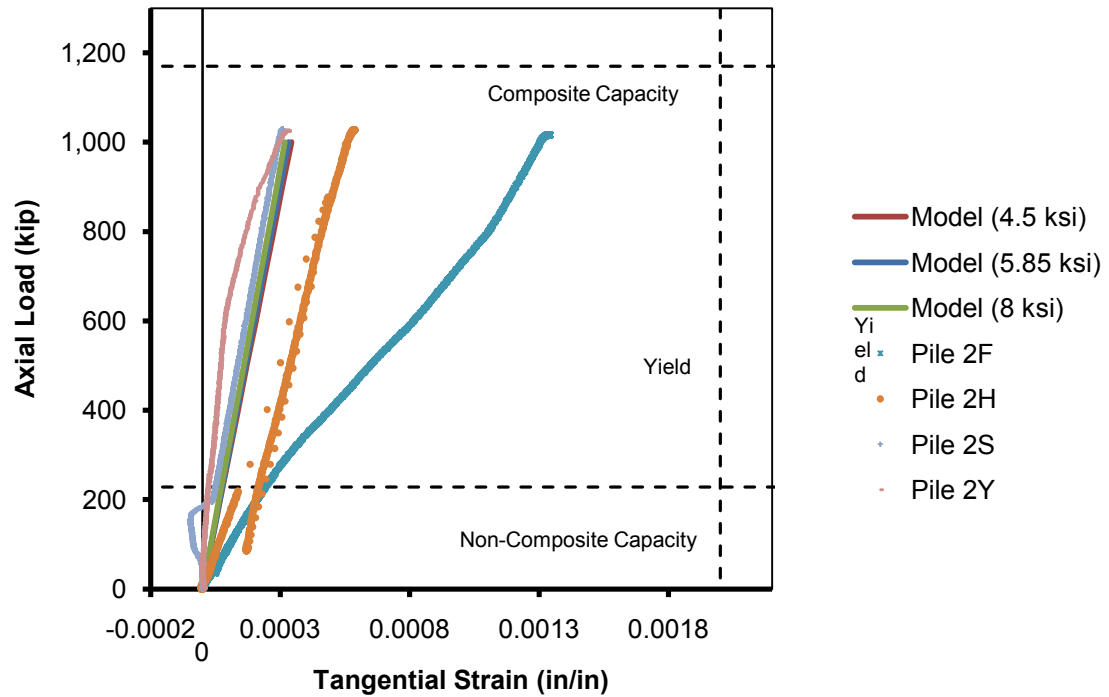


Figure 4.7: Full Cross Section Loading – Axial Load vs. Tangential Strains, 10-³/₄" (0.5" wall)

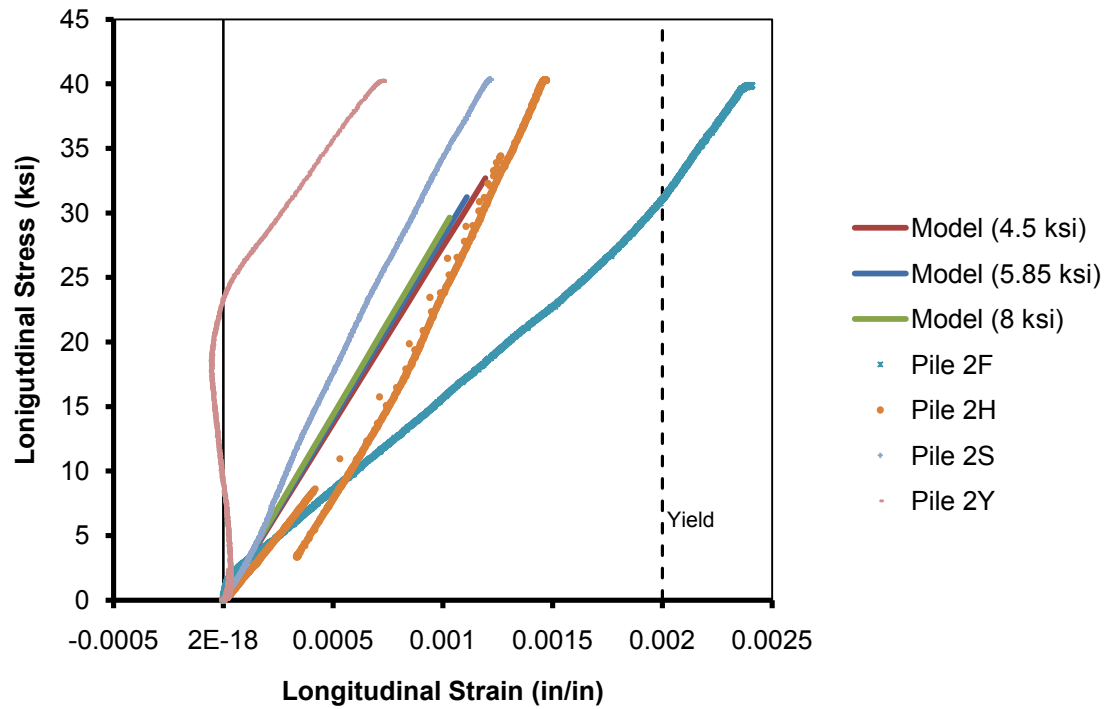


Figure 4.8: Full Cross Section Loading – Longitudinal Stress vs. Longitudinal Strains, 10-³/₄" (0.5" wall)

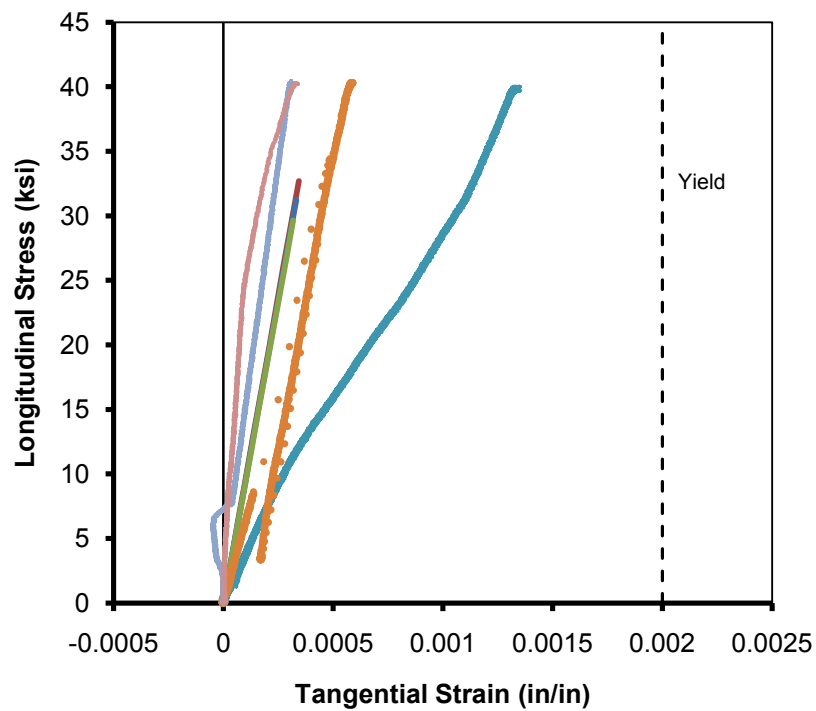


Figure 4.9: Full Cross Section Loading – Longitudinal Stress vs. Tangential Strains, 10-³/₄" (0.5" wall)

In Figure 4.8, a trend can be seen with pile sections 2H and 2S. Trials 2F and 2Y both had the same issues with the location of the strain gauges and a small section of the end surfaces not being perfectly flat as pile section 2H and 2S. Pile section 2F was found to have a small section of the steel shell and concrete core that was slightly higher than the rest of the cross section and this was located on the same side as the strain gauge. This caused the strain gauge to be at a location of greater pressure like section 1J of the 10- $\frac{3}{4}$ " (0.375" wall). Conversely pile section 2Y, had a spot that was higher than the rest but, the strain gauge was located on the opposite side of the high spot. This caused the strain gauge to experience very little compressive strain, until the high spot flattened out and then the strains started to increase with the load. Pile section 2H has a load unload loop in the data as there was a small section of elevated concrete on the surfaces when the loading occurred. This small section was loaded until it began to crack at which the load increased at a quicker rate. After this concrete crushed and the head was loading the entire surface again it loaded back up until the maximum of the load frame. The finite element model was able to accurately simulate the stress-strain relationship for this cross section, more so than for the thinner walled sections of the same size. The model stress-strain relationship appeared directly between the two runs that were loaded simultaneously without the irregularities on the loaded surfaces.

In Figure 4.9, it can be seen that three of the four tests were in relatively good agreement. Pile section 2F had a much larger tangential strain than the rest, as was the case for the longitudinal strains. These large tangential strains were caused by the same problem as the longitudinal strains, which occurred due to the strain gauge being located at a location with a deformity on the top surface, causing the location to be loaded more heavily. The finite element model was able to better simulate the tangential

strains, and the variation in concrete strengths did not affect the overall stiffness enough to influence the strains appreciably.

4.2.3 12 ³/₄" specimen (0.375" wall)

This specimen size had the overall largest cross section of all specimen tested, and was predicted to have the greatest capacity. The nominal capacities from the AASHTO LRFD (2010) composite (Eqn. 2-5) and non-composite (Eqn. 2-6) design methods are presented in Table 4.4.

Table 4.4:
12-³/₄" (0.375" wall) Nominal Capacity

Design Method	Nominal Capacity
Composite	1234 kips
Non-composite	346 kips

The load was applied concentrically to the capacity of the load frame, 1,000 kips. Figure 4.10 and Figure 4.11 illustrates the load vs. longitudinal strains and tangential strains, respectively, of all the 12-³/₄" (0.375" wall) specimens. These loads were converted into longitudinal stresses like the other sections loaded in this manner, by transforming the concrete to an equivalent steel area (Appendix C) for a comparison of the stress-strain response (Figure 4.12 and Figure 4.13) for both the longitudinal and tangential strains. All of these figures also illustrate the simulated response from the finite element models.

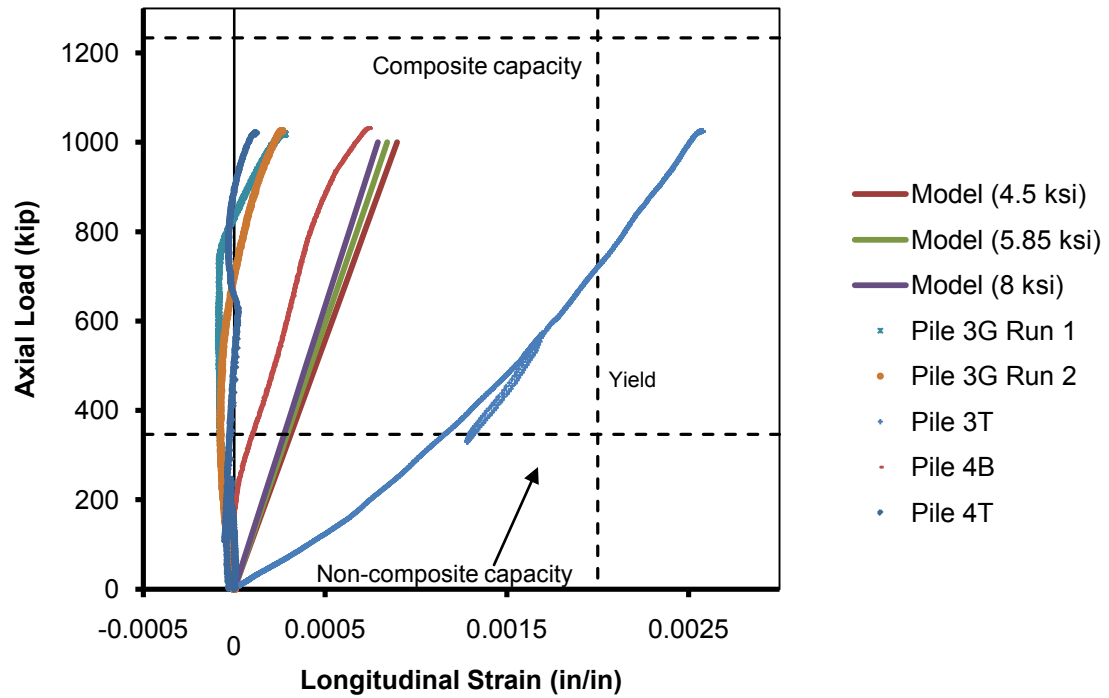


Figure 4.10: Full Cross Section Loading – Axial Load vs. Longitudinal Strains, 12-³/₄" (0.375" wall)

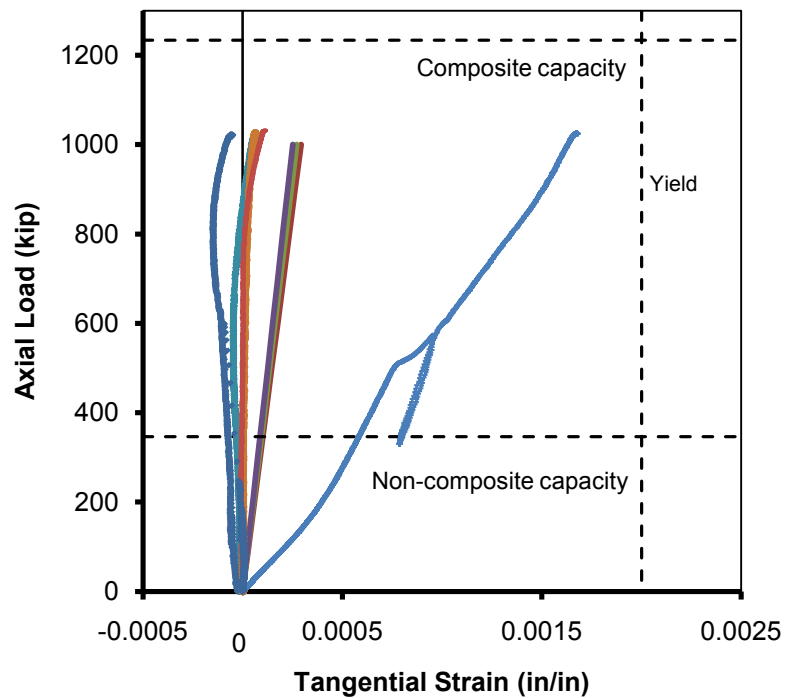


Figure 4.11: Full Cross Section Loading – Axial Load vs. Tangential Strains, 12-³/₄" (0.375" wall)

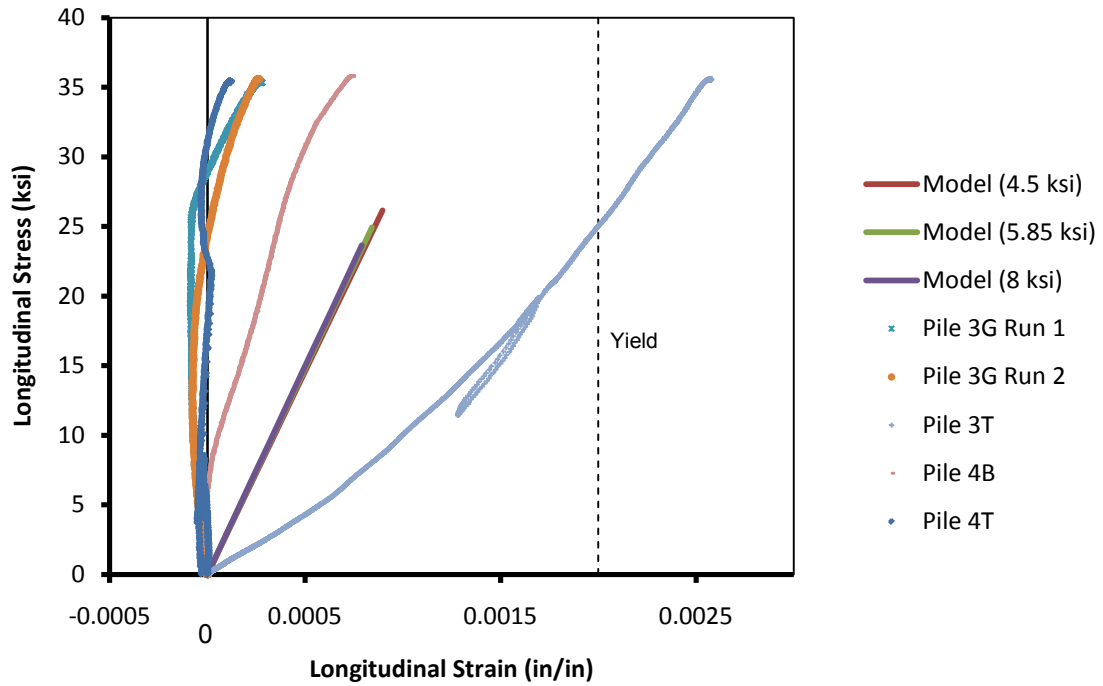


Figure 4.12: Full Cross Section Loading – Longitudinal Stress vs. Longitudinal Strains, 12-³/₄" (0.375" wall)

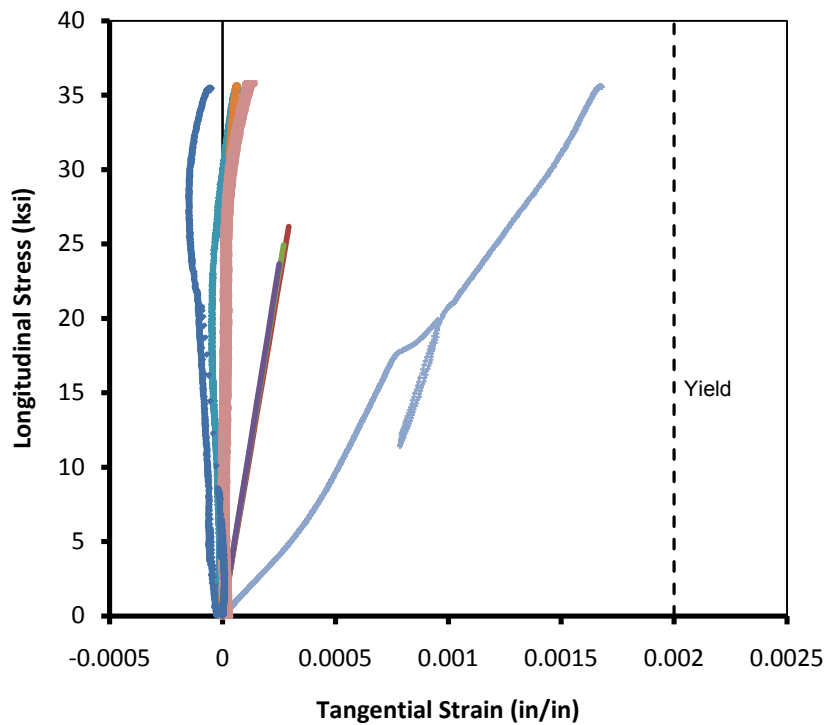


Figure 4.13: Full Cross Section Loading – Longitudinal Stress vs. Tangential Strains, 12-³/₄" (0.375" wall)

Figure 4.12 and Figure 4.13 show that both the longitudinal and tangential strains recorded during testing stayed at or near zero. This is a very different behavior from that exhibited by all of the other specimens tested in this loading configuration, but these specimens had different shell configurations. The shell on the 12- $\frac{3}{4}$ " specimens was spiral welded as opposed to the two 10- $\frac{3}{4}$ " piles which were seam welded. This spiral appears to have changed the way load was transferred throughout the section and, as such, the model was not able to simulate the true strains experienced by the sections. The model calculated the strains at their respective locations, however these strains were much greater than those experienced by the sections due to the seam being in the orientation that it is and re-directing much of the strain in the cross section. There was one 12- $\frac{3}{4}$ " section where the strain gauges did record a much higher value than the rest of the 12- $\frac{3}{4}$ " sections. In this test, the strain gauge happened to be above the seam and also in a location where the top surface had a high spot. Because the spiral welded shell changes the way the load is transferred through the member, the finite element model was not able to simulate the strains of the actual test.

4.2.4 Summary of Full Cross Section Loading

From an analysis of the testing on the three different cross sections, definite trends were observed from the data. For the 10- $\frac{3}{4}$ " (0.375" wall) the samples were near the theoretical yield point of the steel shell in the longitudinal direction at the frame capacity (1000 kip). These specimens exhibited the largest strains observed during testing. From the data, there appears to be a leveling off of the strains at the maximum loads; however, this was attributed to the test frame reaching its maximum load and not the beginning of the yielding of the steel shell. This was verified by running the same sample again and recording almost identical strains and stresses, proving that the

sample was still in its linear elastic behavior. For the 10- $\frac{3}{4}$ " (0.5" wall) samples, the longitudinal strain was smaller than the thinner (0.375") walled specimens as expected. These larger samples were not near their yield limit under the maximum load, but there was a similarity in slopes between the different tests of the same size configuration. This slope matched well with the finite element model that was created. The 12- $\frac{3}{4}$ " samples though did not show a similar trend to that of the smaller diameter test specimens. These samples exhibited almost no strains in either the longitudinal or tangential directions from the testing. This was attributed to the way the spiral seam on the sections transfer the load throughout the section. The tangential strains for the all of the different sized samples were much smaller than the longitudinal strains (roughly 50%). This could be attributed to the entire cross section being loaded simultaneously, with the load being spread between both materials.

The trends in the recorded data also matched observations from the finite element models, except for the case of the 12.75" samples. These discrepancies again can be attributed to the way the steel shell section of the 12.75" samples were made (spiral welded), which appears to modify the transfer of load through the cross section. There were some limitations in the testing procedure though, the displacements that were predicted by the model were very small, and the instrumentation used in the testing were not accurate enough to record the miniscule deflections seen in the sections. Based on the comparisons of the model response to the experimental results, it was concluded that the model that was developed can accurately predict the strains of a stub section that is uniformly loaded and seam welded, however it should not be used with a spiral weld. All additional data from this testing can be seen in Appendix B.

4.3 Section Core Only Loading

Compression testing of the stub section by loading only the core area was performed on a total of 12 different stub-sections, four for each cross section size. Unlike the previous test regime, where the whole stub section was loaded, only the concrete core was loaded using a one-inch thick steel plate on both sides between the loading head and the pile stub-sections (Figure 3.16). For all of the tests, load, longitudinal displacement, longitudinal strain at mid-height, and tangential (transverse) strain at mid-height were measured. To determine the stresses applied to these samples a transformed section analysis was done, converting the concrete core to an equivalent steel section (Eqn. 4-1), same as with the entire cross section loading. This was done for comparison between the two tests, along with the way the stress is transferred through the cross section under this core only loading. The load is transferred to the center of the section which the center area being equally loaded between the two sides, this are then increases with the loading until under maximum load the entire section is equally loaded. Also, the transformation to a equivalent concrete section could not be used as this would neglect the bond that is present between the two materials. As such the stress was calculated using the same equivalent steel section as when the entire cross section was loaded.

The steel properties used for this were the same as those used for the full cross section loading, with an elastic modulus of 29,000 ksi and an overall yield strength of 57.5 ksi for the steel shell, and an elastic modulus of 3,800 ksi for the concrete core. With this loading scenario the nominal capacities were assumed to be the same as the full section capacities because the design methods are not applicable to this scenario. This test was intended to evaluate the capacity that could be achieved with

consideration of the effects of confining the concrete core. Unfortunately in these tests, none of the specimens failed before the capacity of the testing machine was reached.

4.3.1 10 ³/₄" specimen (0.375" wall)

This size configuration was the smallest cross section tested. For all of the specimens, the load was applied concentrically to the concrete core only to a maximum of 1,000 kips, the capacity of the testing frame. Figure 4.14 and Figure 4.15 illustrates the load vs. longitudinal strains and tangential strains, respectively, of all the 10-³/₄" (0.375" wall) specimens. These applied loads were recorded from the tests, and the loads were transformed into longitudinal stresses for comparison of the stress-strain response. The stresses were determined by transforming the steel to an equivalent concrete area (Appendix C) and the stress-strain response can be seen in Figure 4.16 and Figure 4.17 for the longitudinal and tangential strains, respectively. All of these figures also show the response from the three runs of the finite element model created.

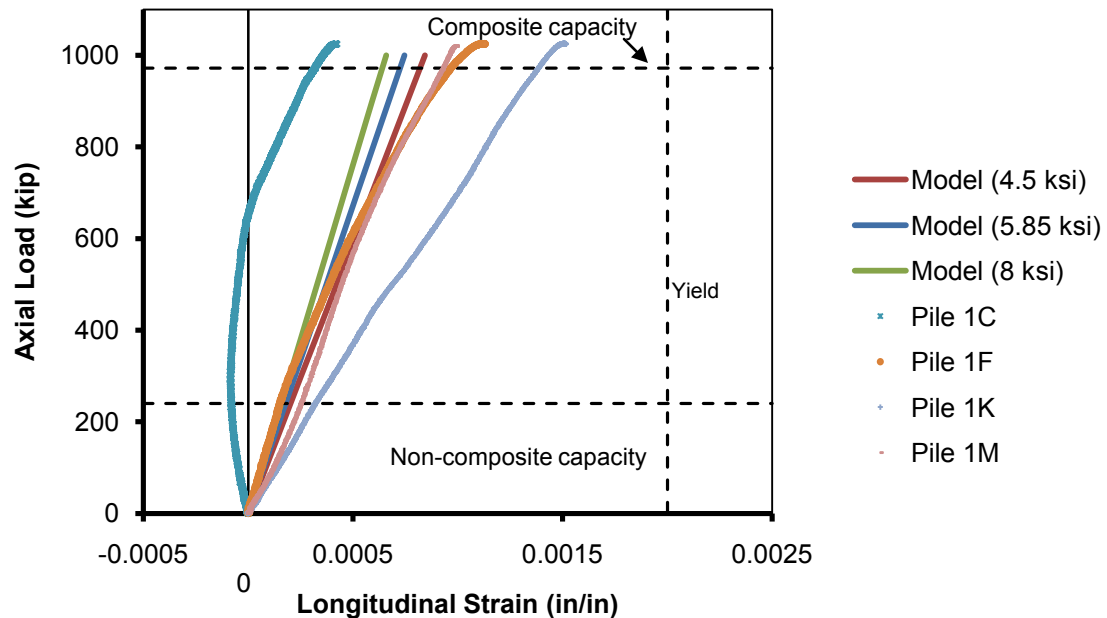


Figure 4.14: Section Core Only Loading – Axial Load vs. Longitudinal Strains, 10-³/₄" (0.375" wall)

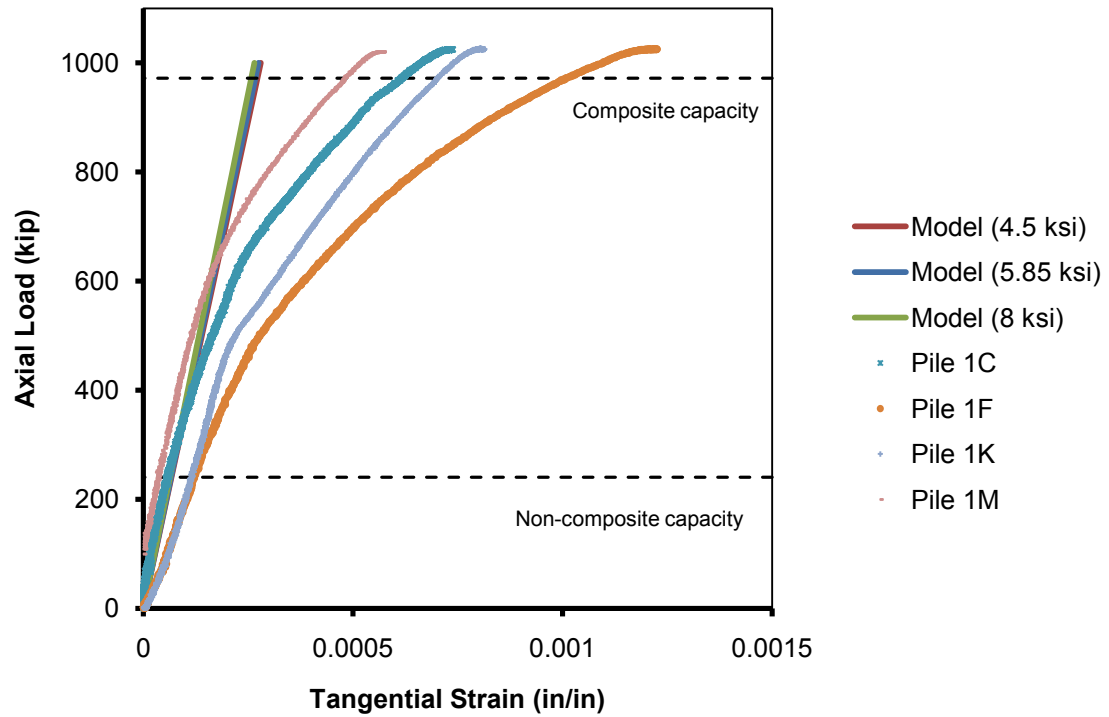


Figure 4.15: Section Core Only Loading – Axial Load vs. Tangential Strains, 10^{-3/4}" (0.375" wall)

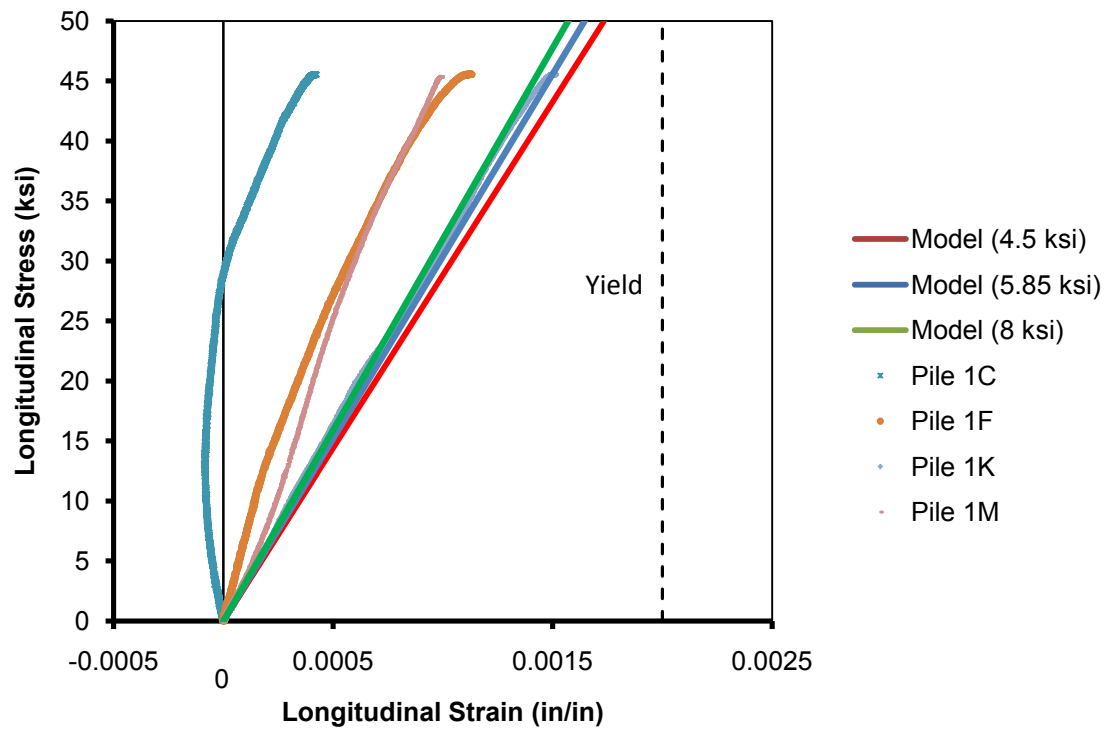


Figure 4.16: Section Core Only Loading – Longitudinal Stress vs. Longitudinal Strains, 10^{-3/4}" (0.375" wall)

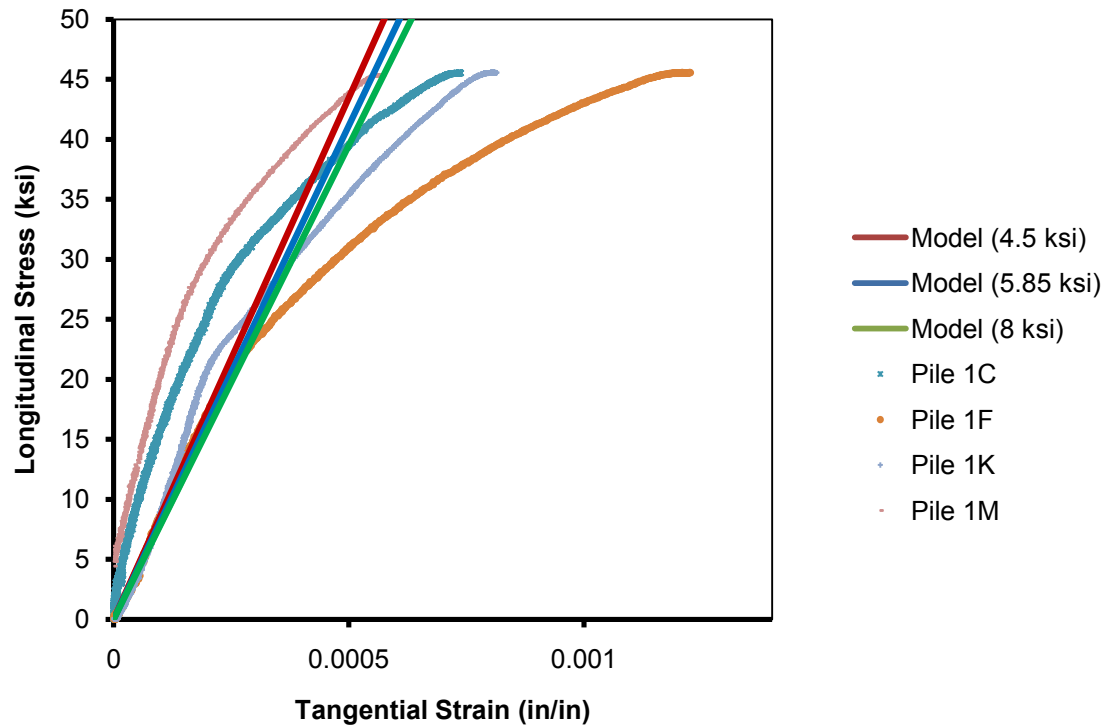


Figure 4.17: Section Core Only Loading – Longitudinal Stress vs. Tangential Strains, 10-³/₄" (0.375" wall)

Figure 4.16 shows the longitudinal stress versus longitudinal strains from the testing of all specimens of this sample size. Pile section 1C had a region of the cross section surface that was slightly elevated and the strain gauge recorded strains around zero until the elevated section was leveled out during loading, at which point the whole section was simultaneously loaded. These results exhibited strains below the elastic limit and a nearly proportional increase in strain with the loading, demonstrating that the steel shell remained in the linear elastic loading phase with respect to the direction of loading. The longitudinal strains recorded are much smaller than those from loading the whole section. This is caused by the steel not being loaded by the loading frame. The strain in the steel is coming from the expansion of the concrete core that is being loaded and the distribution of load into the shell through bond. For this loading scenario, the finite element model was able to accurately simulate the vertical strains for this section

under concrete core loading. With the exception of (Pile 1C), the model overestimates the strain response. The model exhibited a strain of around 0.0015ϵ at maximum, and the largest strain from the three results was around 0.0015ϵ .

Figure 4.17 shows the longitudinal stress versus the tangential strains from the testing. All four trials showed very similar strains in the steel shell, which are much higher than those observed from the scenario where the entire cross section was loaded. This is because the steel shell was not loaded in this test and, as such, the concrete core is resisting more axial load and due to Poisson's effect pushing out in the radial direction which induces strains in the steel in the radial direction. For this scenario the finite element model underestimates the amount of strain in the tangential direction under this loading. The maximum tangential strain from the model was around 0.0006ϵ while the test loading produced a strain of 0.0007ϵ at maximum load. In addition, the stress strain relationship in the tangential direction is non-linear, while in the linear elastic range of loading. This could be one of the major reasons the finite element model is not able to simulate the strains correctly. This could be caused by a softening effect at higher loads as more of the section is being stressed uniformly in the longitudinal direction.

4.3.2 10 $\frac{3}{4}$ " specimen (0.5" wall)

The 10- $\frac{3}{4}$ in. diameter with the $\frac{1}{2}$ in. wall test section had the same outer diameter, but a thicker steel shell than the other 10- $\frac{3}{4}$ in. pile. For all of the specimens, the load was applied concentrically to the concrete core only to a maximum of 1,000 kips, the capacity of the testing frame. Figure 4.18 and Figure 4.19 illustrates the load vs. longitudinal strains and tangential strains, respectively, of all the 10- $\frac{3}{4}$ " (0.5" wall) specimens. These applied loads were recorded from the tests, and these loads were

transformed into longitudinal stresses for comparison of the stress-strain response. The stresses were determined by transforming the steel to an equivalent steel area (Appendix C), and the stress-strain response can be seen in Figure 4.20 and Figure 4.21 for the longitudinal and tangential strains, respectively. All of these figures also show the response from the three runs of the finite element model created.

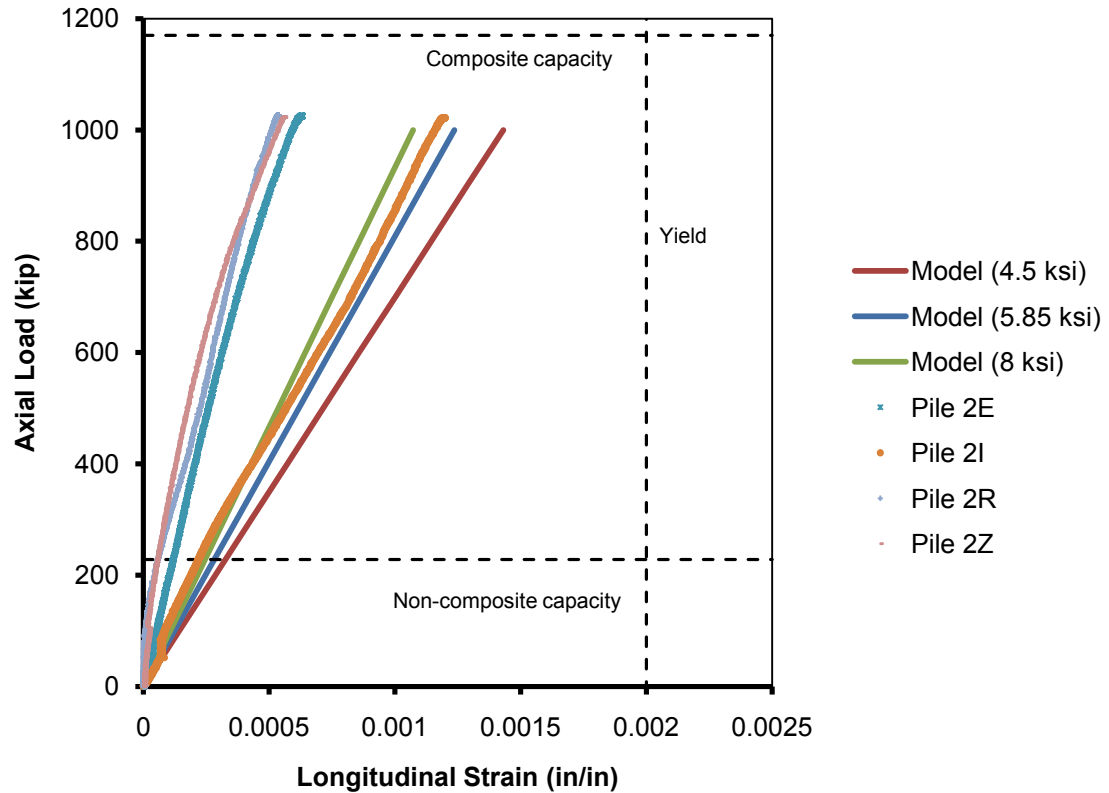


Figure 4.18: Section Core Only Loading – Axial Load vs. Longitudinal Strains, 10- $\frac{3}{4}$ " (0.5" wall)

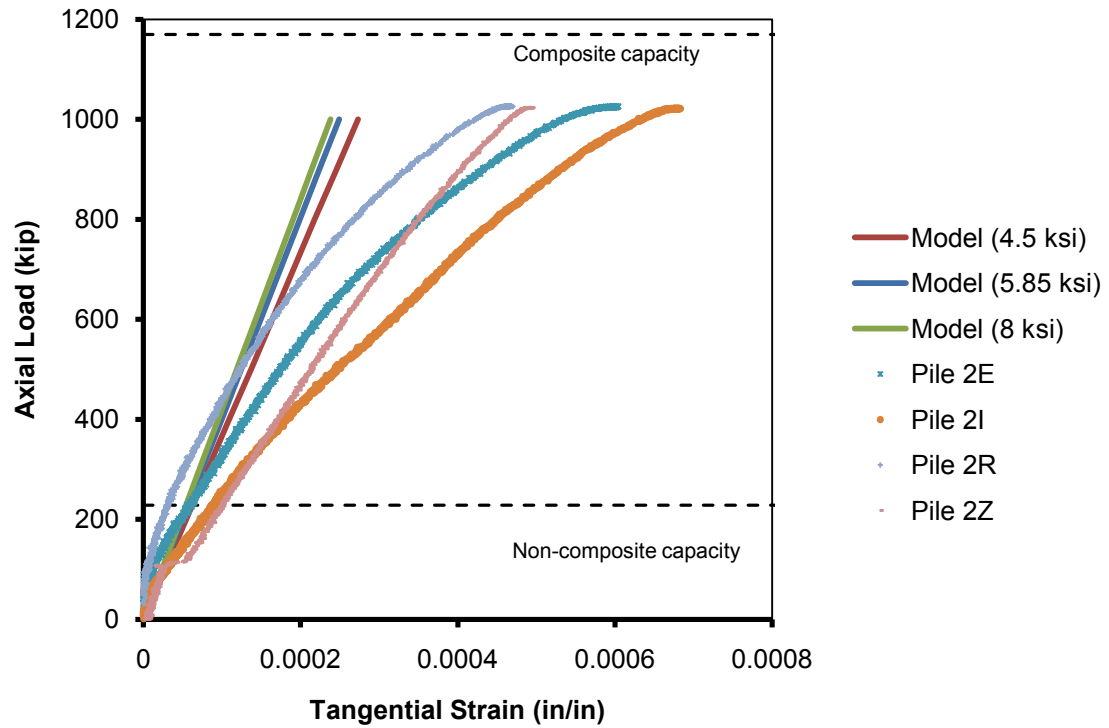


Figure 4.19: Section Core Only Loading – Axial Load vs. Tangential Strains, 10-³/₄" (0.5" wall)

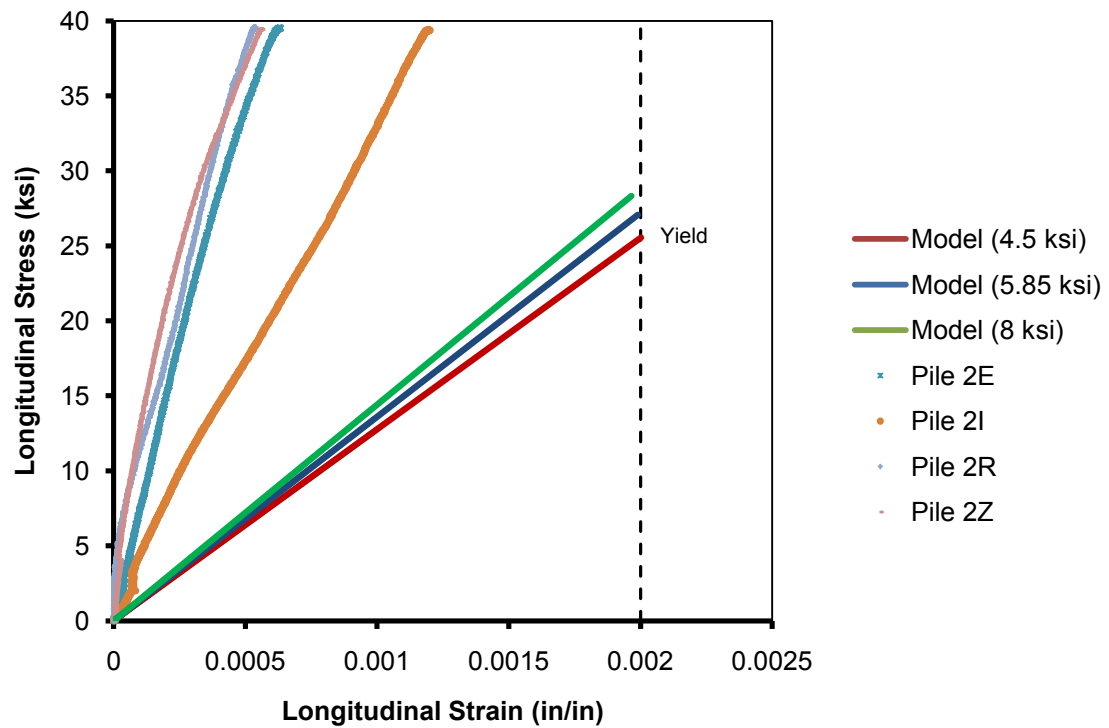


Figure 4.20: Section Core Only Loading – Longitudinal Stress vs. Longitudinal Strains, 10-³/₄" (0.5" wall)

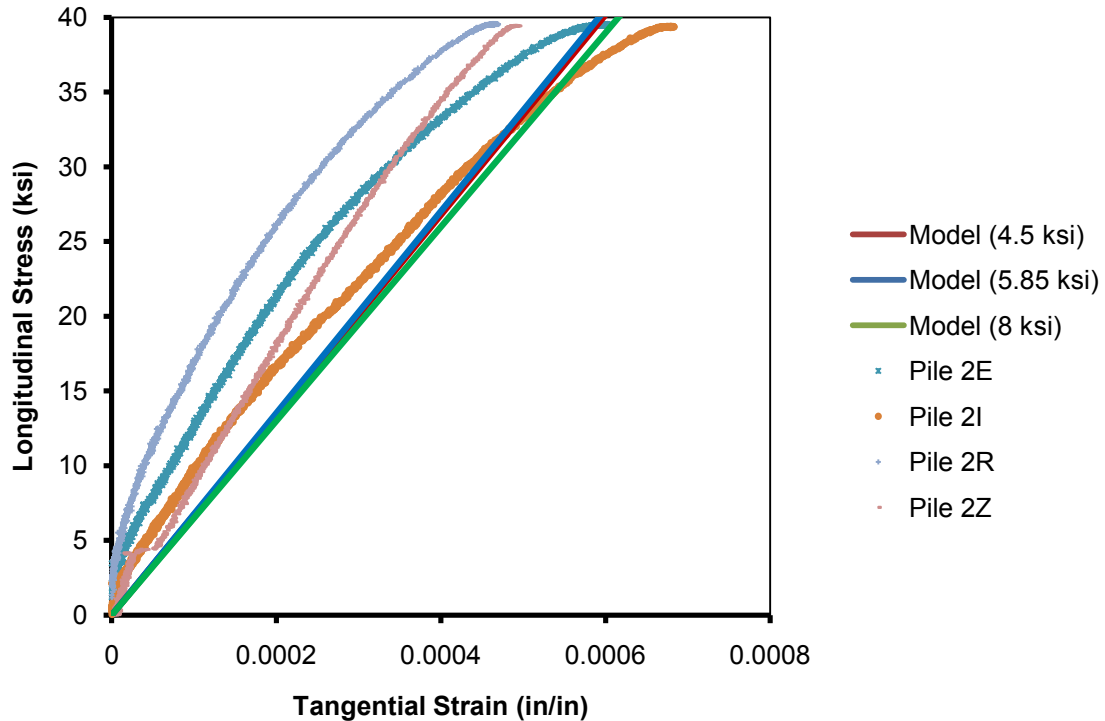


Figure 4.21: Section Core Only Loading – Longitudinal Stress vs. Tangential Strains, 10- $\frac{3}{4}$ " (0.5" wall)

Figure 4.20 shows the longitudinal strains recorded from the tests on the 10- $\frac{3}{4}$ " (0.5" wall) cross section, where only the concrete core was loaded. One test, on pile 2I, had a high spot where the strain gauge was located, which caused the gauge to experience more strain at that location. The other three runs all show very good agreement with each other under core loading. The finite element model overestimated the longitudinal strains when compared to the test results, the largest strains from the model were more than 0.0015 ϵ while the largest from the samples were 0.0012 ϵ . Also the maximum strains from these samples (0.002 ϵ) were slightly larger than those strains experienced by the 10- $\frac{3}{4}$ " (0.375" wall) specimens (0.0017 ϵ). This was caused by the thicker steel shell reduces the area of concrete.

Figure 4.21 shows the longitudinal stress versus the tangential strains from the testing. All four trials showed very similar strains in the steel shell, which are much

higher than those observed during the loading of the entire cross section scenario. Again this is because the steel shell was not loaded in this test and, as such, the concrete core is resisting more axial load and due to Poisson's effect pushing out in the radial direction which induces strains in the steel in the radial direction. For the 10- $\frac{3}{4}$ " (0.5" wall) the tangential strains appear more linear than for the thinner wall (0.375"). This could be caused by the thicker wall section having less of a softening effect at the higher loads. The finite element model again overestimates the amount of strain in the tangential direction under this loading.

4.3.3 12 $\frac{3}{4}$ " specimen (0.375" wall)

The 12- $\frac{3}{4}$ " (0.375" wall) specimen was spiral-welded, and had the largest cross section of any specimen tested. Figure 4.22 and Figure 4.23 illustrates the load vs. longitudinal strains and tangential strains, respectively, of all the 12- $\frac{3}{4}$ " (0.375" wall) specimens. These applied loads were recorded from the tests, and the loads were transformed into longitudinal stresses for comparison of the stress-strain response. The stresses were determined by transforming the steel to an equivalent steel area (Appendix C) and the stress-strain response can be seen in Figure 4.24 and Figure 4.25 for the longitudinal and tangential strains, respectively. All of these figures also show the response produced from the three runs of the finite element model created

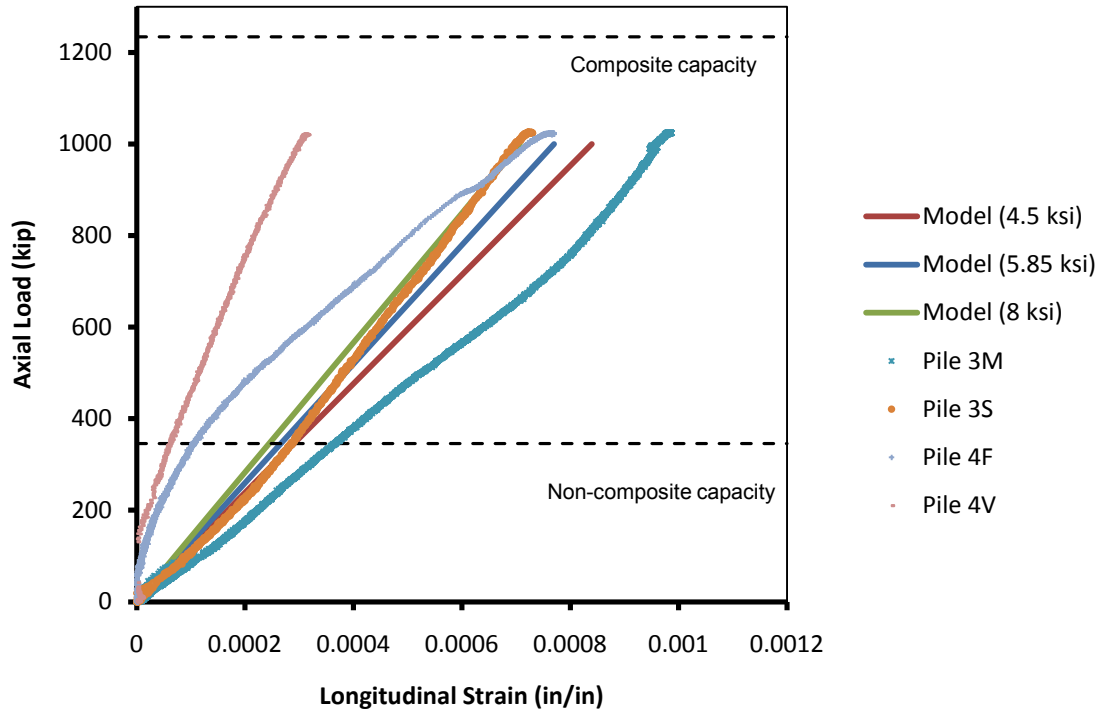


Figure 4.22: Section Core Only Loading – Axial Load vs. Longitudinal Strains, 12- $\frac{3}{4}$ " (0.375" wall)

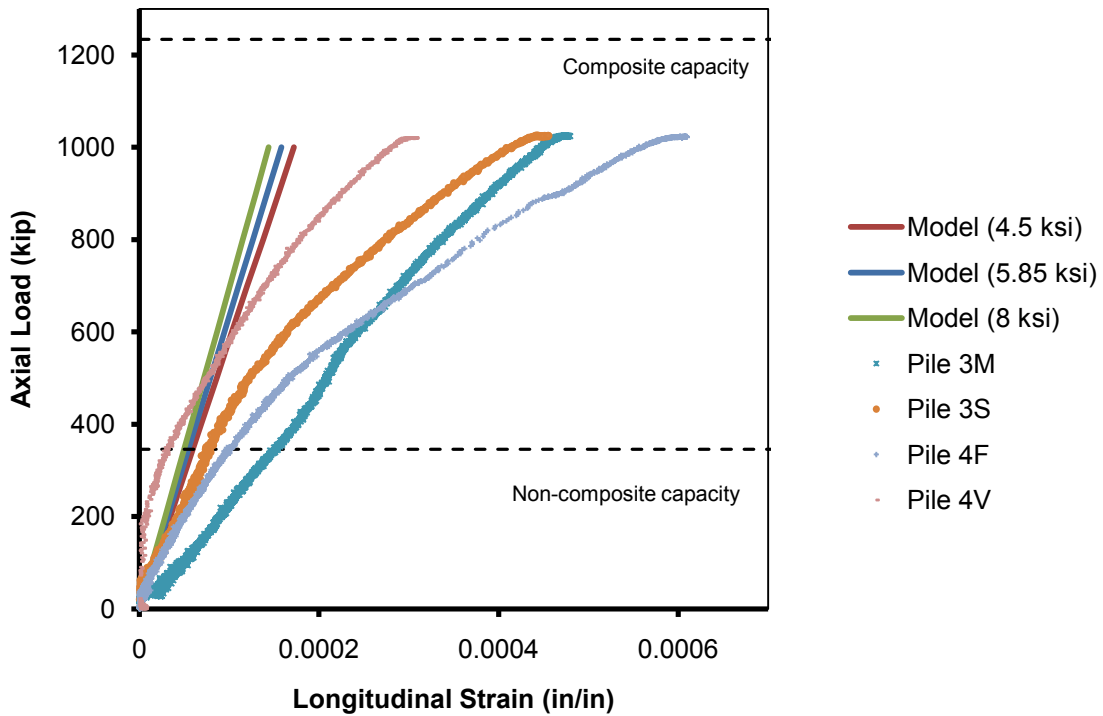


Figure 4.23: Section Core Only Loading – Axial Load vs. Tangential Strains, 12- $\frac{3}{4}$ " (0.375" wall)

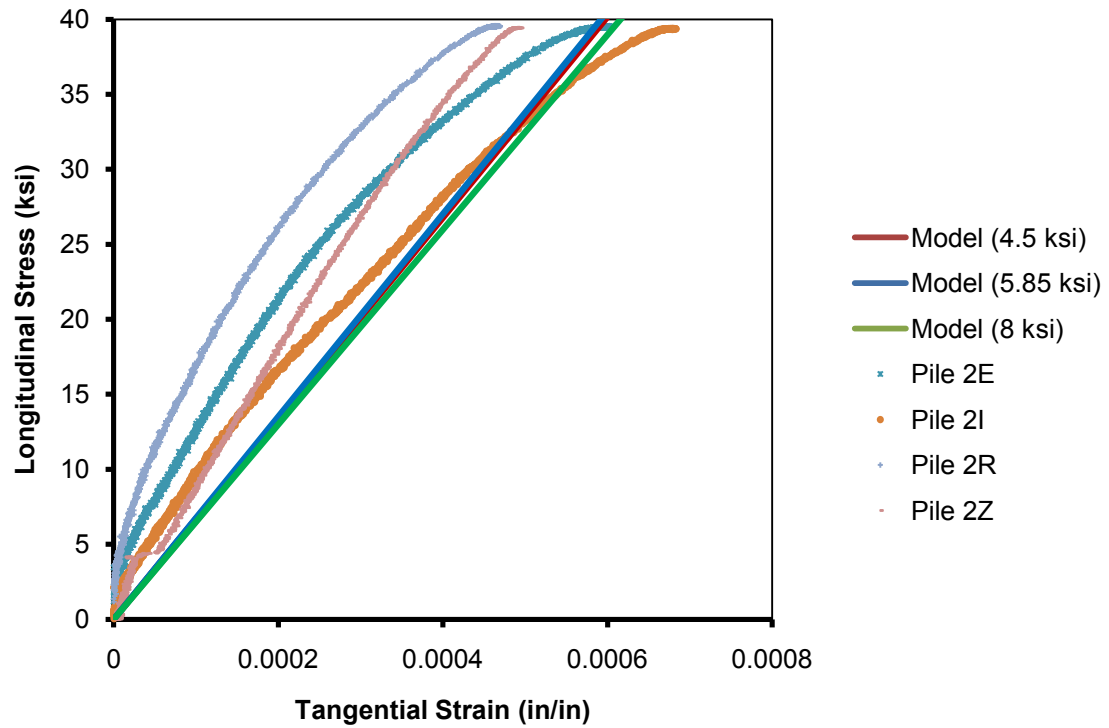


Figure 4.24: Section Core Only Loading – Longitudinal Stress vs. Longitudinal Strains, 12-³/₄" (0.375" wall)

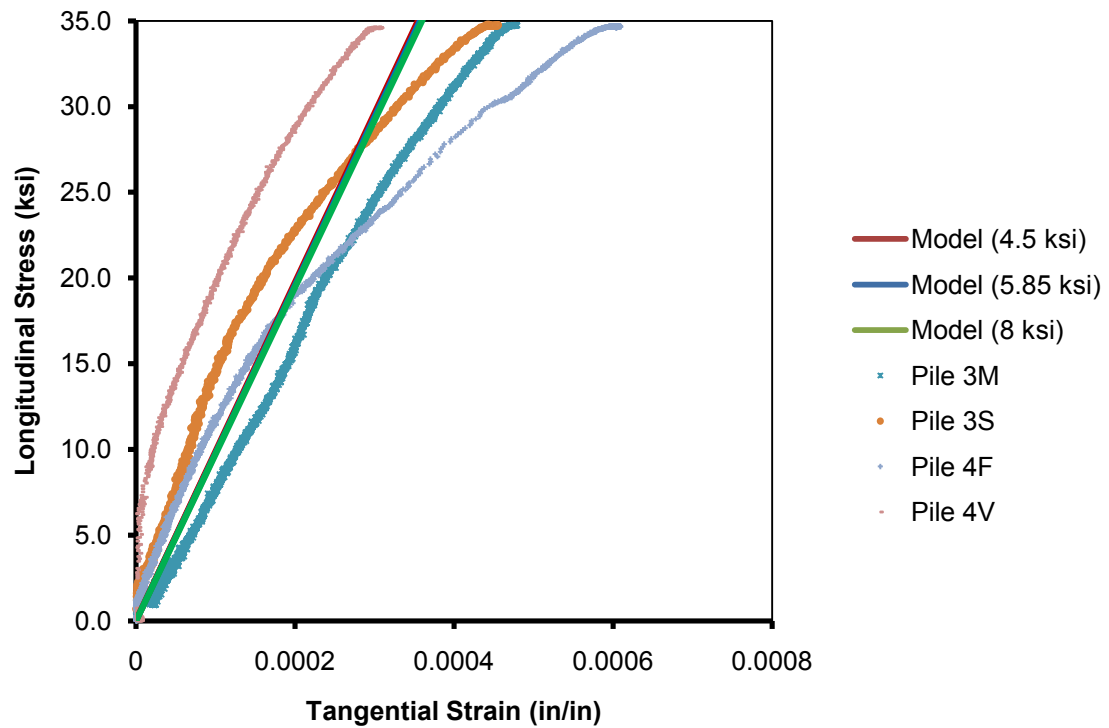


Figure 4.25: Section Core Only Loading – Longitudinal Stress vs. Tangential Strains, 12-³/₄" (0.375" wall)

Figure 4.24 shows the longitudinal strains that were recorded during the testing of the 12- $\frac{3}{4}$ " (0.375" wall) sections. For the loading of the concrete core section, the weld on the steel shell did not appear to affect the strains like when the whole surface was loaded. When only the core was loaded, the recorded strains were larger than zero, however they were not much larger than zero. All the tests experienced similar trends, and the finite element model was able to accurately simulate the fairly linear behavior. The predicted strain was very close to one test trial, however the other three trials all experienced less strains than the model predicted. This seems to be caused by the test of Pile 4V, which had a near linear relationship, whereas each of the other three tests all have a portion of the test where it appears to be non-linear.

Figure 4.25 shows the longitudinal stress versus the tangential strains from the testing. All four trials showed very similar strains in the steel shell, because the steel shell was not loaded. For the 12- $\frac{3}{4}$ " (0.375" wall) the tangential strains are more linear like the 10- $\frac{3}{4}$ " (0.5" wall) specimens. The specimens begin to become non-linear throughout the testing, as the end of the data shows a change in slope with the change in stress. This again could be caused by a softening effect at the higher loads, due to more of the section becoming stressed uniformly. The finite element model again underestimates the amount of strain in some of the samples in the tangential direction under this loading. This again could be attributed to the constraints on the model, being in the Cartesian coordinates and not the radial direction, not allowing the core to displace outward, exerting force into the steel shell.

4.3.4 Summary of Section Core Only Loading

From the testing of the sections under the core only loading, definite trends were observed. For the 10- $\frac{3}{4}$ " (0.375" wall) specimens, the strain response was no longer

near the theoretical yield point of the steel shell in the longitudinal direction as they were when the entire cross section was loaded. The three tests, beside Pile 1C, showed similar elastic moduli between the tests. Pile 1C had a spot with a higher elevation that was leveled before the entire core was loaded, which gave strains around zero until the entire core was loaded. The tangential strains for all the specimens appeared to be non-linear while still in the linear elastic region of loading. As a result the finite element model was unable to simulate the end response because it was a linear-elastic model with linear elastic material properties, however in the lower loads the model was able to predict the strains from the specimens.

For the 10- $\frac{3}{4}$ " (0.5" wall) specimens, the longitudinal and tangential strains were smaller than the thinner (0.375") walled specimens as expected, but were similar to each other in magnitude, approximately 0.0005ϵ at the peak load. This was different from the loading of the whole section, where the tangential strains were much smaller than the longitudinal. This is caused by the steel shell only being loaded by the transfer of forces from the concrete core as it is not being physically loaded by the frame. The finite element model overestimated the amount of strain in the longitudinal and tangential direction under this loading.

The 12- $\frac{3}{4}$ " samples for this loading case actually did show a similar trend to that of the other size test specimens loading in the same manner. For the loading of the core only, the spiral weld did not appear to affect the way the load is transferred through the section. The longitudinal and tangential strains were of almost the same magnitude as those in the 10- $\frac{3}{4}$ " (0.5" wall) samples. The longitudinal strains appeared to mostly be linear, while the tangential strains appeared to be almost completely non-linear. The finite element model was not able to fully simulate the longitudinal or tangential strains

for all three of the sizes, the model underestimated the response in some of the sections.

4.4 Push-Through Testing

This test was designed to determine the strength of the bond between the steel shell and concrete core. If this bond is adequate, composite action would be appropriate for design. This test was intended to determine the load at which the core starts to slide through the steel shell, which is the point at which the bond breaks.

In this test, the load was applied at the same rate as the previous tests, until the load on the section decreased by fifteen percent. The loads versus cross head displacement for the 10- $\frac{3}{4}$ " (0.375" wall), 10- $\frac{3}{4}$ " (0.5" wall), and 12- $\frac{3}{4}$ " (0.375" wall) are presented in Figure 4.26, Figure 4.27, and Figure 4.28, respectively. For all of the 10- $\frac{3}{4}$ " specimens, the behavior is characterized by an increase in load until the bond is broken, followed by a gradual decrease in load as the concrete core pushes through the shell. Due to the spiral welds in the shell of the 12- $\frac{3}{4}$ in. samples, the specimens never reach a maximum load or exhibited a load drop off. Instead the core started to move and then the core came in contact with another weld seam, which was not fully flush on the interior. This caused the load to increase again and then there was another small displacement until the core hits the weld seam again. For all specimens, the bond strength was calculated as the peak load at the initial slip divided by the internal surface area. The average bond strengths for each specimen cross sections is presented in Table 4.5. These values for the bond strengths are on the low end of the bond strengths when compared with previous research, which show that the bond strength can vary from 0.3 ksi to around 2 ksi (Harajli 2004). However the higher bond strengths typically are on ribbed rebar and these pile sections have smooth steel walls.

Some notable findings from these tests were that the bond varied between the sections, the largest section did not have the strongest bond, and the bond varied with depth of the pile. The fact that the largest section did not have the strongest bond could have been due to the weld seam impeding on the contact surface of the materials. Each sample tested was taken from various locations through the depth so that the average bond for the type of shell could be found.

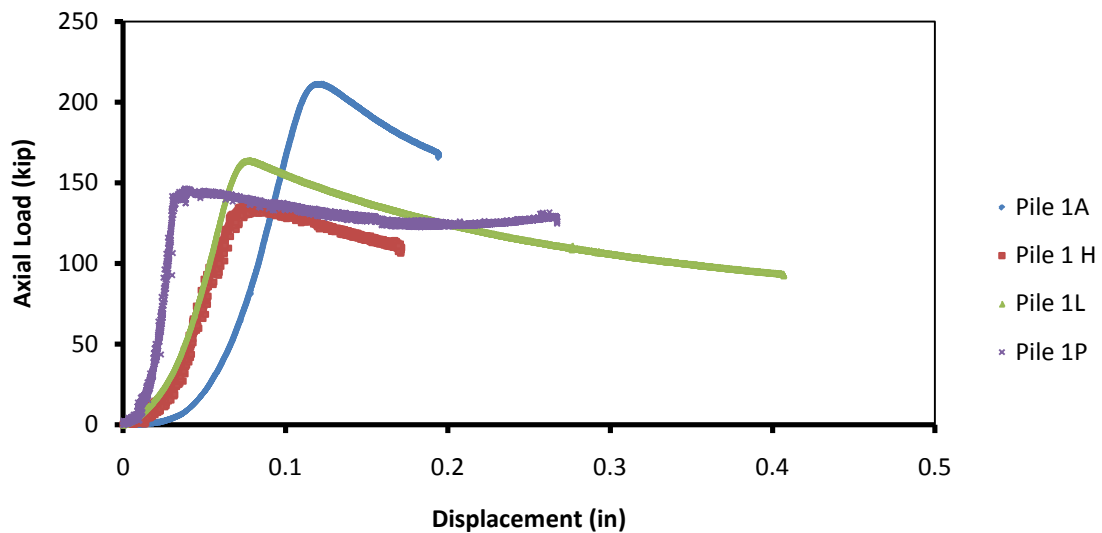


Figure 4.26: Bond Strength – 10-³/₄" (0.375" wall)

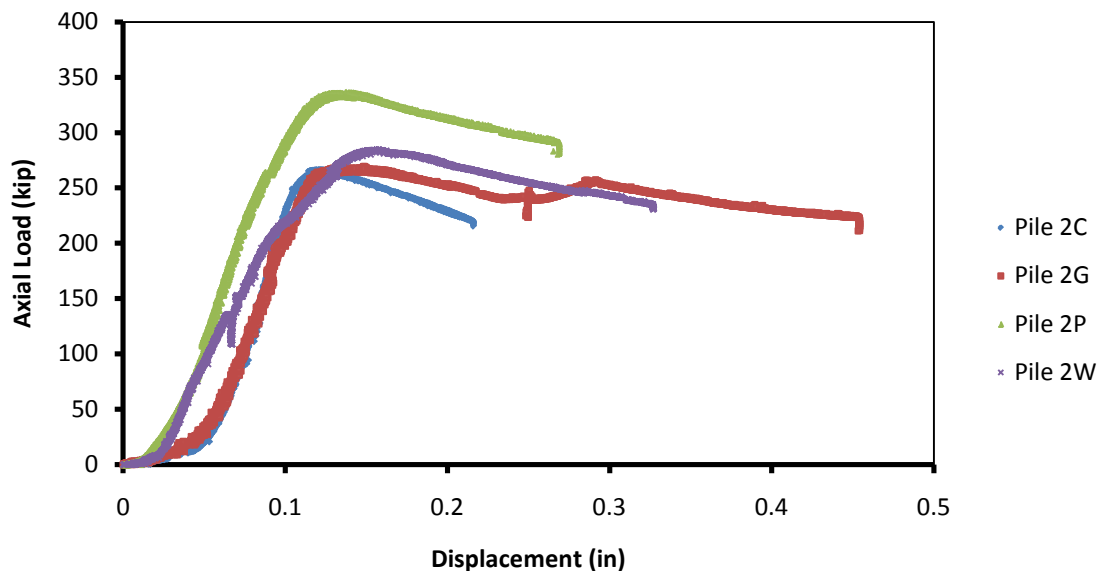


Figure 4.27: Bond Strength – 10-³/₄" (0.5" wall)

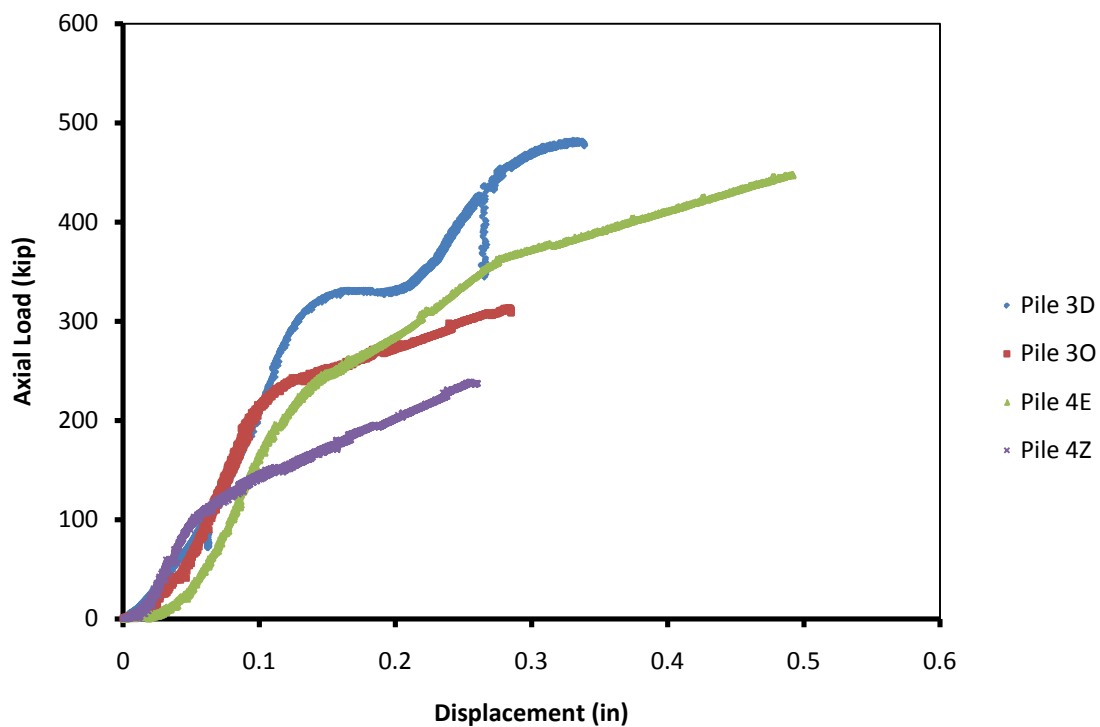


Figure 4.28: Bond Strength – 12- $\frac{3}{4}$ ” (0.375” wall)

**Table 4.5:
Concrete-Steel Bond Strength**

Specimen Name	Depth (ft.)	Pile Size	Bond Strength (ksi)	Average (ksi)
1A	1.5	10- $\frac{3}{4}$ ” (0.375” wall)	0.373	0.291
1H	11.5		0.241	
1L	17.5		0.289	
1P	23		0.259	
2C	4.5	10- $\frac{3}{4}$ ” (0.5” wall)	0.483	0.525
2G	10		0.489	
2P	25.5		0.611	
2W	36		0.517	
3D	5.5	12- $\frac{3}{4}$ ” (0.375” wall)	0.451	0.316
3O	21.5		0.317	
4E	8.5		0.339	
4Z	40		0.157	

4.5 Summary of Analysis

In this section the tests, outlined earlier, were analyzed and compared to the finite element model solutions for the stub-sections under two different types of compression loading. This finite element model comparison included variations in the concrete strength obtained from core testing, along with a revised concrete strength that takes into consideration confinement. The results in this section included the concrete core samples, loading of the entire cross-section, loading of the core section only, and the push-through testing. From the testing, it was observed that the stub pile sections have a greater capacity than the design capacities for both the non-composite and composite section. However, due to the limitations of the testing equipment, the true maximum capacity could not be determined.

5 Conclusion and recommendations

In this study, the structural capacity of cast-in-place steel tubular piling was investigated. Several full length piles were partially driven and filled on-site in as near in-situ conditions as possible. These full length piles were cut up into smaller testable sizes, which also correlate to the short braced lengths for in ground piles. The smaller pile stub sections were run through a set of different tests, with a representative sampling taken from different depths of each pile for each test. The tests included compression tests on the entire stub cross-section, compression tests of the stub section where only the core was loaded, push-through tests, and testing of cored out samples from stub sections. To go along with the testing a linear-elastic finite element model was developed. Through the experimental evaluation of the tested piles stub sections these pile sections are capable of much greater loads than the simplified design equation used by several states. However, due to the limitations in the testing fixtures, a true maximum load and failure mechanism was not found. This research project has led to many interesting conclusions, which are presented below, followed by some possible future work in this area.

5.1 Findings, Observations, and Conclusions

From this research on the pile stub sections, numerous findings, observations, and conclusions were realized. These different developments can be seen in the sections below.

5.1.1 Findings

Some of the findings from this investigation include:

- When loading the entire cross section, there is more strain in the direction of loading, than in the radial direction, due to the load being distributed between both materials.
- When loading only the concrete core, when the steel shell is still present, the radial strains can become greater than those in the direction of loading. As the steel shell is not being loaded in the longitudinal direction like the concrete it would have very little longitudinal strains, however in the tangential direction it would be experiencing the outward force from the concrete core trying to expand radially from the load, while it is compressing.

5.1.2 Observations

Some observations made during this investigation include:

- The thickness of the steel shell wall can vary greatly depending on source and contractor. However most contractors tend to use greater thicknesses than required for ease of drivability.
- Diamond wire-saws are very efficient at cutting through multiple materials, however the saw can leave an end surface with more irregularities, than preferred for testing.
- Even though the concrete core is just dropped down the pile, very few voids were observed in the cut sections.

5.1.3 Conclusions

The following are the conclusions that were reached upon completion of this research:

- From testing of the concrete cores and the concrete cylinders cast on site during the casting of the pile sections, the concrete cores were found to have a compressive strength that is approximately 60% greater than test cylinders cast on site at the same time.
- The concrete strength slightly increases with depth and cross section size, due to the weight of the concrete above it and the confinement from the steel shell not allowing the concrete expand.
- Upon investigation into the design of these types of piles, it was determined that the non-composite section design was typically used as it was simple and the exact mechanics of these pile sections were not fully considered. This non-composite section design netted a capacity for the piling much lower than the tested loads. It should be noted that none of the tested sections failed, and the majority of the sections did not leave the linear elastic range.
- The way the steel shell is fabricated can modify the way the shell transmits the loading through itself, as was seen in the pile sections with the spiral seam. These sections produced much lower strains than the sections with the seam running concurrently with the loading.
- The bond strength (300psi-500psi) in these sections is on the low end of the average bond strength for concrete and steel as determined by other researchers. However due to the surface of the materials neither having modifications to increase the bond, like the ribs on rebar, this average was adequate.

5.2 Recommendations

While numerous finding, observations, and conclusions were drawn from this study, even more questions were brought up by the testing. Some future suggestions for further investigations are presented in this section.

There should be more testing done on these cross sections and other similar cross sections to develop an even better understanding of many different mechanics and reactions of the sections. One future test could be to find the true axial capacity, in different loading configurations. This testing would be beneficial in that a true capacity could be found along with the general failure methods of the different cross sections types and loading configurations. This test would also be another way to verify that full composite section design should be done on these types of piles, if the soil could support it. Also many different cross sections are available and should also be tested to give a better understanding of how all of the different wall thicknesses and outer diameters can control the overall capacity and failure mode of the pile sections. This could give designers the knowledge of what to expect out of each different size before ever choosing one for design. Additional testing of just the steel shell would provide a better understanding of the failure mechanism of the composite system.

For any of the future testing it would be recommended to look into a different cutting method, or advance the diamond wire sawing. This would provide a much better testing surface and there would be fewer irregularities in the samples that need to be accounted for in the test data and the testing would run much smoother. The diamond wire saw worked fairly well for this testing, however the top surface was not always the most planar surface. And to better understand the transfer of the loading through the sections more instrumentation could be used along with imbedding some sensors into the concrete during the casting. These additional sensors could give another

perspective on the transfer of the forces through the sections along with how the concrete core acts without relation to the steel shell.

Also there are many improvements and advancements that could be done to the finite element model that was created as part of this research project. To better account for the way the stub sections are truly constrained a model that is developed in the polar coordinate system would be best. By modeling in this manner, the constraints can better match the actual, along with a better mapped mesh is possible. With the model developed in the Cartesian coordinates, a mapped mesh with rectangular elements is not easily created. This type of mesh is preferred by most users and typically found to give the most accurate results. An advancement that could be made to either model would be to add in a contact element between the two materials. This element could add in the friction between the surfaces, along with different stages of interaction between the materials under different loads.

Another major task that could be done would be to expand the stub section model to a full length section. In this model, the advancements mentioned previously could be beneficial. With a model of the full length pile, different soils could be modeled around the pile to develop a capacity based on the soil the pile is in and the material properties of the concrete and steel used in the pile. One way to model the soil interaction with the pile shell would be to use springs along the length and at the base. For the spring values the modulus of subgrade reaction could be used, however it is typically used for shallow foundations.

Bibliography

American Association of State Highway and Transportation Officials (AASHTO). 2010. AASHTO LRFD Bridge Design Specifications. Washington D.C.: AASHTO.

American Concrete Institute. 2008. Building Code Requirements for Structural Concrete (ACI 318-08) and Commentary. Farmington Hills, MI: American Concrete Institute.

American Institute of Steel Construction Inc. 2005. Steel Construction Manual. Chicago, IL: American Institute of Steel Construction Inc.

ANSYS. 2009. ANSYS® Academic Research, Release 12.0. Canonsburg, PA.

ASTM Standard C31. 2003. Standard Practice for Making and Curing Concrete Test Specimens in the Field. West Conshohocken, PA: ASTM International.

Baig M-N, Fan J, and Nie J. 2006. Strength of Concrete Filled Steel Tubular Columns. Tsinghua Science & Technology 11(6):657-666.

Choi K, and Xiao Y. 2009. Analytical Studies of Concrete-Filled Circular Steel Tubes under Axial Compression. Journal of Structural Engineering.

Coduto D. 2001. Foundation Design Principles and Practices. Upper Saddle River, New Jersey: Prentice Hall.

Fujimoto T, Mukai A, Nishiyama I, and Sakino K. 2004. Behavior of Eccentrically Loaded Concrete-Filled Steel Tubular Columns. Journal of Structural Engineering 130(2):203-212.

Gilbert R, Najjar S, and Choi Y. Incorporating Lower-Bound Capacities into LRFD Codes for Pile Foundations. LRFD and Reliability Based Design for Deep Foundations; 2005; Austin, TX: ASCE. p. 2-2.

Gupta P, Sarda S, and Kumar M. 2007. Experimental and computational study of concrete filled steel tubular columns under axial loads. Journal of Constructional Steel Research 63(2):182-193.

- Harajli M. 2004. Comparison of Bond Strength of Steel Bars in Normal- and High-Strength Concrete. *Journal of Materials in Civil Engineering* 16(4):365-374.
- Hu H-T, Huang C-S, Wu M-H, and Wu Y-M. 2003. Nonlinear Analysis of Axially Loaded Concrete-Filled Tube Columns with Confinement Effect. *Journal of Structural Engineering* 129(10):1322-1329.
- Lam D, and Wong K. Axial Capacity of Concrete Filled Stainless Steel Columns. *Design and Analysis*; 2005; New York, NY: ASCE. p. 105.
- O'Shea M, and Bridge R. 2000. Design of Circular Thin-Walled Concrete Filled Steel Tubes. *Journal of Structural Engineering* 126(11):1295-1303.
- Schneider S. 1998. Axially Loaded Concrete-Filled Steel Tubes. *Journal of Structural Engineering* 124(10):1125-1138.
- Vable M. 2002. *Mechanics of Materials*. New York, NY: Oxford University Press.
- Wisconsin Department of Transportation. 2005. *Wisconsin Highway Construction Specifications*. Wisconsin Department of Transportation.
- Yamamoto T, Kawaguchi J, and Morino S. Experimental Study of Scale Effects on the Compressive Behavior of Short Concrete-Filled Steel Tube Columns. *International Symposium on Advances and Trends in Composite Construction for Building Structures*; 2000; Banff, Alberta, Canada: ASCE. p. 76.

Appendix A – Core Sample Test Data

Table A.1:
Core sample test data

Pile Section	CORE NUMBER	CUT LENGTH (in)	LOAD (LBS)	Pressure (PSI)	Comments
1 B	1	8 1/16	77318	6163	Approx. 5% of surface area has voids; total conical failure from bottom
1 B	2	7 5/8	67558	5399	Approx. 5% of surface area has voids; side sheer, bottom to top
1 B	3	8 1/16	81066	6461	Conical sheer throughout, total failure (exploded)
1 E	1	8	99567	7899	Shear Plane at 45d through middle
1 E	2	8	104058	8251	Shear Plane at approx. 30d from bottom to middle
1 E	3	6 11/16	101179	8025	Broke out of core short, cut on both ends until even; S.P same as previous
1 I	1				Broke Short
1 I	2				Broke Short
1 I	3				Broke Short
1 N	1	8	107420	8520	Conical shear throughout
1 N	2	8	114048	9033	Conical shear throughout
1 N	3	8	123982	9803	Conical shear throughout
1 Q	1	8 1/16	107568	8544	Total conical shear (exploded)
1 Q	2	8 1/16	84854	6754	Conical shear throughout
1 Q	3	8 1/8	95277	7559	Conical shear, bottom to middle, slight

Table A.1, continued

Pile Section	CORE NUMBER	CUT LENGTH (in)	LOAD (LBS)	Pressure (PSI)	Comments
2 D	1	8 inches	118510	9367	Shear Plane vertical down middle
2 D	2	7 7/8 inches	92731	7356	Slight aggregate breakage on one end (<1/4"); Conical shear throughout
2 Q	1	8 1/16 inches	105758	8365	Total conical shear (exploded)
2 Q	2	8 1/8 inches	96196	7553	Slight agg. Breakage at Top, <1/4"; conical shear, total failure (exploded)
2 Q	3	8 inches	97242	7708	Total conical shear (exploded)
2 U	1	8 1/16 inches	100947	7995	Slight agg. Breakage at Top, <1/4"; conical shear, total failure (exploded)
2 U	2	8 inches	93308	7392	Slight agg. Breakage at Top, <1/4"; conical shear, total failure (exploded)
2 U	3	8 1/8 inches	99108	7875	Total conical shear (exploded)
2 X	2	8 inches	122436	9677	Conical shear plane, fractured in middle
2 X	1	8 inches	115731	9176	Shear plane conical; complete failure (exploded)
3 F	1	7 13/16 inches	99540	7905	Slight shear at top to middle; conical
3 F	2	8 1/16 inches	102552	8144	Conical shear, more through middle (vertical)
3 F	3	8 inches	103752	8245	Perfect conical shear
3 F	4	6 7/8 inches	105437	8365	Broke short, cut to longest possible even length; bottom to middle shear
3 K	1				Broke Short
3 K	2				Broke Short

Table A.1, continued

Pile Section	CORE NUMBER	CUT LENGTH (in)	LOAD (LBS)	Pressure (PSI)	Comments
3 K	3				Broke Short
3 K	4				Broke Short
3P	1				Broke Short
3P	2				Broke Short
3P	3				Broke Short
3P	4				Broke Short
3 R	1	8 inches	82416	6545	Conical shear top to middle
4 D	1	8 inches	70624	5638	Approximately 5% of surface area has air voids
4 D	2	8 inches	94634	7517	Shear Plane at 45d through middle
4 D	3	8 inches	76940	6115	Conical shear bottom to middle
4 D	4	8 inches	92703	7362	Conical shear throughout (hour glass shaped break)
4 G	1	8 inches	82710	6569	Total conical failure (exploded)
4 G	2	8 inches	84903	6742	Slight agg. Breakage on one end, <1/4"; surface voids on approx. 5% of surface; complete conical failure
4 G	3	8 1/8 inches	76748	6121	Conical shear, top to middle
4 G	4	8 1/8 inches	83034	6605	Conical shear, bottom to middle
4 Q	1				Broke Short

Table A.1, continued

Pile Section	CORE NUMBER	CUT LENGTH (in)	LOAD (LBS)	Pressure (PSI)	Comments
4 Q	2				Broke Short
4 Q	3				Broke Short
4 Q	4				Broke Short
4 U	1	8 1/16" inches	74749	5966	Slight agg. Breakage on one end, <1/4"; surface voids on approx. 2% of surface; conical shear top to middle
4 U	2	8 1/8 inches	104161	8263	Conical shear bottom to middle
4 U	3	8 inches	89710	7130	Conical shear top to bottom
4 U	4	8 1/8 inches	87241	6933	Slight conical shear bottom to middle - approx. 3" up, 1/2" in from edge
4 Y	1	8 inches	111625	8764	Conical failure
4 Y	2	8 1/8 inches	101956	7965	Conical failure
4 Y	4	8 1/8 inches	100121	7857	Conical fracture, top to bottom

Appendix B – Additional Compression Data

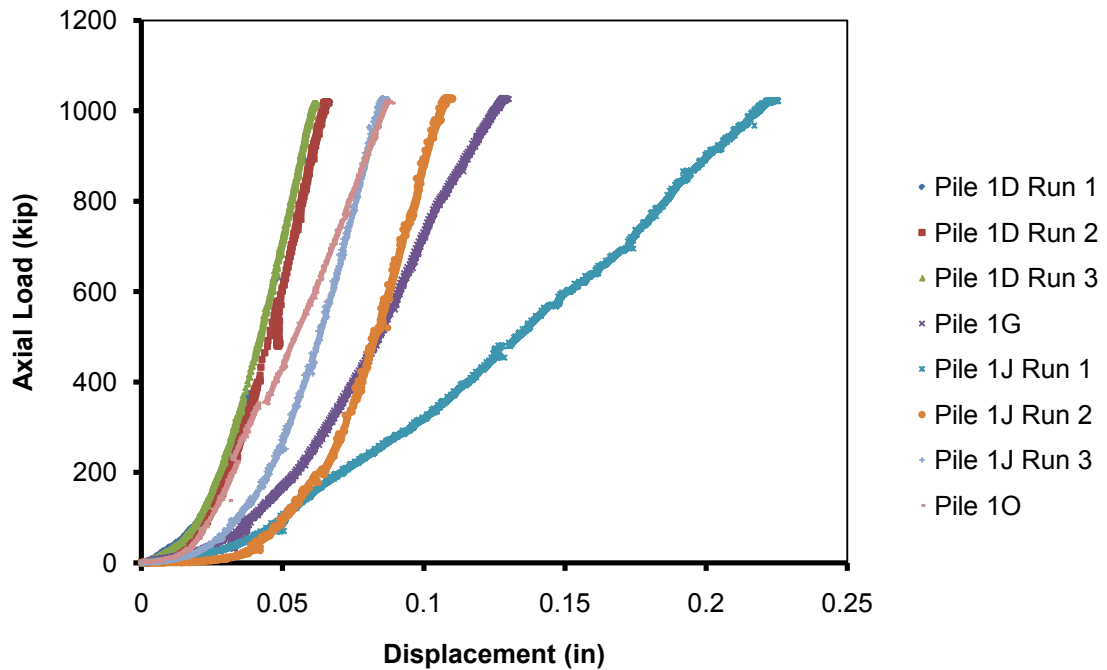


Figure B.1: Full Cross Section Loading – Axial Load vs. Displacement, 10-³/₄" (0.375" wall)

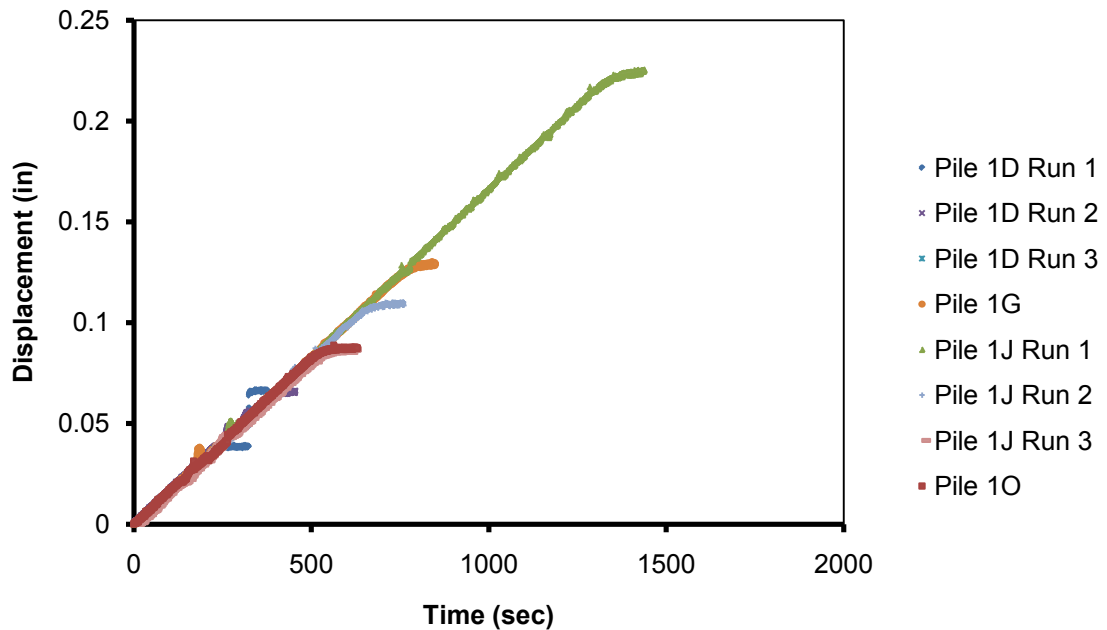


Figure B.2: Full Cross Section Loading - Displacements, 10-³/₄" (0.375" wall)

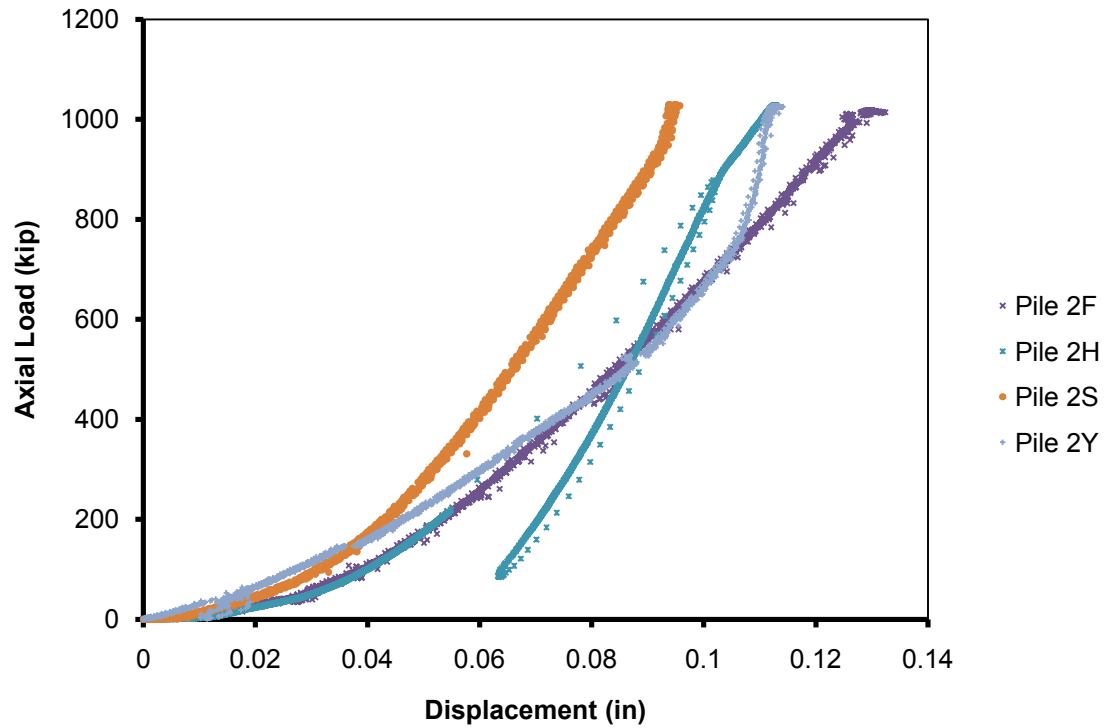


Figure B.3: Full Cross Section Loading – Axial Load vs. Displacement, 10-³/₄" (0.5" wall)

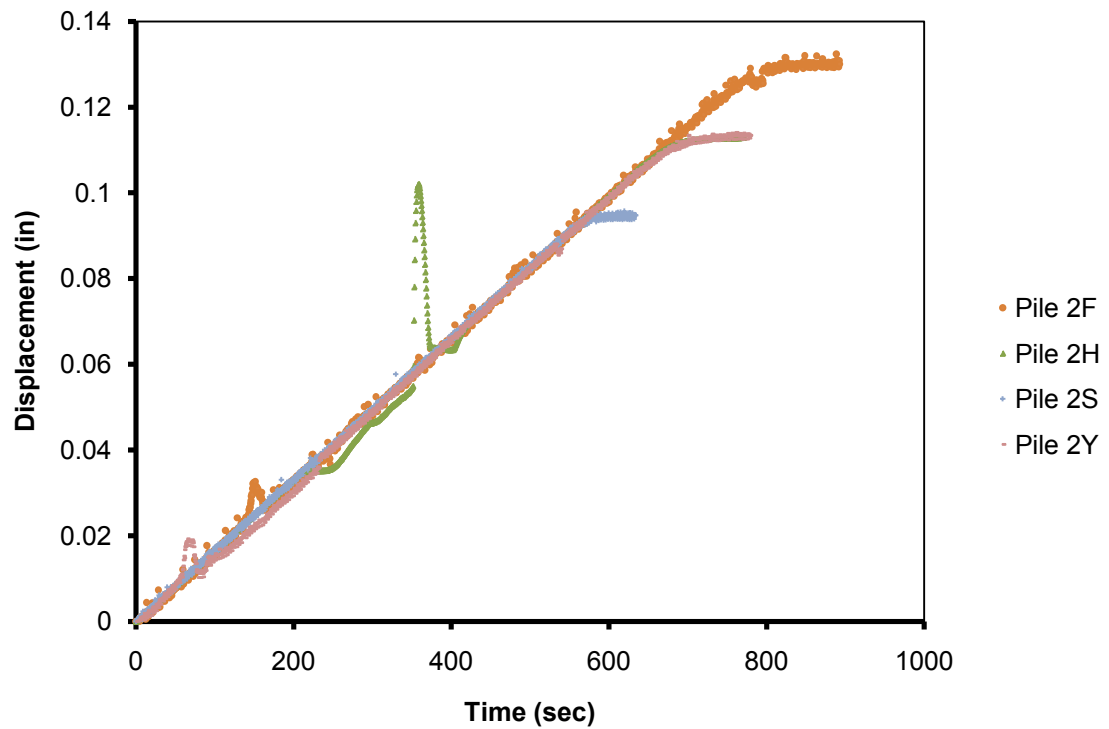


Figure B.4: Full Cross Section Loading – Displacements, 10-³/₄" (0.5" wall)

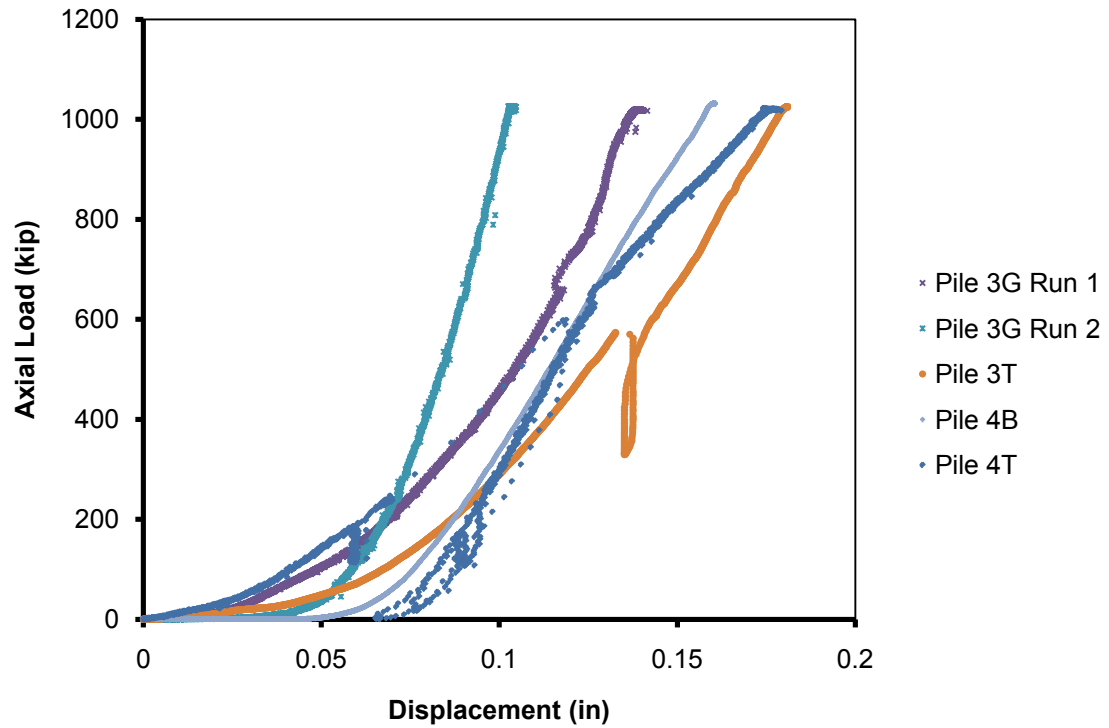


Figure B.5: Full Cross Section Loading – Axial Load vs. Displacement, 12-³/₄" (0.375" wall)

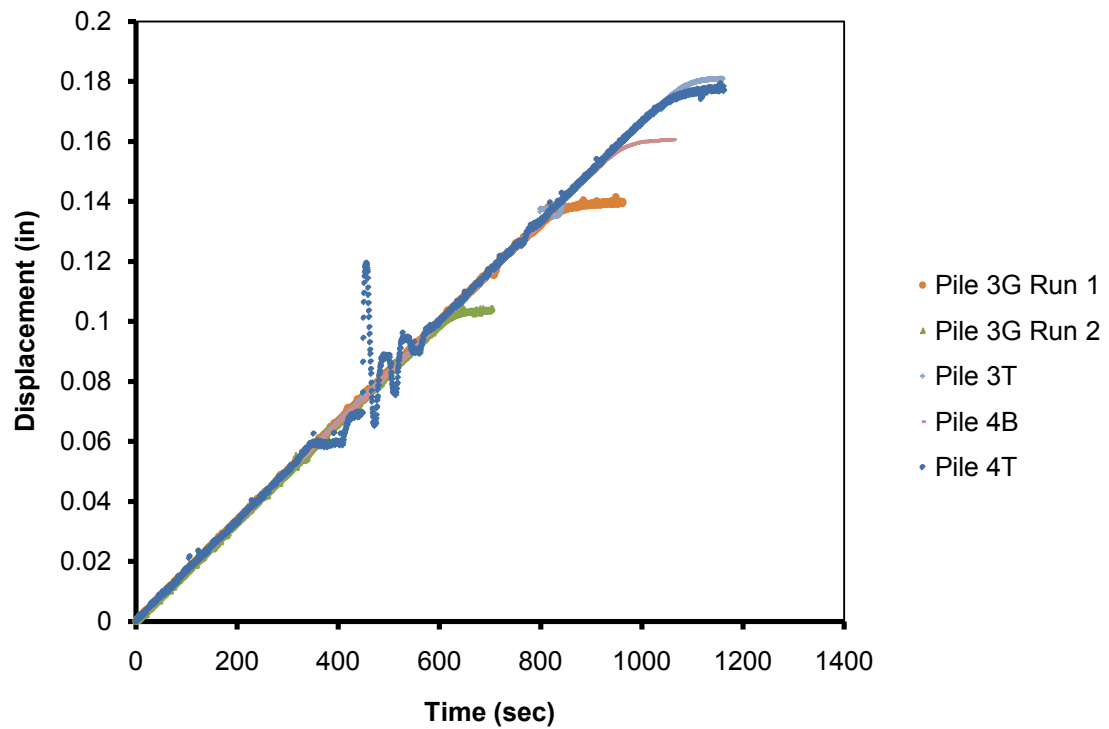


Figure B.6: Full Cross Section Loading – Displacements, 12-³/₄" (0.375" wall)

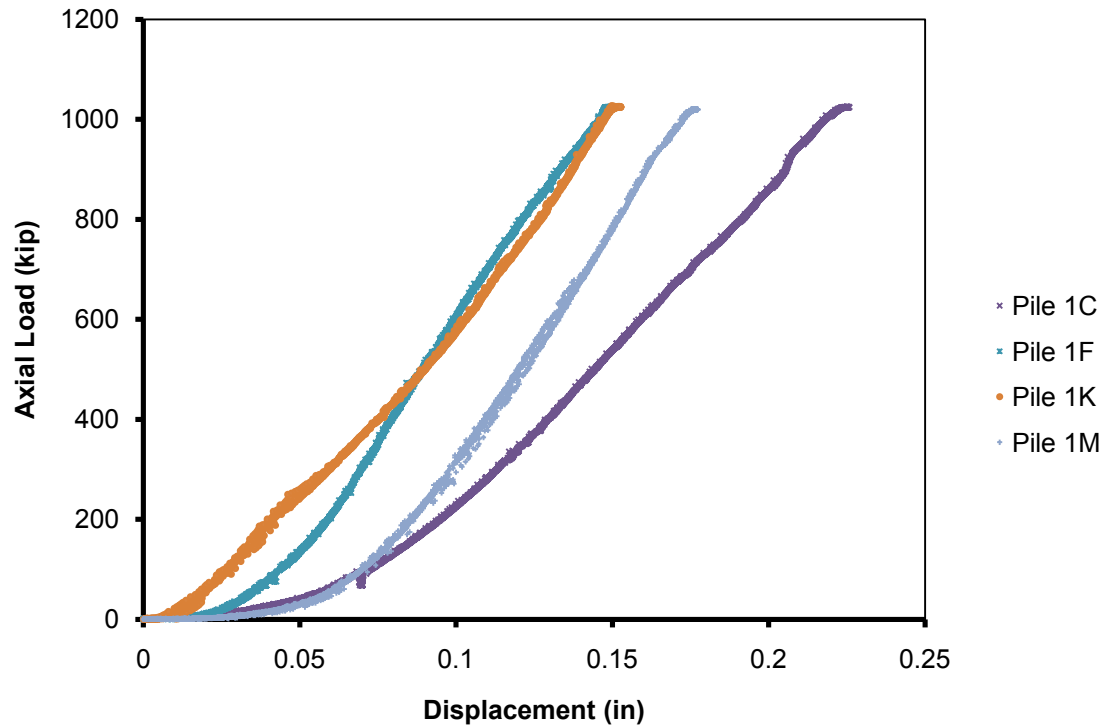


Figure B.7: Section Core Only Loading – Axial Load vs. Displacement, 10^{-3/4}" (0.375" wall)

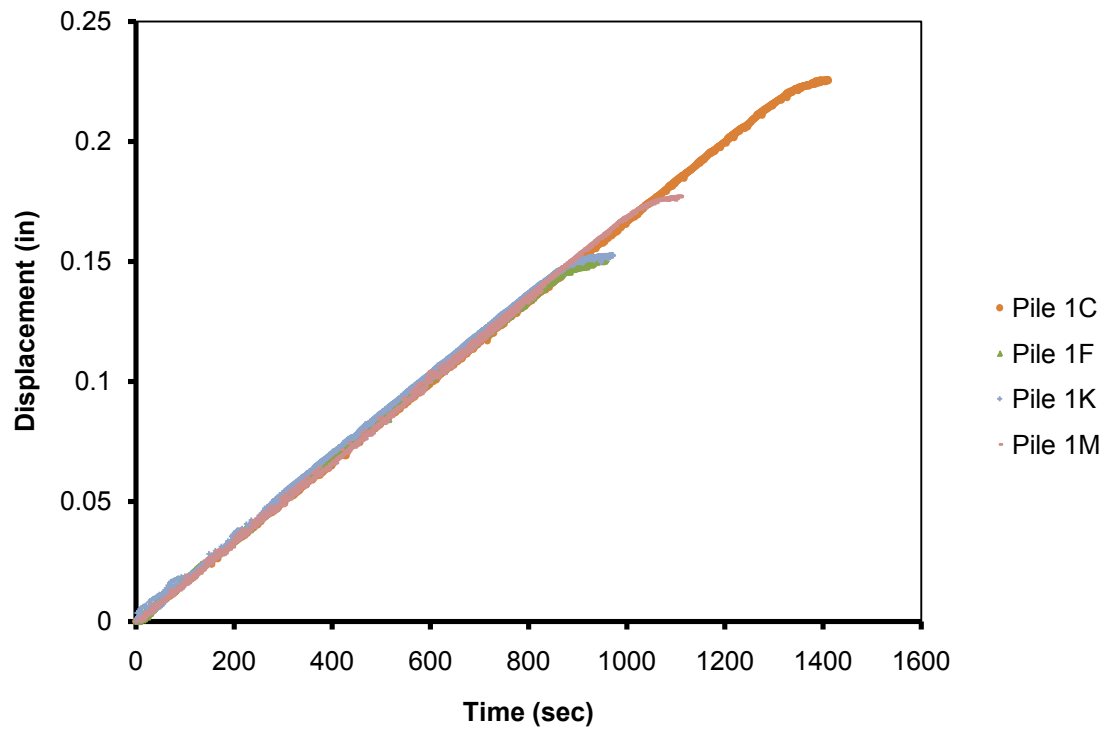


Figure B.8: Section Core Only Loading – Displacements, 10^{-3/4}" (0.375" wall)

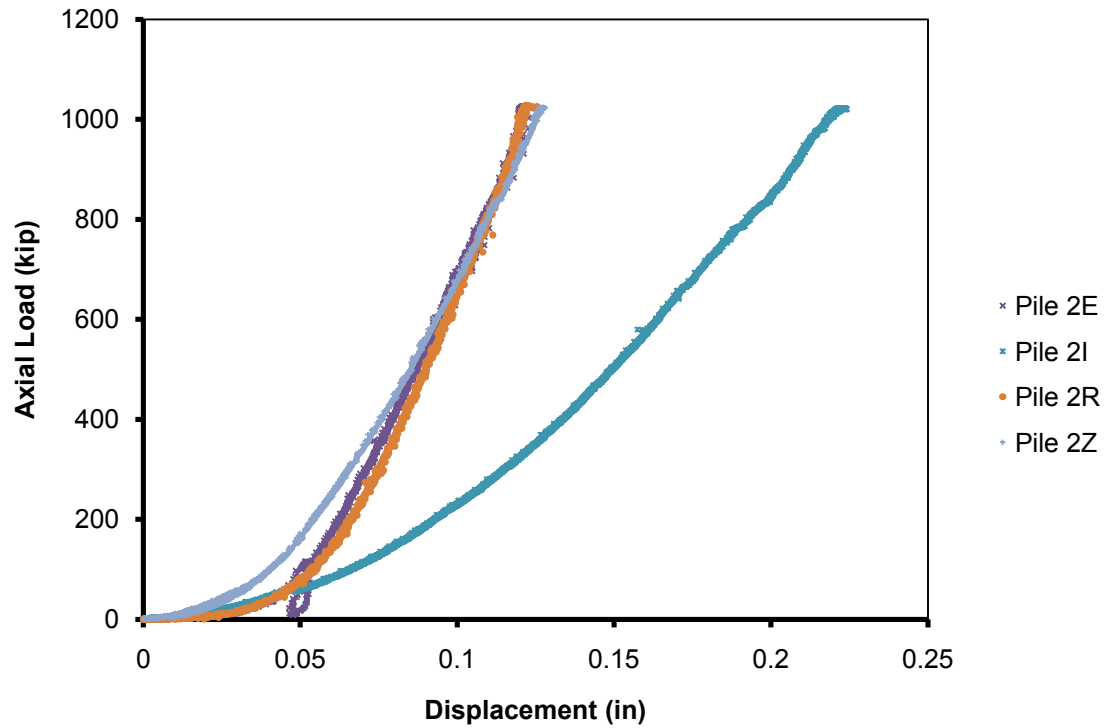


Figure B.9: Section Core Only Loading – Axial Load vs. Displacement, 10-³/₄" (0.5" wall)

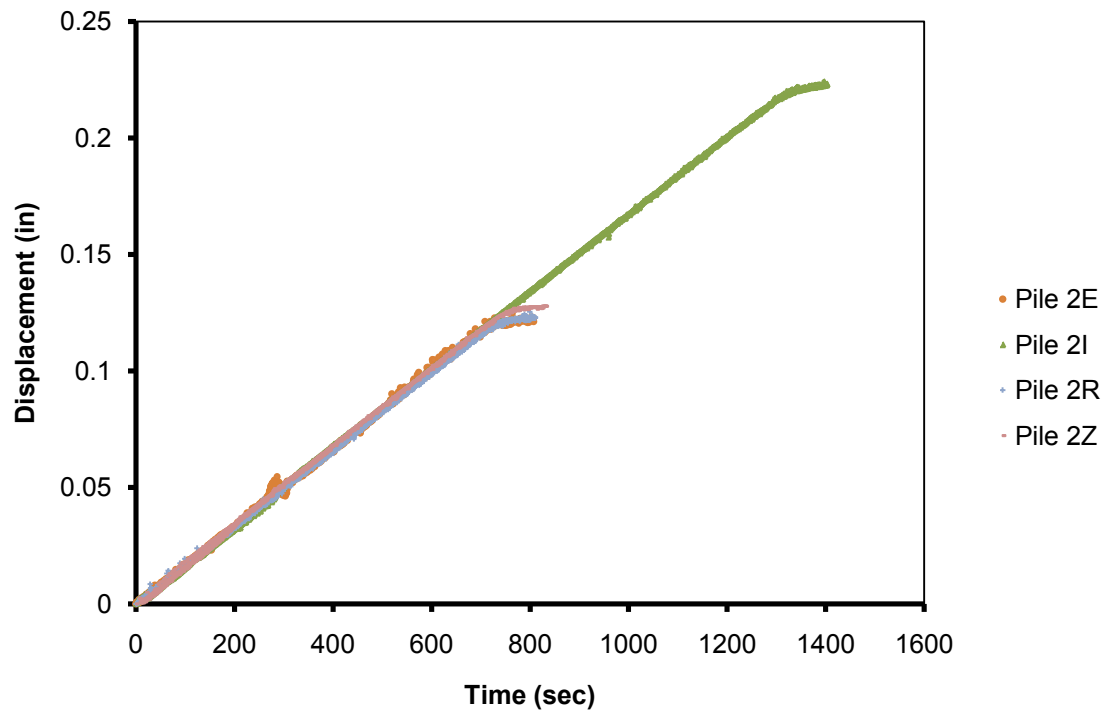


Figure B.10: Section Core Only Loading – Displacements, 10-³/₄" (0.5" wall)

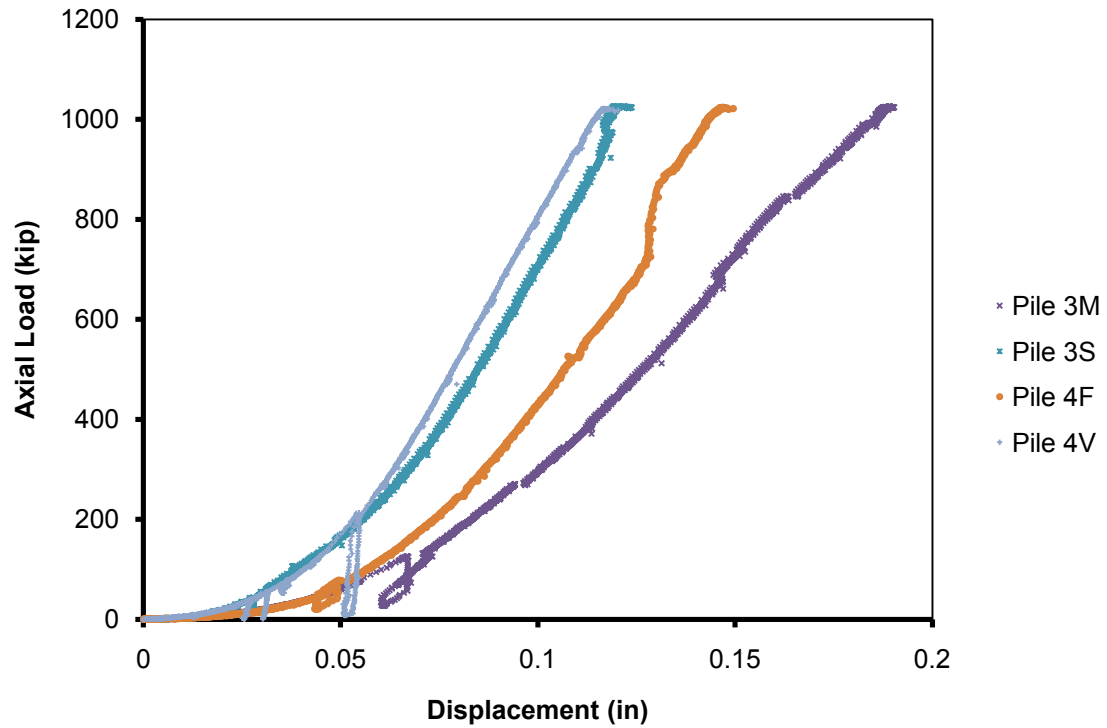


Figure B.11: Section Core Only Loading – Axial Load vs. Displacement, 12-³/₄" (0.375" wall)

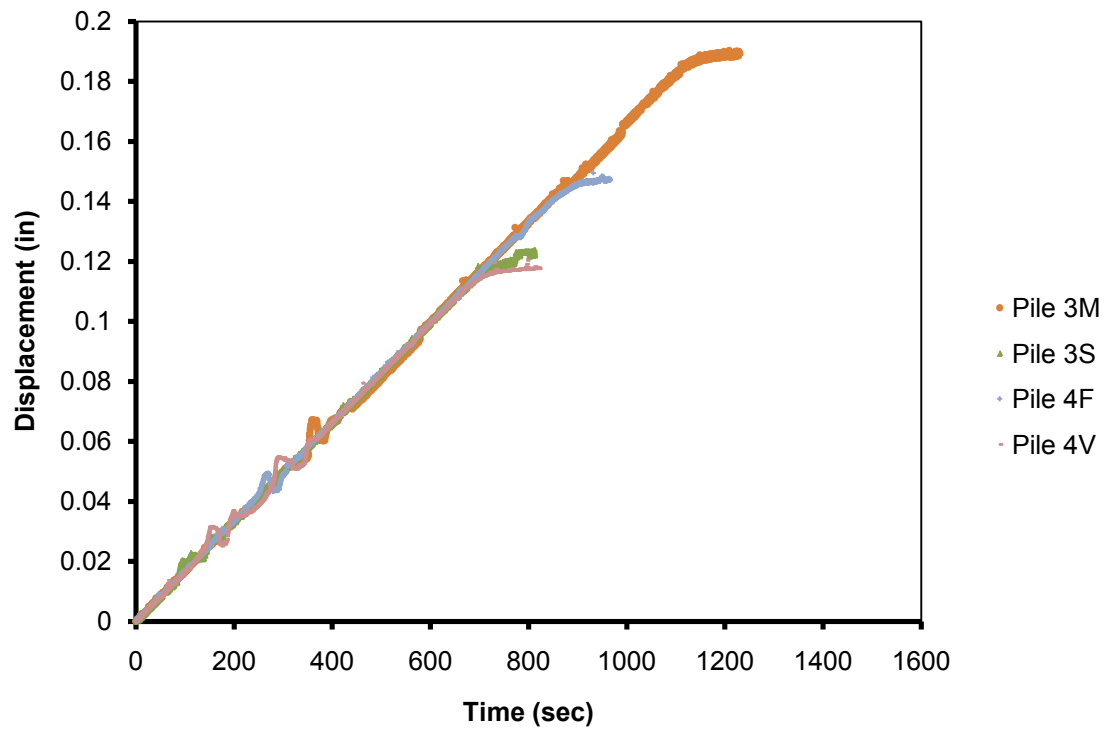


Figure B.12: Section Core Only Loading – Displacements, 12-³/₄" (0.375" wall)

Appendix C – Calculations

C.1 Transformed Section Calculations

$$f_c := 4.5 \frac{\text{kip}}{\text{in}^2} \quad \text{Concrete Compressive Strength}$$

$$E_s := 29000 \frac{\text{kip}}{\text{in}^2} \quad \text{Modulus of elasticity of the steel}$$

$$E_c := 57000 \sqrt{\frac{\text{lb}}{\text{in}^2}} \sqrt{f_c} = 3.824 \times 10^3 \frac{\text{kip}}{\text{in}^2} \quad \text{Modulus of elasticity of the concrete}$$

$$n := \frac{E_s}{E_c} = 7.584 \quad \text{Modular ratio}$$

Transformed area to an effective steel area

10-3/4" (0.375" wall)

$$\left[\frac{(10.75\text{in})^2 \pi}{4} - \frac{(10\text{in})^2 \pi}{4} \right] + \frac{\frac{(10\text{in})^2 \cdot \pi}{4}}{n} = 22.578 \cdot \text{in}^2$$

10-3/4" (0.5" wall)

$$\left[\frac{(10.75\text{in})^2 \pi}{4} - \frac{(9.75\text{in})^2 \pi}{4} \right] + \frac{\frac{(9.75\text{in})^2 \cdot \pi}{4}}{n} = 25.945 \cdot \text{in}^2$$

12-3/4" (0.375" wall)

$$\left[\frac{(12.75\text{in})^2 \pi}{4} - \frac{(12\text{in})^2 \pi}{4} \right] + \frac{\frac{(12\text{in})^2 \cdot \pi}{4}}{n} = 29.491 \cdot \text{in}^2$$

C.2 Transformed Section Example

Example

10-3/4" (0.375" wall)

$$P := 1000 \text{ kip}$$

Applied Load

$$A_c := \frac{(10 \text{ in})^2 \cdot \pi}{4} = 78.54 \cdot \text{in}^2$$

Area of concrete core

$$A_{cs} := \frac{\frac{(10 \text{ in})^2 \cdot \pi}{4}}{n} = 10.356 \text{ in}^2$$

Area of concrete core transformed to equivalent steel

$$\frac{\frac{P}{A_c}}{E_c} = 3.33 \times 10^{-3}$$

Strain in concrete core

$$\frac{\frac{P}{A_{cs}}}{E_s} = 3.33 \times 10^{-3}$$

Strain in equivalent steel section

C.3 10^{-3/4}” (0.375” wall) Member Capacities

$$d_p := 10.75 \cdot \text{in}$$

$$w_t := .375 \text{in}$$

Member Sizing

$$d_c := d_p - 2w_t$$

Diameter of the concrete core

$$d_r := 0 \cdot \text{in}$$

Diameter of the reinforcement

$$l := 1.5 \cdot \text{ft}$$

Unbraced length of member

General Material Properties

$$f_c := 4.5 \cdot \frac{\text{kip}}{\text{in}^2}$$

Strength of the concrete

$$f_y := 55 \cdot \frac{\text{kip}}{\text{in}^2}$$

Strength of the steel

$$f_{pe} := 0 \cdot \frac{\text{kip}}{\text{in}^2}$$

Effective stress in prestressing steel after loss

$$f_{yr} := 60 \cdot \frac{\text{kip}}{\text{in}^2}$$

Yield strength of the steel reinforcement

$$E := 29000 \cdot \frac{\text{kip}}{\text{in}^2}$$

Modulus of elasticity of the steel

$$E_c := 57000 \sqrt{\frac{\text{lb}}{\text{in}^2}} \sqrt{f_c} = 3.824 \times 10^3 \frac{\text{kip}}{\text{in}^2}$$

Modulus of elasticity of the concrete

$$E_p := 0 \cdot \frac{\text{kip}}{\text{in}^2}$$

Modulus of elasticity of prestressing tendons

$$\epsilon_{cu} := .003$$

Failure strain in concrete in compression

$$n := \frac{E}{E_c} \quad n = 7.584$$

Modular ratio

$$K := 1.0$$

Effective length factor

$$r := \sqrt{\frac{d_c^2 + d_p^2}{2}} \quad r = 10.382 \cdot \text{in}$$

Radius of gyration for the steel shell

Longitudinal Reinforcement

$$d_b := 0 \cdot \text{in}$$

Diameter of the reinforcement

$$N_b := 0$$

Number of reinforcing bars

Prestressing Steel

$$d_{ps} := 0 \cdot \text{in}$$

Diameter of the prestressing

Area Calculations

$$A_g := \frac{\pi \cdot d_p^2}{4}$$

$$A_g = 90.763 \cdot \text{in}^2$$

Gross Area of the pile

$$A_c := \frac{\pi \cdot d_c^2}{4}$$

$$A_c = 78.54 \cdot \text{in}^2$$

Area of the concrete

$$A_s := A_g - A_c$$

$$A_s = 12.223 \cdot \text{in}^2$$

Area of the steel shell

$$A_r := \frac{\pi \cdot d_r^2}{4} \cdot N_b$$

$$A_r = 0$$

Area of the reinforcing steel

$$A_{ps} := \frac{\pi \cdot d_{ps}^2}{4}$$

$$A_{ps} = 0$$

Area of the prestressing

LRFD Axial Load Capacity Calculations

$$P_n := .80 \cdot \left[.85 \cdot f_c \cdot (A_c - A_r) + f_y \cdot A_r - A_{ps} \cdot (f_{pe} - E_p \cdot \varepsilon_{cu}) \right]$$

$$P_n = 240.332 \cdot \text{kip}$$

$$P_n = 120.166 \cdot \text{ton}$$

Nominal Axial resistance without flexure

Factored Axial Load Capacity

$$\phi := .75$$

$$P_r := \phi \cdot P_n$$

$$P_r = 180.249 \cdot \text{kip}$$

$$P_r = 90.124 \cdot \text{ton}$$

Factored Axial resistance without flexure

LRFD Composite Section Axial Load Calculations

$$E_e := E \cdot \left(1 + \frac{.40}{n} \cdot \frac{A_c}{A_s} \right)$$

$$E_e = 3.883 \times 10^4 \cdot \frac{\text{kip}}{\text{in}^2}$$

$$F_e := f_y + 1.00 \cdot f_{yr} \cdot \frac{A_r}{A_s} + .85 \cdot f_c \cdot \frac{A_c}{A_s}$$

$$F_e = 79.578 \cdot \frac{\text{kip}}{\text{in}^2}$$

$$\lambda := \left(\frac{K \cdot l^2}{r \cdot \text{ft} \cdot \pi} \right)^2 \frac{F_e}{E_e}$$

$$\lambda = 1.405 \times 10^{-3}$$

$$\frac{K \cdot l}{r} = 1.734$$

If $\lambda < 2.25$

$$P_{n1} := .66^{\lambda} \cdot F_e \cdot A_s \quad P_{n1} = 972.099 \cdot \text{kip} \quad P_{n1} = 486.05 \cdot \text{ton} \quad \text{Nominal Axial resistance}$$

If $\lambda > 2.25$

$$P_{n2} := \frac{.88 \cdot F_e \cdot A_s}{\lambda} \quad P_{n2} = 6.094 \times 10^5 \cdot \text{kip} \quad P_{n2} = 3.047 \times 10^5 \cdot \text{ton}$$

Factored Axial Load Capacity

$$\phi := .75$$

$$P_n := \begin{cases} P_{n1} & \text{if } \lambda < 2.25 \\ P_{n2} & \text{otherwise} \end{cases}$$

$$P_n = 972.099 \cdot \text{kip}$$

$$P_r := \phi \cdot P_n$$

$$P_r = 729.074 \cdot \text{kip} \quad P_r = 364.537 \cdot \text{ton} \quad \text{Factored Axial resistance}$$

C.4 10^{-3/4}” (0.5” wall) Member Capacities

$$d_p := 10.75 \cdot \text{in}$$

$$w_t := .5 \text{in}$$

Member Sizing

$$d_c := d_p - 2w_t$$

Diameter of the concrete core

$$d_r := 0 \cdot \text{in}$$

Diameter of the reinforcement

$$l := 1.5 \cdot \text{ft}$$

Unbraced length of member

General Material Properties

$$f_c := 4.5 \cdot \frac{\text{kip}}{\text{in}^2}$$

Strength of the concrete

$$f_y := 55 \cdot \frac{\text{kip}}{\text{in}^2}$$

Strength of the steel

$$f_{pe} := 0 \cdot \frac{\text{kip}}{\text{in}^2}$$

Effective stress in prestressing steel after loss

$$f_{yr} := 60 \cdot \frac{\text{kip}}{\text{in}^2}$$

Yield strength of the steel reinforcement

$$E := 29000 \cdot \frac{\text{kip}}{\text{in}^2}$$

Modulus of elasticity of the steel

$$E_c := 57000 \sqrt{\frac{\text{lb}}{\text{in}^2}} \sqrt{f_c} = 3.824 \times 10^3 \frac{\text{kip}}{\text{in}^2}$$

Modulus of elasticity of the concrete

$$E_p := 0 \cdot \frac{\text{kip}}{\text{in}^2}$$

Modulus of elasticity of prestressing tendons

$$\epsilon_{cu} := .003$$

Failure strain in concrete in compression

$$n := \frac{E}{E_c} \quad n = 7.584$$

Modular ratio

$$K := 1.0$$

Effective length factor

$$r := \sqrt{\frac{d_c^2 + d_p^2}{2}} \quad r = 10.262 \cdot \text{in}$$

Radius of gyration for the steel shell

Longitudinal Reinforcement

$$d_b := 0 \cdot \text{in}$$

Diameter of the reinforcement

$$N_b := 0$$

Number of reinforcing bars

Prestressing Steel

$$d_{ps} := 0 \cdot \text{in}$$

Diameter of the prestressing

Area Calculations

$$A_g := \frac{\pi \cdot d_p^2}{4}$$

$$A_g = 90.763 \cdot \text{in}^2$$

Gross Area of the pile

$$A_c := \frac{\pi \cdot d_c^2}{4}$$

$$A_c = 74.662 \cdot \text{in}^2$$

Area of the concrete

$$A_s := A_g - A_c$$

$$A_s = 16.101 \cdot \text{in}^2$$

Area of the steel shell

$$A_r := \frac{\pi \cdot d_r^2}{4} \cdot N_b$$

$$A_r = 0$$

Area of the reinforcing steel

$$A_{ps} := \frac{\pi \cdot d_{ps}^2}{4}$$

$$A_{ps} = 0$$

Area of the prestressing

LRFD Axial Load Capacity Calculations

$$P_n := .80 \cdot \left[.85 \cdot f_c \cdot (A_c - A_r) + f_y \cdot A_r - A_{ps} \cdot (f_{pe} - E_p \cdot \varepsilon_{cu}) \right]$$

$$P_n = 228.465 \cdot \text{kip}$$

$$P_n = 114.233 \cdot \text{ton}$$

Nominal Axial resistance without flexure

Factored Axial Load Capacity

$$\phi := .75$$

$$P_r := \phi \cdot P_n$$

$$P_r = 171.349 \cdot \text{kip}$$

$$P_r = 85.675 \cdot \text{ton}$$

Factored Axial resistance without flexure

LRFD Composite Section Axial Load Calculations

$$E_e := E \cdot \left(1 + \frac{.40}{n} \cdot \frac{A_c}{A_s} \right)$$

$$E_e = 3.609 \times 10^4 \cdot \frac{\text{kip}}{\text{in}^2}$$

$$F_e := f_y + 1.00 \cdot f_{yr} \cdot \frac{A_r}{A_s} + .85 \cdot f_c \cdot \frac{A_c}{A_s}$$

$$F_e = 72.737 \cdot \frac{\text{kip}}{\text{in}^2}$$

$$\lambda := \left(\frac{K \cdot l^2}{r \cdot \text{ft} \cdot \pi} \right)^2 \frac{F_e}{E_e}$$

$$\lambda = 1.413 \times 10^{-3}$$

$$\frac{K \cdot l}{r} = 1.754$$

If $\lambda < 2.25$

$$P_{n1} := .66^{\lambda} \cdot F_e \cdot A_s \quad P_{n1} = 1.17 \times 10^3 \cdot \text{kip} \quad P_{n1} = 585.215 \cdot \text{ton} \quad \text{Nominal Axial resistance}$$

If $\lambda > 2.25$

$$P_{n2} := \frac{.88 \cdot F_e \cdot A_s}{\lambda} \quad P_{n2} = 7.291 \times 10^5 \cdot \text{kip} \quad P_{n2} = 3.646 \times 10^5 \cdot \text{ton}$$

Factored Axial Load Capacity

$$\phi := .75$$

$$P_n := \begin{cases} P_{n1} & \text{if } \lambda < 2.25 \\ P_{n2} & \text{otherwise} \end{cases}$$

$$P_n = 1.17 \times 10^3 \cdot \text{kip}$$

$$P_r := \phi \cdot P_n$$

$$P_r = 877.823 \cdot \text{kip} \quad P_r = 438.911 \cdot \text{ton} \quad \text{Factored Axial resistance}$$

C.5 12-3/4" (0.375" wall) Member Capacities

$$d_p := 12.75 \cdot \text{in}$$

$$w_t := .375 \text{in}$$

Member Sizing

$$d_c := d_p - 2w_t$$

Diameter of the concrete core

$$d_r := 0 \cdot \text{in}$$

Diameter of the reinforcement

$$l := 1.5 \cdot \text{ft}$$

Unbraced length of member

General Material Properties

$$f_c := 4.5 \cdot \frac{\text{kip}}{\text{in}^2}$$

Strength of the concrete

$$f_y := 55 \cdot \frac{\text{kip}}{\text{in}^2}$$

Strength of the steel

$$f_{pe} := 0 \cdot \frac{\text{kip}}{\text{in}^2}$$

Effective stress in prestressing steel after loss

$$f_{yr} := 60 \cdot \frac{\text{kip}}{\text{in}^2}$$

Yield strength of the steel reinforcement

$$E := 29000 \cdot \frac{\text{kip}}{\text{in}^2}$$

Modulus of elasticity of the steel

$$E_c := 57000 \sqrt{\frac{\text{lb}}{\text{in}^2}} \sqrt{f_c} = 3.824 \times 10^3 \frac{\text{kip}}{\text{in}^2}$$

Modulus of elasticity of the concrete

$$E_p := 0 \cdot \frac{\text{kip}}{\text{in}^2}$$

Modulus of elasticity of prestressing tendons

$$\epsilon_{cu} := .003$$

Failure strain in concrete in compression

$$n := \frac{E}{E_c} \quad n = 7.584$$

Modular ratio

$$K := 1.0$$

Effective length factor

$$r := \sqrt{\frac{d_c^2 + d_p^2}{2}} \quad r = 12.381 \cdot \text{in}$$

Radius of gyration for the steel shell

Longitudinal Reinforcement

$$d_b := 0 \cdot \text{in}$$

Diameter of the reinforcement

$$N_b := 0$$

Number of reinforcing bars

Prestressing Steel

$$d_{ps} := 0 \cdot \text{in}$$

Diameter of the prestressing

Area Calculations

$$A_g := \frac{\pi \cdot d_p^2}{4}$$

$$A_g = 127.676 \cdot \text{in}^2$$

Gross Area of the pile

$$A_c := \frac{\pi \cdot d_c^2}{4}$$

$$A_c = 113.097 \cdot \text{in}^2$$

Area of the concrete

$$A_s := A_g - A_c$$

$$A_s = 14.579 \cdot \text{in}^2$$

Area of the steel shell

$$A_r := \frac{\pi \cdot d_r^2}{4} \cdot N_b$$

$$A_r = 0$$

Area of the reinforcing steel

$$A_{ps} := \frac{\pi \cdot d_{ps}^2}{4}$$

$$A_{ps} = 0$$

Area of the prestressing

LRFD Axial Load Capacity Calculations

$$P_n := .80 \cdot \left[.85 \cdot f_c \cdot (A_c - A_r) + f_y \cdot A_r - A_{ps} \cdot (f_{pe} - E_p \cdot \varepsilon_{cu}) \right]$$

$$P_n = 346.078 \cdot \text{kip}$$

$$P_n = 173.039 \cdot \text{ton}$$

Nominal Axial resistance without flexure

Factored Axial Load Capacity

$$\phi := .75$$

$$P_r := \phi \cdot P_n$$

$$P_r = 259.558 \cdot \text{kip}$$

$$P_r = 129.779 \cdot \text{ton}$$

Factored Axial resistance without flexure

LRFD Composite Section Axial Load Calculations

$$E_e := E \cdot \left(1 + \frac{.40}{n} \cdot \frac{A_c}{A_s} \right)$$

$$E_e = 4.086 \times 10^4 \cdot \frac{\text{kip}}{\text{in}^2}$$

$$F_e := f_y + 1.00 \cdot f_{yr} \cdot \frac{A_r}{A_s} + .85 \cdot f_c \cdot \frac{A_c}{A_s}$$

$$F_e = 84.673 \cdot \frac{\text{kip}}{\text{in}^2}$$

$$\lambda := \left(\frac{K \cdot l^2}{r \cdot \text{ft} \cdot \pi} \right)^2 \frac{F_e}{E_e}$$

$$\lambda = 9.985 \times 10^{-4}$$

$$\frac{K \cdot l}{r} = 1.454$$

If $\lambda < 2.25$

$$P_{n1} := .66^{\lambda} \cdot F_e \cdot A_s \quad P_{n1} = 1.234 \times 10^3 \cdot \text{kip} \quad P_{n1} = 616.964 \cdot \text{ton} \quad \text{Nominal Axial resistance}$$

If $\lambda > 2.25$

$$P_{n2} := \frac{.88 \cdot F_e \cdot A_s}{\lambda} \quad P_{n2} = 1.088 \times 10^6 \cdot \text{kip} \quad P_{n2} = 5.44 \times 10^5 \cdot \text{ton}$$

Factored Axial Load Capacity

$$\phi := .75$$

$$P_n := \begin{cases} P_{n1} & \text{if } \lambda < 2.25 \\ P_{n2} & \text{otherwise} \end{cases}$$

$$P_n = 1.234 \times 10^3 \cdot \text{kip}$$

$$P_r := \phi \cdot P_n$$

$$P_r = 925.446 \cdot \text{kip} \quad P_r = 462.723 \cdot \text{ton} \quad \text{Factored Axial resistance}$$